Dynamics and Kinematics of an Estuarine Network

by

William Bryce Corlett

M.S., University of Southampton, 2013
B.S.C.E., Old Dominion University, 2012
B.S., Old Dominion University, 2012

Submitted to the
Joint Program in Oceanography/Applied Ocean Science & Engineering
in partial fulfillment of the requirements for the degree of

Doctor of Philosophy

at the

MASSACHUSETTS INSTITUTE OF TECHNOLOGY

and the

WOODS HOLE OCEANOGRAPHIC INSTITUTION

September 2019

Signature redacted

Author .....
Joint Program in Oceanography/Applied Ocean Science & Engineering
Massachusetts Institute of Technology
& Woods Hole Oceanographic Institution
August 2, 2019

Signature redacted

Certified by .....
Dr. W. Rockwell Geyer
Senior Scientist, Woods Hole Oceanographic Institution
Thesis Supervisor

Signature redacted

Accepted by .....
Prof. Glenn R. Flierl
Chair, Joint Committee for Physical Oceanography
Massachusetts Institute of Technology
& Woods Hole Oceanographic Institution

Dynamics and Kinematics of an Estuarine Network

by

William Bryce Corlett

Submitted to the Joint Program in Oceanography/Applied Ocean Science & Engineering
Massachusetts Institute of Technology & Woods Hole Oceanographic Institution
on August 2, 2019, in partial fulfillment of the requirements for the degree of
Doctor of Philosophy

Abstract

This thesis addresses the dynamics of estuarine networks, based on hydrographic observations in Newark Bay, a sub-estuarine network connected to the Hudson River estuary through New York Harbor. Estuarine networks differ from simple estuaries in that they may have multiple connections to the ocean, multiple freshwater sources, and often contain complex junctions between estuarine segments. The Newark Bay estuarine network is connected to the sea through two tidal straits, and is fed by multiple internal and external sources of fresh water. The estuarine network is also naturally divided into a series of reaches, each of which is characterized by a different cross-sectional geometry. This thesis focuses on the hydrographic variability and varying exchange flow within the Newark Bay estuarine network. Shipboard hydrographic measurements reveal the time-dependent formation of salinity fronts between reaches of the estuary. Each front is generated by a different mechanism; however, all are generated by tidal flow through channel junctions during ebb tide, and are advected landward during flood tide. Mooring-based measurements confirm that these fronts form during nearly every tidal cycle, and that the fronts are associated with substantial changes in local salinity on tidal timescales. The effect of tidal processes, such as frontal advection, on the exchange flow is investigated by applying the isohaline total exchange flow (TEF) framework to mooring-based observations in multiple reaches of the estuarine network. This reveals that over half of the exchange flow is driven by tidal processes at all sites within the estuary. Both the TEF-based salt balance and the standard Eulerian salt balance indicate that tidal processes are also responsible for at least half of the landward salt flux at most sites within the estuary; TEF and Eulerian salt balances are nearly identical. Tidal processes within the estuary are in large part associated with fronts. The large influence of tidal processes on the exchange flow in Newark Bay is thus likely due to the prevalence of channel junctions within the estuarine network.

Thesis Supervisor: Dr. W. Rockwell Geyer
Title: Senior Scientist, Woods Hole Oceanographic Institution

Acknowledgments

The studies contained in this thesis were largely funded as part of a National Science Foundation Coastal SEES project (Grant OCE-1325136), which was developed to investigate the effects of anthropogenic modifications on the physical processes in estuaries. Additional funding was provided by the J. Seward Johnson Fund at Woods Hole Oceanographic Institution, and by Hudson River Foundation Graduate Fellowship GF/01/17.

My success, and my involvement in this research, would not have been possible without the team of support I have had at home, at WHOI and MIT, and in the estuarine and oceanographic physics communities. Many thanks go to Bob Pickart for seeing the spark of scientific ability in me, and for his valuable advice in observational oceanography. Thank you Fiamma, Meg, and the Academic Programs Office at WHOI, for enabling me to switch specialties mid-program, and for continuing to support me throughout my career at WHOI. And Rocky, my utmost thanks are yours for seeing my potential and for continuing to push me to reach it during every weekly meeting we've shared.

To my committee: Anthony, Claudia, Dave, and Heidi—thank you for providing invaluable advice on countless aspects of my research, and for continuing to guide me toward seeing the broader impacts of my research, and my research's place in the larger field of estuarine physics.

There would be no thesis without data from Newark Bay, and the collection of data in 2016 was in large part due to the meticulous planning and hard work on the part of Jay Sisson. Vital help in the collection of shipboard measurements was also provided by the crews of the R/V Sharp and R/V Caleta. The examination of the exchange flow throughout the Newark Bay estuarine network would not have been possible without access to data collected from moorings within the estuarine network in 2008 and 2009 as part of Hudson River Foundation Grant 008/07A; many thanks go to Bob Chant for access to this data, and for numerous helpful conversations regarding the characteristics of Newark Bay.

Finally, this thesis would not have been possible without the ongoing support of my academic peers, my friends, and my wife and family. Thank you all for listening to countless practice talks, helpfully critiquing my presentations and figures, editing papers, and inspiring new ways of looking at estuarine dynamics. This marathon would not have been successful without your assistance at every step of the journey.

THIS PAGE INTENTIONALLY LEFT BLANK

Contents

List of Figures

THIS PAGE INTENTIONALLY LEFT BLANK

Chapter 1

Introduction

The fundamental elements of estuarine physics are the salinity structure and exchange of water within an estuary (Pritchard, 1952a; Hansen & Rattray, 1965, 1966). In the typical estuarine regime, sea water encounters fresh water from riverine sources (Pritchard, 1967). Sea water and fresh water are mixed along the length of the estuary, mainly due to tidally generated turbulence. This mixing of salt water and fresh water requires a persistent exchange flow that draws salt water in from the ocean and transports mixed water out of the estuary (Knudsen, 1900). Although classical treatments of the estuarine circulation depict the circulation and mixing processes within an estuary based on a relatively uniform salinity gradient and distribution of mixing (Pritchard, 1952a; Hansen & Rattray, 1965), later studies emphasize the potential for pronounced along-estuary variations in the strength of these processes (Cokelet & Stewart, 1985; Largier, 1992; O'Donnell, 1993).

The physical processes in estuaries have fundamental significance to the ecology, biogeochemistry, sediment transport, and human activities within the estuarine environment. Because many species within estuaries are acutely sensitive to salinity (Bœuf & Payan, 2001; Levinton et al., 2011; He et al., 2017), the large salinity ranges within estuaries contribute to the high biodiversity found in these systems (Levings et al., 1983). The availability of both light and nutrients, which influence phytoplankton productivity in estuaries (Mallin et al., 1993), is dependent on a complex suite of physical processes, including spring-neap fluctuations in stratification (Jay & Smith, 1990) and sediment resuspension (Cloern, 1987), spatial variations in horizontal velocity (Kingsford & Suthers, 1996), and variations in the strength of the exchange flow (Mackas & Harrison, 1997). Sediment transport is one of the most im-

portant processes affected by estuarine physics (Postma, 1961; Festa & Hansen, 1978), with consequences for turbidity, shoaling, and contaminant transport. The extensive literature on estuarine sediment trapping processes (Migniot, 1971; Jay & Musiak, 1994; Woodruff et al., 2001; Traykovski et al., 2004; Schoellhamer, 2011; Ralston et al., 2012; Shellenbarger et al., 2015) exemplifies the complexity of the physical interactions between tidal flow, the estuarine circulation, stratification, and turbulent processes in determining the fate of sediment within estuaries. Some of these studies, notably Traykovski et al. (2004), Ralston et al. (2012), and Shellenbarger et al. (2015), highlight the importance of the frontal salinity structures within estuaries in controlling the position and intensity of sediment trapping processes.

Because estuaries are connected to both riverine and oceanic environments, they are natural locations for commercial ports. Excavations near Marseille (Morhange & Marriner, 2008), Rome (Delile et al., 2018), and Amsterdam (Beerenhout, 1994) have shown that the ancient Greeks and Romans often used estuaries as sites for commercial harbors. At many of these sites, the steady accumulation of trapped sediment required constant dredging of the main channels to maintain safe depths for ships (Salomon et al., 2012; Di Donato et al., 2018). Over the past century, the focus of dredging has in many ports shifted toward deepening shipping channels in response to increasing ship sizes (Winterwerp et al., 2013; Tran & Haasis, 2015). Channel dredging is particularly relevant to estuarine dynamics in light of the feedback processes between the dynamics and the depth of an estuary. Ralston and Geyer (2019) found that the deepening of the Hudson River has increased the tidal amplitude and shifted the head of the exchange flow farther upstream. Channel deepening has also increased local concentrations of suspended sediment by up to an order of magnitude in some Northern European estuarine harbors by modifying the asymmetry between flood and ebb tide (de Jonge et al., 2014; van Maren, Winterwerp, & Vroom, 2015). These effects may be exacerbated by the construction of side channels, which can modify the along-estuary salinity gradient (Okubo, 1973; van Maren et al., 2009) as well as the local tidal amplitude (Alebregtse et al., 2013).

While most estuarine dynamics research has focused on individual estuaries with one predominant channel, many estuarine environments contain multiple channels and tributaries, and may have multiple fresh water sources as well as multiple connections to the ocean. Chesapeake Bay, Narragansett Bay, Puget Sound, and the Changjiang estuary are

examples of such systems, which this thesis will refer to as "estuarine networks". While attempts have been made to characterize such systems in terms of the average characteristics of the overall estuary (e.g., Geyer & MacCready, 2014), the variability between different segments of estuarine networks renders such simplifications problematical. Individual branches of an estuarine network, such as the York River and James River within Chesapeake Bay (Friedrichs, 2009), are estuaries in their own right and contain distinctive characteristics. Because these sub-estuaries are connected within the larger estuarine network, they are also influenced by the dynamics and fresh water of other components of the estuarine network (Hayward et al., 1982; Chao et al., 1996). Moreover, the junctions and interconnections among components of an estuarine network may lead to processes that would not occur in simple estuaries. For example, Chesapeake Bay supplies both salt water and fresh water to the estuarine circulation in Baltimore Harbor (Stroup et al., 1961). These waters mix within the harbor and exit at a mixed salinity, creating a three-layer exchange flow (Long, 1977). Such a regime typically occurs in context with an estuarine network.

Estuarine networks are often associated with globally significant ports, such as Rotterdam (de Kok, 2002), Singapore (Simoons, 2010), and New York (Chant et al., 2018). The estuarine processes that occur within these estuarine networks are relevant to the actual function of the ports, in context with the currents that may affect ship operations and resilience of the built environment (Frittelli, 2008), sediment transport and trapping processes that affect the maintenance of navigation channels (W.-h. Li et al., 2007; de Nijs et al., 2009), and exchange processes that determine the fate of contaminants that are inevitably discharged into the waters of major industrial ports (Crawford et al., 1995; Balcom et al., 2008). Even the supply of fresh water may be influenced by the dynamics of an urban estuarine network. In the Changjiang estuary, for example, much of the municipal fresh water for the city of Shanghai (pop. 25 million) comes from within the estuarine network, and episodic variations in the exchange flow induce salt water intrusions on the local water supply (Zhu et al., 2018), with significant consequences for municipal water management.

The Newark Bay estuarine network, which contains the Port of New York and New Jersey (Suszkowski, 1978), offers a unique case study from which to examine both natural and human-induced aspects of the circulation of an estuarine network. Newark Bay is a sub-estuary network of the Hudson River—Raritan Bay estuary system, and has multiple connections to the ocean as well as multiple sources of fresh water (Fig. 1-1). Most sea water

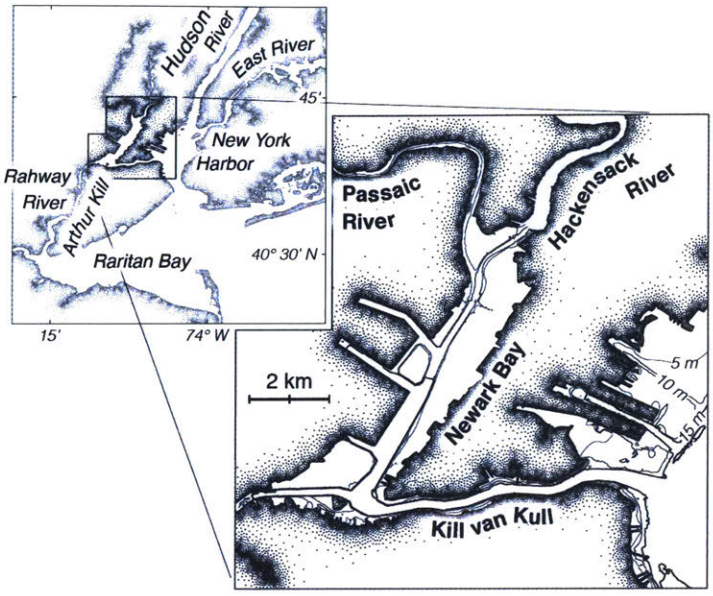

Figure 1-1: The Newark Bay estuarine network and the surrounding waterways.

enters the estuarine network through Kill van Kull in response to a net clockwise circulation around Staten Island (Suszkowski, 1978; Blumberg et al., 1999). This circulation is driven by a sea level gradient between New York Harbor and Raritan Bay (Kaluarachchi et al., 2003), which is likely caused by the mean wind stress (Chant et al., 2006). Most (85%) fresh water comes from the Passaic River, and much of the rest comes from the Hackensack River. The estuarine network has also been substantially modified over the past century to support the Port of New York and New Jersey (Halonen, 2011). Chant et al. (2018) found that the most recent deepening of the channel at the mouth of Newark Bay has substantially increased the tidal-residual circulation, but the effects of channel modifications on tidal processes and the exchange flow throughout the estuarine network have not yet been resolved.

Natural and man-made junctions divide the Newark Bay estuarine network into a series of distinct reaches (Fig. 1-1). At the junction between New York Harbor and Kill van Kull, the width of the channel abruptly decreases by one-third. The channel is roughly 20 m deep and 300 m wide in Kill van Kull and Arthur Kill. The channel is further punctuated by a series of abrupt bathymetric transitions in Newark Bay due to the natural geometry of the system as well as human-induced channel modifications. These modifications include the creation of two side channels to support Port Elizabeth and Port Newark (Marshall, 2004), as well as an abrupt transition in channel depth from 20 to 13 m in the middle of Newark Bay. In the shallower northern half of Newark Bay, the channel is roughly 250 m wide and is

flanked by a 600 m wide shoal. Depths on the shoal range from two to five meters. The main channel divides at the northern end of Newark Bay as it enters the Passaic and Hackensack rivers. North of the confluence, the Passaic is 5 m deep and 150 m wide, and the Hackensack is 10 m deep and 200 m wide. Because of different basin geometries, the tidal prism of the Passaic—the volume of water that is transported into the river during flood tide and out during ebb tide—is roughly four times smaller than that of the Hackensack River (Shrestha et al., 2014).

Tides within the estuarine network are largely semidiurnal, with a mean range of 1.5 m (Mathew & Winterwerp, 2017). Tidal velocity and water level are 90 degrees out of phase within Newark Bay (Chant et al., 2011). Tidal velocity and water level are 45 degrees out of phase in the adjacent Hudson River (Nepf & Geyer, 1996); consequently, tidal velocities within the Harbor lag velocities within the sub-estuary by 45 degrees, or roughly 90 minutes. This causes some low-salinity water from the Hudson River to be transported into Newark Bay through Kill van Kull (Corlett & Geyer, 2018). Some low-salinity water also enters the estuarine network from the Rahway River through Arthur Kill (Chant et al., 2006).

This thesis uses observations in the Newark Bay estuarine network to examine the hydrographic variability and varying exchange flow within an estuarine network, in light of both natural and human-induced aspects of the estuarine geometry. The hydrographic variability of the system is described in Chapter 2, revealing the importance of tidal flow through channel junctions in the generation of fronts. The spatial- and temporal-varying exchange flow is examined in Chapter 3, revealing that tidal processes are dominant throughout much of the estuarine network. These results are placed in the context of estuarine parameter space in Chapter 4. Chapter 5 provides a succinct summary of the thesis and reviews the ecological and societal implications of the results.

THIS PAGE INTENTIONALLY LEFT BLANK

Chapter 2

Frontogenesis at estuarine junctions*

2.1 Abstract

Observations of Newark Bay, a sub-estuary network characterized by multiple junctions, reveal that fronts are generated by tidal flow through transitions in channel geometry. Three types of fronts are observed, and most are associated with changes in channel geometry and tidal velocity phase-shifts. A lift-off front forms at the mouth of the sub-estuary during ebb tide in response to the abrupt seaward channel expansion. While forming, the front is enhanced by a tidal velocity phase-shift; flood tide persists in the main estuary until 90 minutes after the start of ebb tide in the sub-estuary. A second lift-off front forms during ebb tide at a channel-side-channel junction and is enhanced by a lateral baroclinic circulation induced by baroclinic and barotropic tidal velocity phase-shifts between the main channel and side channel. The lateral circulation also bifurcates the along-channel ebb flow at the surface, generating a surface front above the lift-off front. At the head of Newark Bay, a second surface front forms during ebb tide at the confluence of two tributary estuaries. This confluence front is rotated across the mouth of the primary fresh water source by high velocities from the adjacent tributary estuary and is maintained through much of ebb tide by lateral straining and mixing. Although the overall stratification of Newark Bay would categorize it as a partially-mixed estuary, these fronts divide the density structure of the sub-estuary into a series of nearly homogeneous segments between channel junctions, in a manner that is more commonly associated with fjords.

*Manuscript submitted to Estuaries and Coasts on November 8, 2018, with 2nd author W. Rockwell Geyer.

2.2 Introduction

Partially-mixed estuaries are often portrayed as having near-uniform along-channel salinity and stratification gradients (Hansen & Rattray, 1965; MacCready & Geyer, 2010). However, observations frequently reveal significant variability in the strength of these gradients, especially in fjords. In Puget Sound, for example, horizontal gradients in salinity and stratification are larger over shallow sills than along deep basins (Ebbesmeyer & Barnes, 1980). At bathymetric transitions, horizontal salinity gradients are concentrated in fronts (Lavelle et al., 1991); these fronts divide the fjord into a series of distinct segments (Cokelet & Stewart, 1985). The frontal processes within fjords may also be relevant to partially-mixed and well-mixed estuarine regimes, as fronts form in all types of estuaries (Largier, 1993; Geyer & Ralston, 2015).

Along-channel estuarine fronts are generated by a variety of mechanisms, which are manifest in the tendency equation of the along-channel salinity gradient, derived from the along-estuary derivative of the salt conservation equation:

$$\underbrace{\frac{\partial}{\partial t}\frac{\partial s}{\partial x}}_{1} + \underbrace{u \cdot \nabla \frac{\partial s}{\partial x}}_{2} = \underbrace{-\frac{\partial u}{\partial x}\frac{\partial s}{\partial x}}_{3} \underbrace{-\frac{\partial v}{\partial x}\frac{\partial s}{\partial y}}_{4} \underbrace{-\frac{\partial w}{\partial x}\frac{\partial s}{\partial z}}_{5} \underbrace{-\frac{\partial}{\partial x}\frac{\partial(\overline{s'w'})}{\partial z}}_{6}. \tag{2.1}$$

This equation describes the tendency (term 1) and advection (term 2) of the local salinity gradient, as well as the generation of along-channel fronts through the convergence of the along-channel salinity gradient (term 3), the twisting of a cross-channel gradient (term 4), the shearing of stratification (term 5), and the sharpening of the along-channel salinity gradient by a mixing gradient (term 6). Although all of these mechanisms may generate fronts, frontogenesis by along-channel convergence is most commonly discussed (term 3; J. H. Simpson & Nunes, 1981; Largier, 1992; MacDonald & Geyer, 2005; Ralston et al., 2010).

The formation of along-channel convergence fronts was first investigated by J. E. Simpson and Linden (1989). Through a series of lock exchange experiments, they determined that convergences may be generated by locally intensified horizontal salinity gradients. The locally intensified horizontal pressure gradient, in turn, produces an along-channel convergence. In a modeling study of the Hudson estuary, Geyer and Ralston (2015) demonstrated that frontogenesis may also occur at channel expansions, where velocity convergences are

produced by the hydraulic response of stratified flow to the change in width or depth. During ebb tide, stratified flow lifts off from the bed at seaward channel expansions, generating along-channel convergences between rapid ebb flow on the landward side of the lift-off zone and stagnant or weakly-ebbing flow on the seaward side (Horner-Devine et al., 2015). This convergence concentrates the along-channel salinity gradient at the bed in a lift-off front (Geyer & Ralston, 2015).

During flood tide, on the other hand, the buoyant surface layer is often arrested by saline inflow at landward channel expansions (J. H. Simpson & Nunes, 1981; Huzzey, 1982). The inflow subducts beneath the surface layer, generating a velocity convergence between inflow on the seaward side of the plunge line and nearly-stagnant flow on the landward side (Largier, 1992; Marmorino & Trump, 1996). This convergence concentrates the surface salinity gradient in a tidal intrusion front. During formation, both lift-off fronts and tidal intrusion fronts are essentially arrested gravity currents (Benjamin, 1968; Pelegri, 1988), in which the baroclinic propagation speed of the front matches the speed of the oncoming flow. Consequently, the internal hydraulic state of the flow is often critical at locations of frontogenesis (Armi & Farmer, 1986).

Lift-off fronts and tidal intrusion fronts also share similar propagation characteristics. Lift-off fronts tend to propagate landward as gravity currents after the change of tide; Geyer and Farmer (1989), for example, described the landward propagation of a lift-off front as a salt wedge during flood tide at the mouth of the Fraser River. In some cases, these propagating fronts induce the formation of new bottom fronts during the following ebb tide by initiating along-channel convergences at more landward locations (J. E. Simpson & Linden, 1989). Tidal intrusion fronts may propagate after the change of tide as well; these fronts propagate seaward during ebb tide, and in some cases leave estuaries as plume fronts (Nunes, 1982). However, tidal intrusion fronts may also propagate after initially forming during flood tide. For instance, Brubaker and Simpson (1999) observed that these fronts may be advected landward from bathymetric transitions and dissipate as flood tide intensifies.

Fronts also form at bathymetric transitions through non-buoyant processes. At channel confluences, for example, laterally-convergent streams produce fronts (Best, 1987; Rhoads & Sukhodolov, 2001). When the confluence is asymmetric, i.e., one of the flows is stronger than the other, the resulting lateral shear may rotate the front into the along-channel direction (De Serres et al., 1999; Riley et al., 2014). These fronts may also exhibit cross-front buoyancy

gradients, which are produced by either contrasting water properties (Farmer et al., 1995) or tidal phase-shifts between channels (Warner et al., 2002; Giddings et al., 2012).

Confluence fronts, lift-off fronts, and tidal intrusion fronts each form at channel junctions, located either within an estuary or between an estuary and the receiving waters (e.g., lift-off fronts). These junctions provide either the geometry or phase-shifts that are conducive to frontogenesis. Phase-shifts at junctions may also modify the process of frontogenesis by altering the horizontal salinity gradient (Pritchard & Bunce, 1959; Alebregtse et al., 2013) and the along-channel velocity gradient (Warner et al., 2003). Warner et al. (2002), for example, observed that phase-shifts between channels may generate either convergent or divergent along-channel salinity gradients at a junction depending on the phase of the tide. A phase-shift at a junction between a channel and side channel may enhance the lateral salinity gradient, generating a lateral bottom front (van Maren et al., 2009). These bottom fronts propagate into side channels as part of a tidal lock exchange process produced by the channel-side channel phase-shift (Allen & Price, 1959; Hayward et al., 1982). The lock exchange may also influence the along-channel salinity gradient by alternately exporting freshwater into the main channel at the surface and saline water into the channel at the bed.

In this observational study, we examine how junctions affect the formation of salinity fronts in the Newark Bay sub-estuary network, and how these fronts contribute to a heterogeneous estuarine structure. The chapter is structured as follows: section 2.3 reports our observation methods; section 2.4 analyzes the influence of junctions on the formation of salinity fronts; and section 2.5 discusses the effects of fronts on the heterogeneity of the sub-estuary network.

2.3 Methods

Shipboard and moored observations of the Newark Bay sub-estuary network and New York Harbor were conducted in the spring and early summer of 2016. From March 17 through July 5, four moorings were deployed along the axis of the sub-estuary, each within a region of distinctly different channel geometry (Fig. 2-1). From south to north, these moorings are labelled New York Harbor (NYH), Kill van Kull (KvK), Newark Bay (NB), and Passaic River (PR). All moorings were equipped with near-bed and near-surface RBR conductivity-temperature-depth (CTD) sensors; near-bed CTD sensors were mounted 0.5 m above the

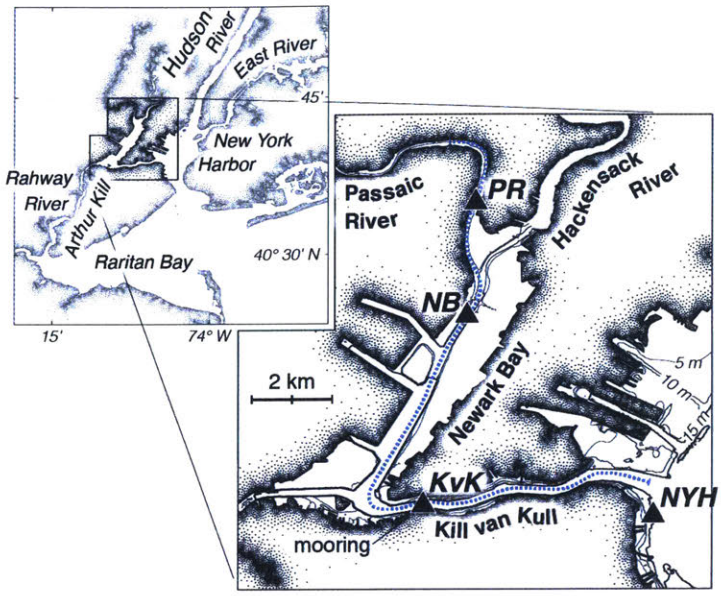

Figure 2-1: Locations of moorings and along-channel hydrographic sections within the Newark Bay sub-estuary network. Black triangles depict the locations of moorings, and the blue dotted line indicates the track of along-channel hydrographic sections. The inset shows the surrounding waterways.

bed and near-surface sensors were mounted 1 m below the water surface. All CTD sensors sampled water properties once per minute. Moorings NYH and NB were also equipped with bottom-mounted 1 MHz Nortek AWAC acoustic Doppler current profilers (ADCPs), which measured velocities in 0.5 m depth bins throughout the water column every ten minutes; the center of the bottom depth bin was located roughly 1.75 m above the bed. Mooring KvK was equipped with a bottom-mounted 600 kHz RDI ADCP, which measured velocities in 0.5 m depth bins throughout the water column every 15 minutes; the center of the bottom depth bin of the ADCP was located 1.6 m above the bed. Mooring PR was equipped with a 2 MHz Nortek Aquadopp ADCP, though data from this ADCP was not recovered due to corrosion by sea water; while deployed, the housing was breached by a propeller. Some loss of CTD data occurred at all moorings due to biofouling. Consequently, comprehensive data coverage of the sub-estuary with moored instruments ceased on May 30. All mooring-based data were interpolated onto a 10-minute sampling interval for processing and analyses.

To capture the along-channel variability of estuarine characteristics, shipboard measurements of velocity and salinity were made over semidiurnal tidal periods using a downward-facing 1200 kHz RDI ADCP and continuously profiling RBR CTDs. The ADCP measured velocities throughout the water column in 0.25 m depth bins once per second; the aver-

age horizontal resolution is equivalent to one profile every 2.5 m. The CTDs measured water properties at a rate of 12 Hz, producing salinity profiles with a vertical resolution of 0.1 m roughly every 70 m along the channel. For analyses of shipboard measurements, data were subsampled onto the vertical resolution of ADCP measurements and the horizontal resolution of CTD measurements. Shipboard surveys took place during two periods of the mooring deployment. The first period (May 11–14) coincided with larger-than-average (perigean) spring tides and relatively high discharge conditions (Fig. 2-2, top panel), and the second (June 30–July 1) occurred during smaller (apogean) spring tides and low discharge conditions. All along-channel sections fall along the transect shown in figure 2-1, which follows the primary axis of the sub-estuary from NYH to PR.

2.4 Results and analysis

2.4.1 Overall structure and variability

During the observation period, mean discharge from the Passaic and Hackensack rivers was 15 m^3/s (Fig. 2-2, top panel)—the 42^{nd} percentile of the overall historical record, and the 6^{th} percentile of the seasonal climatology (USGS gages 01389500 and 01378500, 1920–2015). Freshwater discharge in the adjacent Hudson River estuary was above average relative to overall historical conditions, but below average relative to the seasonal climatology (at the 66^{th} and 9^{th} percentiles, respectively; USGS gage 01358000, 1946–2015). The tidal range within the sub-estuary was larger than average during the observation period; the alignment of lunar perigee with spring tides produced two perigean springs and three apogean springs (Fig. 2-2, bottom panel). Tidal water level amplitudes ranged from roughly 0.5 m during neap tides to 1.0 m during perigean spring tides. Mean tidal velocities within the sub-estuary ranged from 0.5 to 0.9 m/s over the same period.

The salinity time series at the moorings exhibit variations due to the tides, spring/neap modulations, and fluctuations in river flow (Fig. 2-2). In New York Harbor, the spring/neap cycle significantly influences subtidal surface salinity variability; the surface of the Harbor is up to 10 psu fresher during neap tides than during perigean spring tides. Within the sub-estuary, the influence of the spring/neap cycle is more evident in near-bed salinity variability, although the response rapidly weakens toward the head of the sub-estuary. In the Passaic River, subtidal salinity variability is strongly influenced by fluctuations in river flow. Tidal

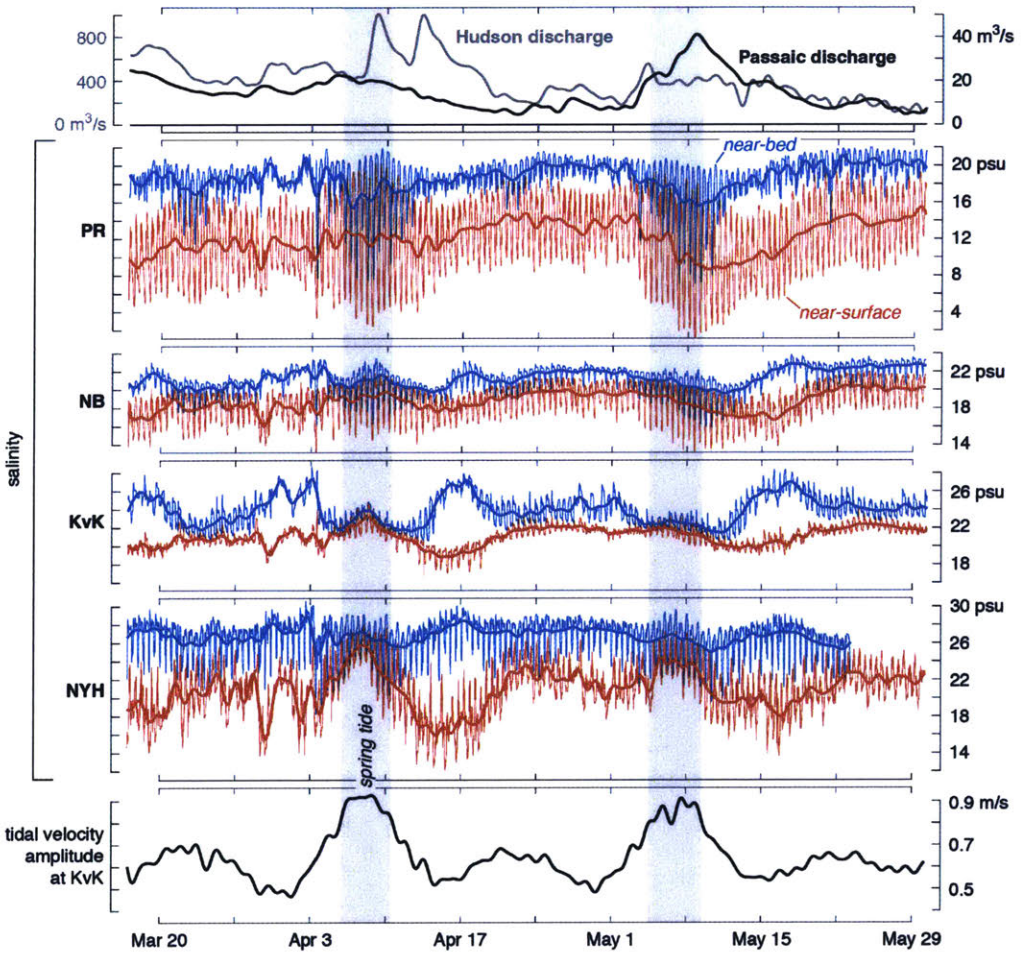

Figure 2-2: Time series of environmental conditions and salinity over the period of full moored data coverage. 33-hour filtered salinity measurements are superimposed over 10-minute data to show subtidal variability. Perigean spring tides are shaded in grey.

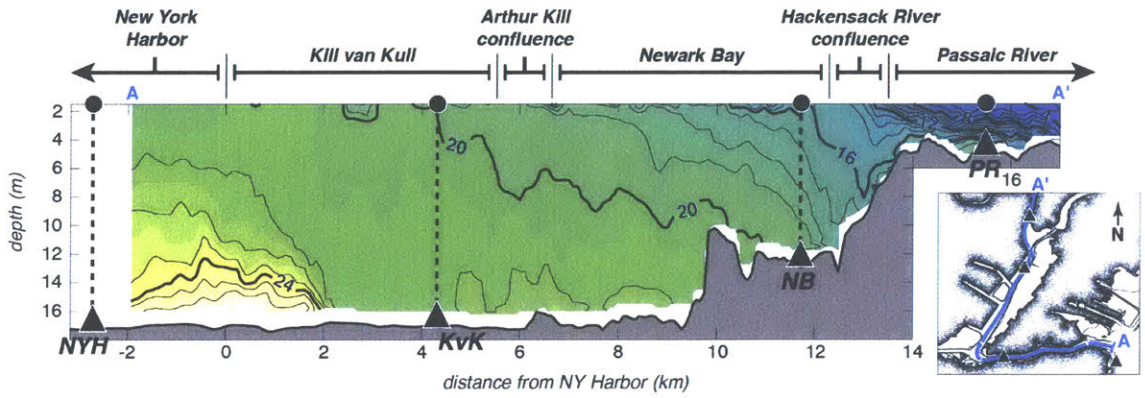

Figure 2-3: Mooring locations relative to the end-of-ebb along-channel salinity structure of the sub-estuary during spring tides and high discharge. Isohalines are indicated with both black contour lines and color shading.

salinity variability is most notable at moorings PR and NYH; however, all moorings exhibit rapid tidal salinity fluctuations. The varying tidal signal between moorings indicates that the strength of the horizontal salinity gradient changes over scales less than the tidal excursion.

Spatial structure

The spatial heterogeneity of salinity and stratification is confirmed by an along-channel salinity section obtained at the end of ebb tide (Fig. 2-3). Although the section presents a snapshot of tidal conditions, its depiction of the sub-estuary is consistent with the mean characteristics of the moored time series. Stratification is largest at the landward and seaward boundaries of the sub-estuary. Conditions within Newark Bay are partially-mixed, and Kill van Kull is largely well-mixed. Between regions of different stratification, the along-channel salinity gradient is concentrated in fronts. A bottom front at the mouth of the sub-estuary separates the Harbor from Kill van Kull, and a surface front separates the Passaic River from the Hackensack River confluence. Salinity and stratification gradients are more gradual between Kill van Kull and Newark Bay; however, a weak bottom front is observed near 12 km, and a weak surface front is observed near 10 km.

Temporal evidence of fronts

The salinity measured at each mooring rapidly increases during flood tide, consistent with the passage of fronts (Fig. 2-4). Fronts that are advected landward during flood tide produce a rapid increase in salinity at a stationary mooring, as the sharp horizontal salinity gradient

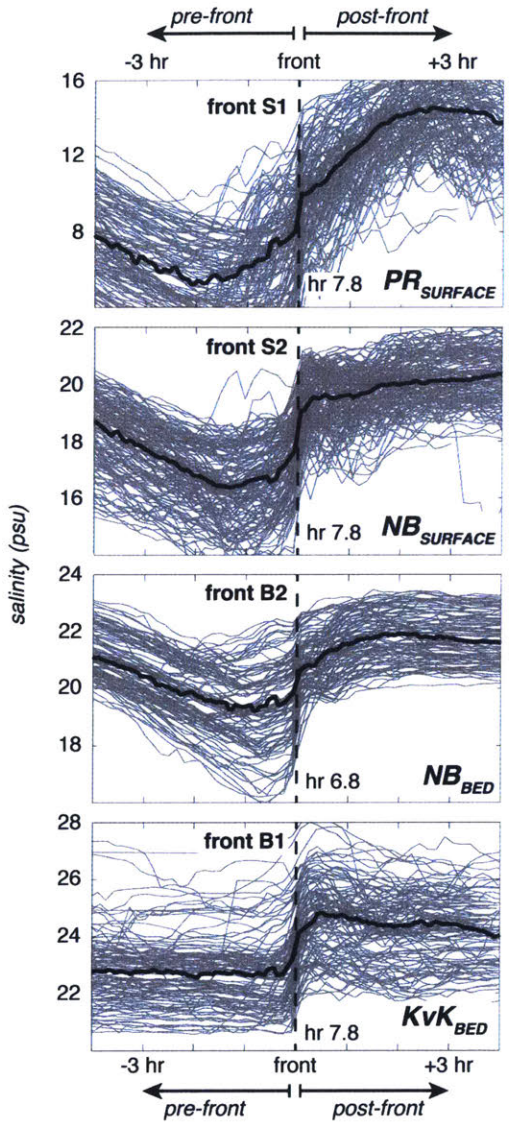

Figure 2-4: Temporal increases in salinity attributed to the landward advection of fronts at each mooring. Time series are aligned such that all fronts occur at the mean tidal hour of frontal advection. Tidal hours are given in reference to the depth-averaged velocity at each mooring; hour 0 occurs at the start of ebb tide, and hour 6 occurs at the start of flood tide. Note that the salinity scale at mooring PR is twice as large as the scales at moorings NB and KvK.

is translated into a rapid temporal change in salinity. The rapid increases in salinity in the moored observation records that are associated with the passage of fronts are at least two standard deviations larger than the mean temporal salinity gradient. The tidal cycles at each mooring that contain these rapid changes in salinity are shown in grey in figure 2-4; repeated hydrographic sections (discussed in §2.4.2) confirm that these tidal fluctuations are indeed generated by advected salinity fronts. To emphasize the characteristics of the fronts, the tidal salinity time series shown in figure 2-4 are aligned such that all rapid increases in salinity occur at the mean tidal hour of frontal advection at each mooring. The average tidal salinity variability at each mooring after co-locating frontal measurements is shown in black. This process of identifying advected fronts within the moored salinity records reveals that bottom fronts pass moorings KvK and NB in over 70% of tidal cycles, and surface fronts pass moorings PR and NB in over 90% of tidal cycles.

The consistent observations of frontal advection throughout the three-month record permit the characterization of the fronts at each mooring. At mooring KvK, the recurrent bottom front (labelled B1) increases near-bed salinity by an average of 2 psu in early flood tide. The salinity difference across the front fluctuates over the observation record by less than 1 psu. The large subtidal salinity fluctuations evident in figure 2-4 are instead produced by the effects of the spring/neap cycle on the mean tidal salinity at the mooring; the mean flood tide salinity at mooring KvK decreases by roughly 3 psu from neap tides to perigean spring tides. Front B1 passes the mooring by two hours into flood tide on average, which suggests that the front originates roughly 2.5 km seaward of the mooring, assuming that the front is primarily advected by depth-averaged tidal velocities. This location is consistent with the observed location of the bottom front in Kill van Kull in figure 2-3. However, the salinity gradient across the front in the mooring observations is much weaker than the salinity gradient across the front in the hydrography. This suggests that the front is significantly modified by tidal processes before passing mooring KvK.

The recurring bottom front in Newark Bay (labelled B2) increases the near-bed salinity at mooring NB by an average of 2 psu roughly 30 minutes after the start of flood tide. The salinity difference across the front is significantly influenced by spring/neap variability; the difference in salinity across front B2 increases by an average of 1.7 psu from neap tides to perigean spring tides. The relationship between the strength of the front and the spring/neap cycle suggests that the process of frontogenesis for front B2 is influenced by the tidal salinity

range. The time at which the bottom front (B2) passes the mooring, conversely, fluctuates nearly independently of spring/neap and discharge variability; most measurements of the front occur 20–70 minutes after the start of flood. This range suggests that the front forms roughly 0.5 km downstream of the mooring, assuming that the front is advected landward by near-bed velocities similar to those observed at the mooring.

The recurring surface front at mooring NB (labelled front S1) increases the surface salinity by an average of 3 psu in early flood tide. The salinity difference across this front is similarly influenced by the spring/neap cycle, increasing by an average of 1.7 psu from neap tides to perigean spring tides. This suggests that the process of formation for this front is influenced by the tidal salinity range. The time at which the front passes the mooring also fluctuates over the spring/neap cycle, decreasing from 2.2 to 1.4 hours into flood from neap tides to perigean spring tides. This suggests that the front consistently forms in the same location, at most 2.5 km seaward of the mooring, assuming that the front forms at the start of flood tide and is advected landward by tidal velocities.

The surface front at mooring PR increases the near-surface salinity by an average of 7 psu in early flood tide, which is consistent with the salinity difference across the front observed at the mouth of the Passaic River in figure 2-3. At the mooring, the salinity difference across the front ranges from 2–14 psu over the observation record, producing the vertical spread of salinity measurements shown in figure 2-4. Most of this variability is due to fluctuations in river flow; the salinity difference increases from an average of 4 psu during low discharge to 8 psu during peak discharge. The front is typically observed two hours after the start of flood tide, although the time of observation does fluctuate from tide to tide; most observations of front S2 occur between 1.3 and 2.4 hours into flood tide.

2.4.2 Formation and evolution of fronts

Repeated hydrographic surveys in each region of the sub-estuary provide insight into the formation and evolution of these fronts. All fronts observed at the moorings form at junctions during ebb tide. The fronts are generated by flow through the junctions, and most are modified by tidal phase-shifts. While there are similarities among the frontal locations, each front demonstrates a different mechanism through which junctions influence frontogenesis and frontal evolution.

Front B1

The formation and evolution of bottom front B1 is shown in two-hour intervals in figure 2-5. At the start of ebb tide (hour 0.7), the near-bed salinity gradient within Kill van Kull is nearly uniform. Ebb flow accelerates seaward at the 500-meter channel expansion at the mouth of the sub-estuary (0 km). Although the sub-estuary is beginning to ebb at hour 0.7, the Harbor continues to flood; this phase-shift is evident in the landward near-bed flow observed 2 km seaward of the mouth of Kill van Kull, which opposes the strengthening ebb in the sub-estuary. By maximum ebb (hour 2.5), this landward flow increases the salinity in New York Harbor by roughly 1 psu. Rapid ebb flow within Kill van Kull converges with the landward flow near 0 km at the newly formed front B1. The salinity difference across the front increases from 4 psu to 6 psu by late ebb (hour 4.3), despite a substantial decrease in the volume of saline water on the seaward side of the front. As ebb tide progresses, the front begins propagating landward as a gravity current, traveling 2 km by the start of flood tide (hour 6.2). The Harbor continues to ebb through hour 6.7, isolating the propagating gravity current from a seaward source of salinity. The propagating front continues toward Newark Bay through the remainder of flood tide, passing mooring KvK (hour 8.3), and exiting the survey region.

The mechanism of formation of front B1 is shown in figure 2-6 through the components of the along-channel convergence term in the frontogenesis equation (term 3; Eq. 2.1). The front is initially observed as an along-channel salinity gradient maximum prior to maximum ebb tide (hour 2.5; Fig. 2-6). This salinity gradient maximum is concentrated by an along-channel velocity convergence at the mouth of the sub-estuary. Near-bed velocities reverse from -0.5 m/s on the landward side of the front to +0.1 m/s on the seaward side. This velocity convergence is generated by the response of stratified ebb flow to the seaward channel expansion at 0 km. The hydraulic state of flow within Kill van Kull is supercritical during ebb tide, and the lift-off of the isohaline associated with front B1 at the estuary-sub-estuary junction is consistent with the response of supercritical stratified flow to a channel expansion (MacDonald & Geyer, 2005; Armi & Farmer, 1986). This suggests that front B1 is generated by the hydraulic response of ebb flow to the junction. The front begins propagating landward by late ebb (hour 4.3), in response to weakening ebb velocities in Kill van Kull.

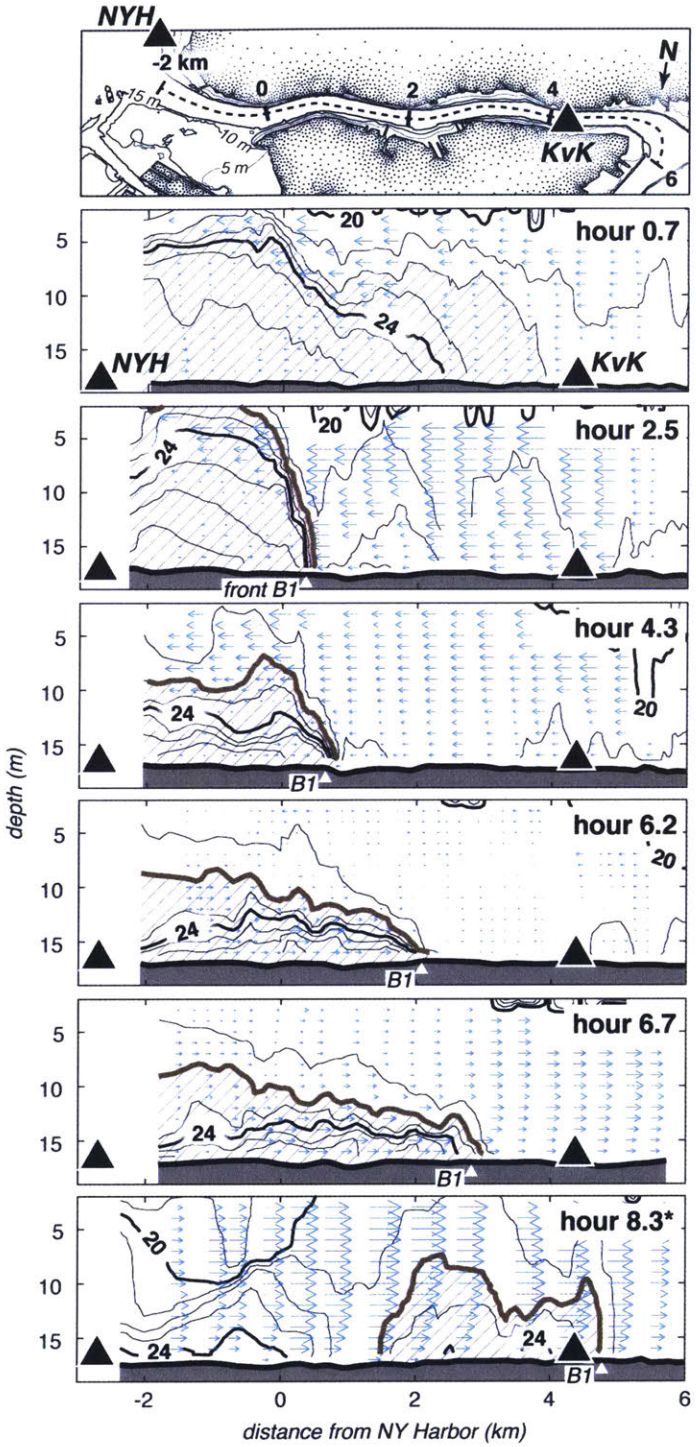

Figure 2-5: Repeated along-channel salinity sections in Kill van Kull from the start of ebb tide (hour 0.7) through maximum flood (hour 8.3). Along-channel velocities are shown with arrows, and shading indicates salinities greater than 22 psu. *Conditions at maximum flood were observed at the end of the previous tidal cycle.

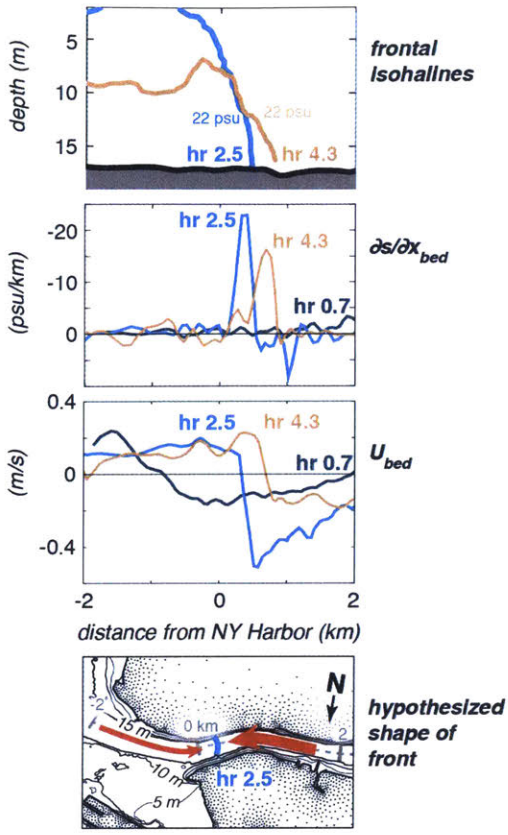

Figure 2-6: Generation of bottom front B1 during ebb tide. The seaward channel expansion at the mouth of Kill van Kull is located at 0 km. Lines are labelled by tidal hour. Positive along-channel salinity gradients and velocities are directed landward.

Both the formation and propagation of front B1 are substantially influenced by the tidal velocity phase-shift between New York Harbor and the sub-estuary. During early ebb tide (hour 2.5; Fig. 2-5), the phase-shift juxtaposes saline, flood tide conditions in the Harbor with fresher, ebb tide conditions in the sub-estuary. This enhances the along-channel salinity and velocity gradients at the mouth of Kill van Kull, both of which enhance the along-channel salinity convergence. Because of the enhanced convergence, the front forms during early ebb; most lift-off fronts instead form during late ebb (Geyer & Ralston, 2015). During early flood tide (hour 6.2), the phase-shift juxtaposes fresher, ebb tide conditions in the Harbor with saline, flood tide conditions in the sub-estuary. This reverses the near-bed salinity gradient at the mouth of Kill van Kull and detaches the propagating gravity current from New York Harbor (hour 8.3). The resulting isolated gravity current makes front B1 visibly different from the lift-off fronts observed at the mouths of salt-wedge estuaries (Geyer & Farmer, 1989; Ralston et al., 2010), which tend to have along-channel salinity gradients

that monotonically increase toward the sea.

Front B2

The second bottom front is observed in Newark Bay; the tidal evolution of this front (front B2) is shown in figure 2-7 in roughly ninety-minute intervals from early ebb tide through maximum flood. A region of enhanced horizontal salinity gradient is observed near the mouth of a side channel at 10.5 km in early ebb tide (hour 1.5; Fig. 2-7); along-channel velocities in this region are weakly divergent. By maximum ebb (hour 3.0), the region is advected seaward, and a weak bottom front forms at this location (front B2). Near-bed velocities at front B2 are convergent; along-channel ebbing velocities on the landward side of the front are stronger than those on the seaward side. The weak initial salinity difference across the front increases to 1 psu by late ebb (hour 4.3), following a reduction of the salinity on the landward side of the front. The salinity on the seaward side of the front remains nearly constant. The front begins propagating landward by the start of flood (hour 6.2), passing mooring NB and exiting the survey region by maximum flood (hour 9.0).

The dynamics of front B2 appear to be related to two factors: the response of ebb flow to the seaward channel expansion at the mouth of the side channel at 10.5 km, and the export of saline water from the same side channel. This is determined by analyses of along-channel variations of the horizontal salinity gradient, near-bed velocities, and repeated lateral hydrographic sections. Along-channel variations in the horizontal salinity gradient and near-bed velocities, the components of the along-channel convergence and cross-channel twisting terms in the frontogenesis equation (terms 3 and 4; Eq. 2.1), are shown during the formation of front B2 in figure 2-8. The front is first observed as a weak along-channel salinity gradient maximum at maximum ebb tide (hour 3.0; Fig. 2-8). The along-channel salinity gradient is drawn together by an along-channel velocity convergence at 10.5 km; ebbing near-bed velocities weaken by roughly 0.3 m/s over 500 m. We hypothesize that the velocity convergence is generated by the response of stratified ebb flow to the lateral channel expansion of the side channel junction, as ebb flow throughout the region is supercritical. The lack of a flow reversal across front B2 suggests that the front should be advected seaward. However, the front remains in nearly the same location through late ebb (hour 4.3).

Strong eastward lateral velocities on the seaward side of front B2 during late ebb tide suggest that the front is maintained and enhanced by the interaction of the main channel

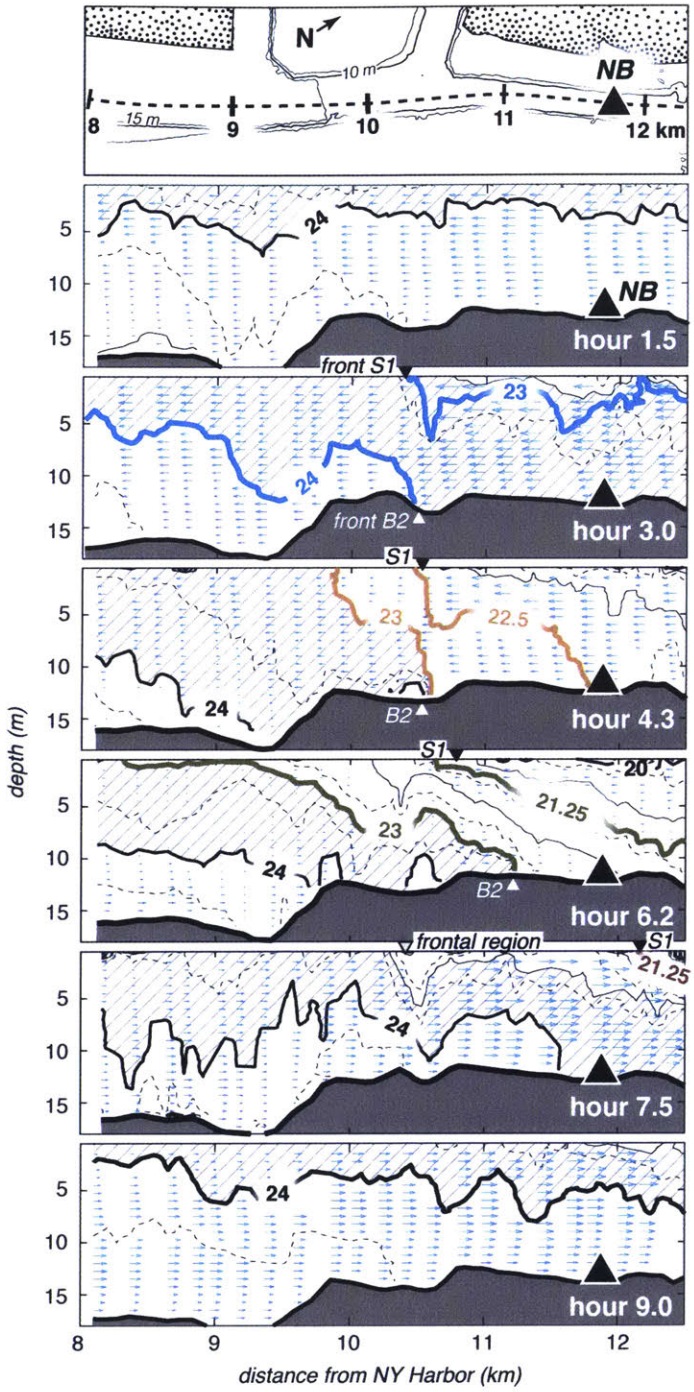

Figure 2-7: Along-channel salinity sections in Newark Bay from early ebb tide (hour 1.5) through maximum flood (hour 9.0). Arrows indicate along-channel velocities, and shading corresponds to salinities between 23 and 24 psu. Isohalines associated with fronts B2 and S1 over time are highlighted with colors that correspond to the changes over time depicted in figures 2-8 and 2-10.

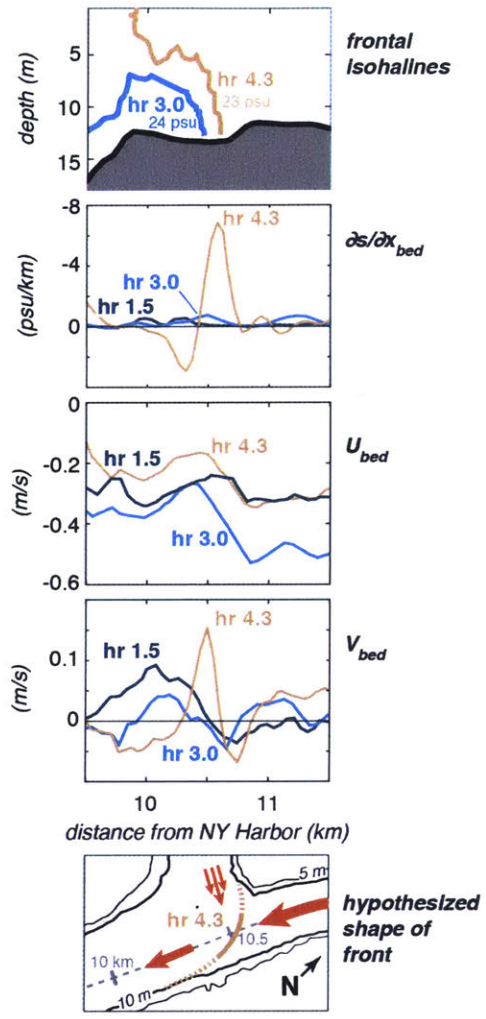

Figure 2-8: Generation of front B2 during ebb tide. The mouth of the side channel is located at 10.5 km. Lines are labelled by tidal hour. Positive cross-channel salinity gradients and velocities are directed eastward (out of the page).

with the side channel (hour 4.3; Fig. 2-8). This is confirmed by repeated lateral hydrographic sections at the junction at a different time under similar environmental conditions (Fig. 2-9; note the lower salinity—the 20 psu isohaline roughly corresponds to the 24 psu isohaline in figure 2-7). The lateral sections are shown in roughly ninety-minute intervals from the end of flood tide through early flood tide. These sections reveal the presence of both baroclinic and barotropic tidal velocity phase-shifts between the main channel and side channel; flood tide persists in the side channel roughly 90 minutes after the start of ebb tide in the main channel. From the end of flood through early ebb tide (hours 11.8–1.3; Fig. 2-9), the near-bed salinity of the main channel is greater than the side channel. The combination of this baroclinic pressure gradient with a lateral barotropic pressure gradient generates a lateral

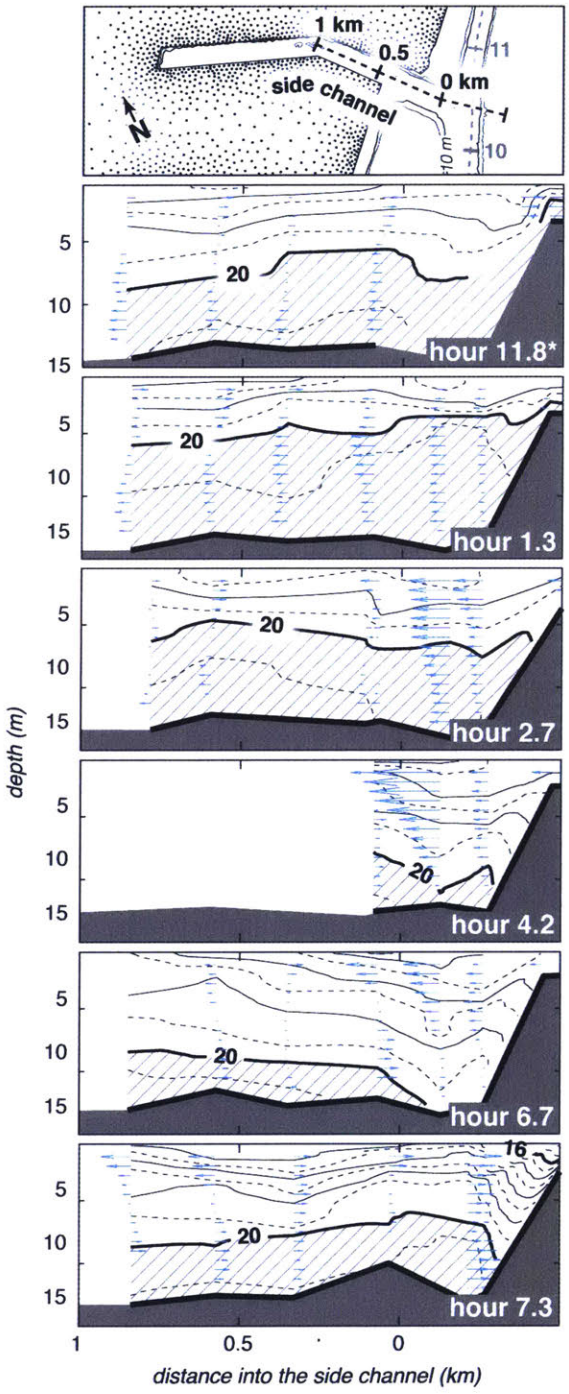

Figure 2-9: Across-channel salinity sections in Newark Bay from the end of flood tide (hour 11.8) through early flood (hour 7.3). Arrows indicate across-channel velocities, and shading corresponds to salinities greater than 20 psu. *Conditions at the end of flood tide were observed at the end of the depicted tidal cycle.

circulation in which salt water is advected into the side channel from the main channel. The near-bed salinity in the main channel decreases as ebb tide progresses (hours 2.7–4.2), due to the seaward advection of fresh water from the Passaic and Hackensack rivers. By late ebb (hour 4.2), the low salinity of the main channel reverses the lateral near-bed baroclinic pressure gradient, which in turn reverses the circulation of the side channel. Consequently, salt water that was trapped in the side channel from the previous flood tide is expelled into the main channel. In figure 2-7, this is the bolus of 24 psu water on the seaward side of the front in late ebb (hours 4.3 and 6.2). The expulsion of salt water from the side channel continues through the end of ebb tide (hour 6.7; Fig. 2-9), maintaining the front as an oblique boundary between fresh water from upstream and salt water from the side channel.

Front S1

A surface front also forms during ebb tide at the seaward channel expansion at the mouth of the side channel (Fig. 2-7). In early ebb (hour 1.5), the surface velocities and salinity gradient throughout Newark Bay are nearly uniform. By maximum ebb (hour 3.0; Fig. 2-7), surface velocities roughly double on the landward side of the side channel at 10.5 km, whereas those on the seaward side remain nearly constant. This convergence is associated with the surface front (front S1). As ebb tide progresses (hour 4.3), the gradient zone remains in nearly the same location, and retains a constant cross-front salinity difference, while the isohalines themselves are advected seaward. From maximum ebb to the end of ebb (hour 6.2), the isohaline associated with the front decreases from 23 psu to 21.25 psu. At the change of the tide, the front propagates landward, retaining the salinity it was associated with at the end of ebb tide. By hour 7.5, the front passes mooring NB, as shown in figure 2-3. It continues landward and exits the survey region as flood tide progresses. After front S1 propagates landward, another surface front forms at the mouth of the side channel (hour 7.5). Although this front also propagates landward, it is stretched and weakened by the divergent surface velocity field at 11 km. Consequently, this second surface front in Newark Bay is dissipated by the time it passes mooring NB (hour 9.0).

We hypothesize that front S1 is generated by the response of along-channel flow to the lateral circulation of the side channel. This is suggested by analyses of along-channel variations of the horizontal salinity gradient and near-surface velocities—components of the along-channel convergence term in the frontogenesis equation (term 3; Eq. 2.1). The

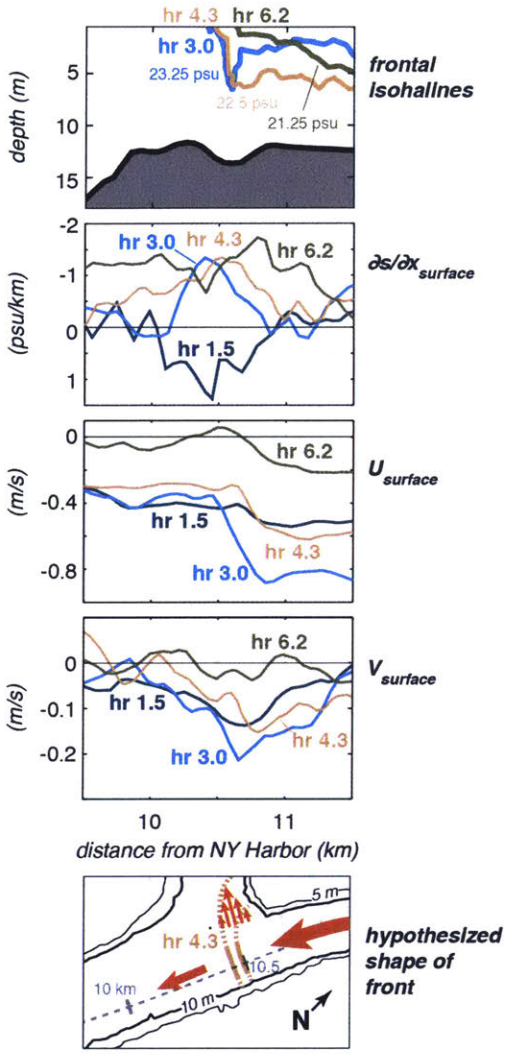

Figure 2-10: Generation of front S1 during ebb tide. The mouth of the side channel is located at 10.5 km. Lines are labelled by tidal hour.

isohalines associated with front S1 during frontogenesis, as well as along-channel variations in the horizontal salinity gradient and near-surface velocities, are shown in figure 2-10. The front is first observed at maximum ebb tide as a weak maximum of the along-channel salinity gradient located above bottom front B2 at 10.5 km (hour 3.0; Fig. 2-10). The salinity gradient maximum is generated by an along-channel velocity convergence, in which surface velocities decrease by roughly 0.5 m/s over a distance of 500 meters. The peak westward lateral velocities located at the along-channel convergence suggests that the surface convergence is generated by the interaction of the main channel with the side channel. This is confirmed by repeated hydrographic sections within the side channel during similar environmental conditions, shown in figure 2-9 from the end of flood tide through early flood

tide.

At the end of flood tide (hour 11.8; Fig. 2-9), the surface salinity within the side channel is less than the salinity in the main channel. The resulting baroclinic pressure gradient generates a lateral circulation that exports fresh water from the side channel at the surface. However, this pressure gradient reverses as fresh water is advected seaward in the main channel (hours 1.3–2.7). By maximum ebb tide (hour 2.7), the reversed baroclinic pressure gradient draws ebbing fresh water into the side channel, generating a weak lateral divergence in the main channel. The along-channel response to this lateral divergence is the weak surface velocity convergence that forms front S1 (hour 3.0; Fig. 2-10). Similar circulation patterns have been described before at the mouths of estuarine harbors (Langendoen & Karelse, 1990), but the resulting along-channel surface front has not been reported. This circulation persists through the end of ebb tide (hour 4.2–6.7; Fig. 2-9), continuously concentrating the along-channel salinity gradient into a surface front at the mouth of side channel. With the change of tide (hour 6.2; Fig. 2-10), along-channel surface velocities on the seaward side of the front reverse direction, halting the seaward advection of fresh water. This couples the front to its end-of-ebb salinity and further draws surface isohalines together, enhancing the front before it is advected landward.

Front S2

The strongest surface front observed in the Newark Bay system occurs at the mouth of the Passaic River; the formation and tidal evolution of this front (front S2) is shown in figure 2-11. At the start of ebb tide (hour 0.5), the surface salinity gradient increases from Newark Bay toward the Passaic. Weak surface velocities within Newark Bay are directed landward, and surface velocities within the Passaic are directed seaward. The resulting surface convergence forms a frontal region at 13 km. By maximum ebb (hour 2.2), this frontal region is advected seaward, and is replaced by surface front S2. This front is located above Hackensack River outflow, which is shown in figure 2-11 as a mid-depth cross-channel velocity maximum. As ebb tide progresses (hours 3.8–6.2), the front remains nearly stationary despite the seaward advection of surface isohalines; the salinity associated with the front decreases from 16 psu at maximum ebb to 11 psu at the end of ebb tide. With the change of tide, the front is advected landward, and passes mooring PR by maximum flood (hour 8.7).

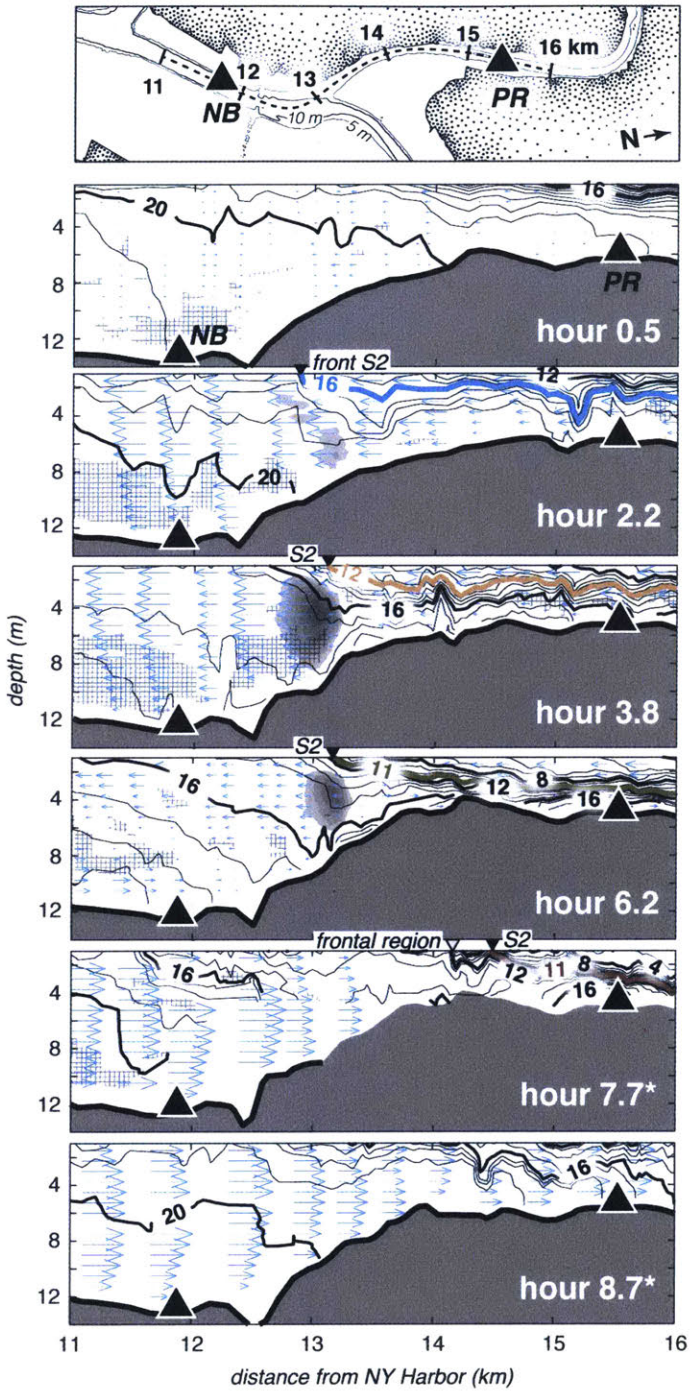

Figure 2-11: Along-channel salinity sections at the mouth of the Passaic River from the start of ebb tide (hour 0.5) through maximum flood (hour 8.7). Arrows indicate along-channel velocities, and cross-hatching indicates regions in which the Richardson number is less than 0.5. Contours of westward cross-channel velocities, which emanate from the Hackensack River, are shown in 10 cm/s increments in grey; velocity contours start at 10 cm/s. Salinity isohalines associated with front S2 over time are shown with colors that correspond to the changes over time shown in figure 2-12.

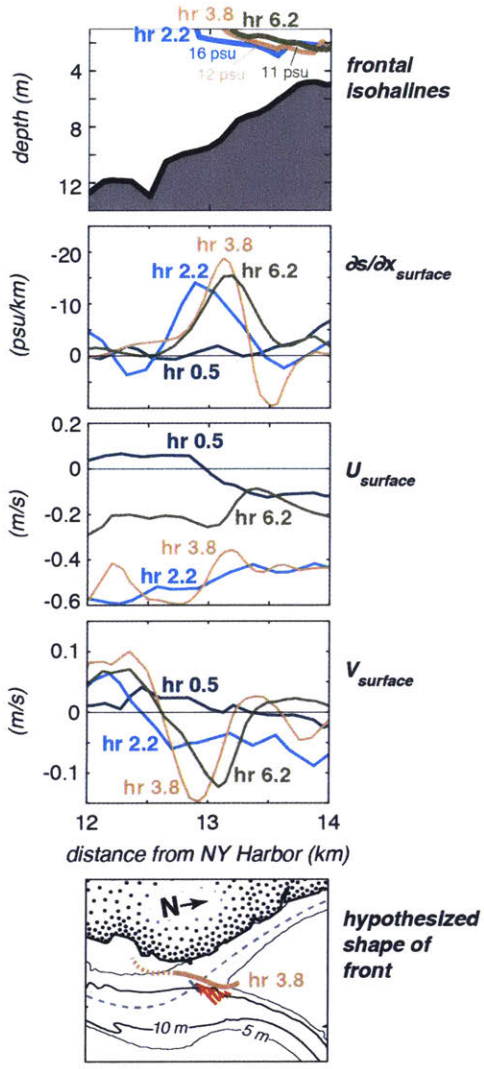

Figure 2-12: Generation of front S2 during ebb tide. The mouth of the Passaic River is located at 13 km. Lines are labelled by tidal hour. Negative cross-channel velocities are directed westward (into the page).

The dynamics of front S2 are associated with the merging of the Passaic and Hackensack rivers during ebb tide (Fig. 2-11). Because of the geometry of the confluence, Hackensack outflow impinges on outflow from the Passaic. The interaction between the two laterally-convergent ebb flows was determined through analyses of the along-channel variations of the horizontal salinity gradient and near-surface velocities—components of the along-channel convergence and cross-channel gradient twisting terms in the frontogenesis equation (terms 3 and 4; Eq. 2.1). These components, as well as the front-associated isohalines, are shown in figure 2-12. The front is first observed in early ebb tide (hour 2.2; Fig. 2-12). Unlike the fronts described above, the along-channel velocity field at the location of front S2 is weakly

divergent. Instead, the front is located in a region of cross-channel shear; westward lateral velocities peak immediately downstream of the front throughout ebb tide (hours 2.2–6.2). We hypothesize that this shear twists the boundary between the Passaic and Hackensack outflows into the along-channel direction. Throughout ebb tide, the magnitude of the along-channel salinity gradient at the front remains nearly constant. This is despite the tripling of cross-front shear from early ebb (hour 2.2) to the end of ebb tide (hour 6.2), which suggests that the strength of the front is not set by shear, but is instead set by the salinity gradient between the Passaic and Hackensack rivers. Consequently, the front is likely generated as a channel-parallel boundary between the two ebbing outflows, and is rotated by the cross-channel shear to be oriented obliquely to the channel. This process is consistent with the formation of confluence fronts, which are generated by the along-channel straining of the interface between convergent flows, and may be rotated into the along-channel direction by geometry-induced flow asymmetries (De Serres et al., 1999; Riley et al., 2014).

Front S2 is maintained by the confluence through the end of ebb, and like front S1, the salinity of the front steadily decreases throughout ebb tide. Although the lateral structure of the front was not resolved, the presence of the front within the along-channel sections in figure 2-11 demonstrates that the front extends over most of the mouth of the Passaic. This, combined with an absence of observations of unmixed fresh water further downstream, suggests that most ebbing fresh water from the Passaic passes through the front before being entrained into the saline and well-mixed Hackensack at the confluence. During late ebb (hour 3.8; Fig. 2-11), ebbing freshwater from the Passaic is entrained into the Hackensack near the bed through a turbulent bottom boundary layer, which is shown by the region of low gradient Richardson number ($Ri < 0.5$) beneath the core of cross-channel velocities associated with the impinging Hackensack. Ebb flow from the Passaic is also entrained into the Hackensack at the surface; the lack of low gradient Richardson numbers near the surface suggests that Passaic fresh water is entrained into the Hackensack at the surface by horizontal mixing, such as through lateral shear instabilities along the front. When the tide turns to flood, the front is advected landward up the Passaic River, preserving the cross-front salinity difference between Passaic and Hackensack water.

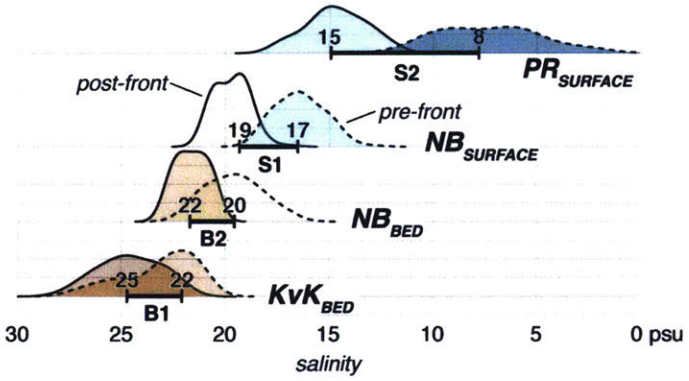

Figure 2-13: Histograms of flood-tide salinity before and after the passage of fronts, measured at moorings KvK, NB, and PR; colors indicate similar mean salinities.

2.4.3 Estuarine heterogeneity by fronts

Over the course of the observation record, the fronts within the Newark Bay sub-estuary generate a heterogeneous along-channel salinity structure. Each front separates significantly different salinities during flood tide, as shown by histograms of the salinity distributions at each mooring location (Fig. 2-13). In addition, the mean flood tide salinity measured before front B1 is similar to the mean flood tide salinity observed after the passage of front B2 at mooring NB. The difference between the two means is less than one standard deviation, which indicates that the region between the two fronts is nearly homogeneous. This is also true for near-bed salinities observed before front B2 and near-surface salinities observed after front S1, as well as near-surface salinities observed before front S1 and after front S2. This shows that, on average, fronts divide the sub-estuary into three nearly homogeneous segments between New York Harbor and the Passaic River. The characterization of the sub-estuary as a segmented system is further supported by the heterogeneous along-channel structure of the sub-estuary observed at the end of ebb in figure 2-3. Because the horizontal density gradient is not continuously distributed along the sub-estuary, Newark Bay has a structure that is more akin to a segmented fjord (e.g. Puget Sound; Ebbesmeyer & Barnes, 1980) than to a more uniform gradient estuary, such as the main stem of the James River (Pritchard, 1952b; Haas, 1977). Because Newark Bay is segmented by fronts, this characterization may also be true for other frontal estuaries and may even be true at small horizontal scales for the more uniform gradient estuaries as well.

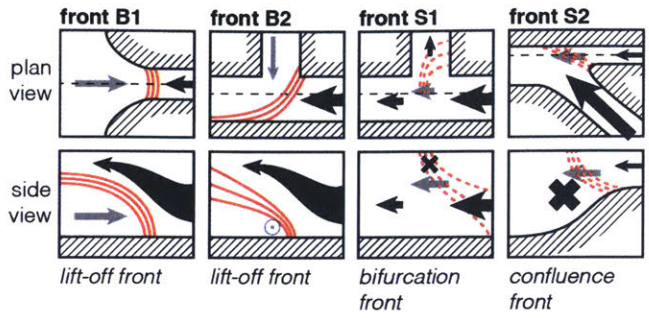

Figure 2-14: Plan and side-view schematics of the formation of the observed fronts, showing velocities in black and isohalines in red. Dashed red lines indicate that the salinity associated with the front changes during ebb tide, whereas the isohalines depicted with solid lines remain nearly stationary. Grey arrows emphasize the unique aspects of each front. For fronts B1 and B2, these are the velocities produced by tidal velocity phase-shifts. For fronts S1 and S2, these represent the advected salinity field, which is decoupled from the location of the front.

2.5 Summary and discussion

This chapter demonstrates that along-channel salinity fronts are generated by tidal flow through geometric transitions, and that these fronts contribute to along-channel estuarine heterogeneity. Several types of fronts are described within the Newark Bay sub-estuary (Fig. 2-14). During ebb tide, a lift-off front forms at the mouth of the sub-estuary from an along-channel convergence produced in response to the abrupt seaward channel expansion. A second lift-off front similarly forms in response to an abrupt seaward expansion at the mouth of a side channel within the sub-estuary. This front is maintained during late ebb by the export of high salinity water from the side channel. At the surface, ebbing fresh water is drawn into the side channel. This bifurcation of surface ebb flow generates an along-channel convergence, which in turn produces a surface front above the lift-off front. We label this a bifurcation front; similar density-driven circulation patterns have been described at the mouths of harbors (e.g. Roelfzema & van Os, 1978; Langendoen & Karelse, 1990), but we are unaware of any descriptions of similar along-channel surface fronts. The strongest surface front—a confluence front—is formed at the head of the sub-estuary by the merging of ebb flows at a channel confluence, and is rotated across the mouth of the primary fresh water source by high velocities from the adjoining tributary estuary. Each of these four fronts is generated at a channel junction, and each front is also modified by either a tidal phase-shift or by the geometry of the junction.

An along-channel phase-shift at the mouth of the sub-estuary, for example, enhances the formation of the lift-off front. These phase-shifts often occur due to transitions in channel geometry (Speer & Aubrey, 1985; Friedrichs & Aubrey, 1994). Both geometric transitions and along-channel phase-shifts are typically abrupt at junctions between short estuaries and the adjacent sea (Aubrey & Speer, 1985), or sub-estuaries and the main estuary (Hayward et al., 1982; Roos & Schuttelaars, 2015). In this chapter, the tidal phase of the sub-estuary leads the main estuary by 45 degrees. Because the start of ebb tide in the sub-estuary occurs while the main estuary is at the end of flood tide, the phase-shift enhances the convergence of the along-channel salinity gradient at the mouth of the sub-estuary. This enhanced along-channel convergence initiates the early formation of the lift-off front. As the front propagates landward during early flood tide, the phase-shift also detaches the gravity current behind the front from the main estuary. This occurs because the start of flood tide in the sub-estuary happens while the main estuary is at the end of ebb tide; the ebbing main estuary advects fresh water from a second source toward the mouth of the sub-estuary, which reverses the along-channel salinity gradient at the junction. The effects of the phase-shift on both frontogenesis and frontal evolution make this lift-off front different from others described at the mouths of estuaries, such as the fronts described by Geyer and Farmer (1989) and Ralston et al. (2010). Because tidal phase-shifts are common at junctions which are also conducive to frontogenesis, we suspect that many lift-off fronts are modified in a manner similar to the front described in this chapter.

Within the sub-estuary, along-channel fronts are modified by lateral barotropic and baroclinic tidal velocity phase-shifts at a channel-side channel junction. Lateral phase-shifts often occur between channels of different geometries (Warner et al., 2002), or of different lengths (van Maren et al., 2009). de Nijs et al. (2009) described how these phase-shifts set up fronts that propagate into side channels; this study finds that lateral phase-shifts also generate fronts within the main channel. During ebb tide, the salinity gradient between fresh water in the main channel and salt water in the side channel induces a lateral circulation that expels salt water into the main channel at the bed, similar to a lock exchange. The expelled salt water maintains the bottom front that forms at the seaward expansion of the side channel. At the same time, the lateral circulation draws fresh water into the side channel, producing a lateral flow divergence at the surface. This induces an along-channel convergence, which forms a surface front above the bottom front. This scenario appears to be

unique to channel-side channel junctions, as most seaward channel expansions exhibit divergent along-channel surface velocities during ebb tide (e.g., Luketina & Imberger, 1987). The process may also require a minimum along-channel salinity gradient at the junction. The southern side channel in Newark Bay, for example, is of similar dimensions to the northern side channel but does not generate a lateral lock exchange, likely due to the smaller tidal salinity range in the deeper, southern half of the sub-estuary. In any case, the fronts resulting from the exchange with the side-embayment contribute to the along-channel heterogeneity of the sub-estuary, consistent with their contribution to along-channel dispersion due to tidal trapping, as discussed by Okubo (1973) and MacVean and Stacey (2010).

This study also identified fronts that are generated by the geometry of confluence junctions. While they have been previously associated with river confluences (Best, 1987; Rhoads & Kenworthy, 1995), such fronts may be quite common in estuaries. The front described in this chapter as well as similar fronts described by Redbourn (1996) and Giddings et al. (2012) demonstrate that such fronts form in estuaries at junctions between channels as well as between a channel and side embayment. The buoyancy gradients across these fronts are induced by different sources of salinity, or by a tidal velocity phase-shift. Farmer et al. (1995) describe a similar front at a barotropic confluence of tidal flows in the Strait of Georgia—Juan de Fuca Strait system. This front is characterized by a frontal interface that is strained by the local velocity field, and numerical model results indicate that the convergence originates at the coast of Stuart Island. This suggests that the front is generated by the confluence of flows around the island rather than by local shear. The plume front described at the mouth at the Connecticut River by O'Donnell (1990) and Garvine (1977) also shares similar characteristics with a confluence front, in that it is generated at a boundary between laterally convergent flows with different salinity sources. Although these examples suggest that confluence fronts may be widespread in estuaries, further studies are needed to clarify the prevalence of fronts formed by lateral convergences and interfacial strain at confluences.

By forming and modifying fronts, the geometric transitions at junctions divide the estuary into a series of distinct, nearly homogeneous segments. The segmented structure of the sub-estuary is suggested by the overall hydrographic section and confirmed by measurements of similar salinities between fronts during flood tide. The division of the sub-estuary by fronts may be a common feature of partially-mixed and well-mixed estuaries. Geyer and

Ralston (2015)'s study of fronts in the Hudson estuary found that fronts can be generated by relatively small changes in geometry, and this study finds that even small differences in salinity across fronts may represent the major part of the along-estuary salinity variation. This suggests that the along-channel gradients, and perhaps the mean circulation, of frontal estuaries are more similar to geometrically-segmented fjords (e.g. Puget Sound; Cokelet & Stewart, 1985) than to the idealized partially-mixed estuaries often described in the literature (Hansen & Rattray, 1965; MacCready & Geyer, 2010).

THIS PAGE INTENTIONALLY LEFT BLANK

Chapter 3

Quantifying the salt balance of a partially-mixed estuarine network

Comparing Eulerian and isohaline approaches

3.1 Abstract

The salinity structure of an estuary is determined by the balance between landward fluxes of salt water and seaward fluxes of fresh water. The processes that generate this balance are typically examined in Eulerian coordinates. However, recent studies have applied an isohaline coordinate system to better quantify the exchange of salt water and fresh water in the presence of significant tidal salt fluxes. This chapter compares the Eulerian and isohaline approaches through the calculation of the time-varying subtidal salt balance at multiple locations within the Newark Bay estuarine network, a set of interconnected reaches at the mouth of the Hudson River estuary. Complex exchange flows, which may contain throughflows of unmodified water or inflows of both high and low salinity, are revealed by applying the isohaline approach to time-varying salinity and velocity measurements at a series of moorings within the estuarine network. These complex exchange flows occur in the presence of multiple channels and multiple sources of fresh water. A form of the isohaline salt balance is derived that accounts for complex exchange flows, and divides the salt balance into fluxes generated by tidal oscillatory and residual processes. The analyses reveal that Eulerian and isohaline estimates of salt fluxes are nearly identical. The analyses also reveal

that the variability of the landward salt flux due to tidal and residual processes does not need to match the variability of the exchange flow. At the mouth of the Newark Bay estuarine network, the landward salt flux is driven by residual processes though the exchange flow is driven by tidal oscillatory processes. At the head of the Newark Bay estuarine network, on the other hand, the effects of tidal oscillatory and residual processes balance to maintain a nearly-constant exchange flow and landward salt flux.

3.2 Introduction

The exchange flow in an estuary is a venerable topic, extending back to Procopius' description of the underflow in the Strait of Bosporus based on the observations of fishermen (History of the Wars VIII, vi. 27), and Marsili (1681)'s deduction that the two-layer circulation in the strait is driven by an along-channel density gradient (Pinardi et al., 2018). The first known quantification of the exchange flow was by Knudsen (1900), who examined the two-layer circulation at the mouth of the similarly stratified Baltic Sea. Knudsen noted that the steady-state salt balance of the Baltic Sea can be expressed as a function of the inflow of saline water from the North Sea and the outflow of fresher water:

$$0 = Q_{\text{in}} S_{\text{in}} - Q_{\text{out}} S_{\text{out}}. \tag{3.1}$$

Q_{in} and Q_{out} are the volume fluxes of the inflow and outflow layers at a cross-section at the mouth of the Baltic Sea, and S_{in} and S_{out} are the salinities of those layers (Burchard et al., 2018). This approach is well-suited to highly stratified regimes in which the exchange is dominated by the residual, density-driven circulation (see also Cokelet & Stewart, 1985). However, the definition of inflow and outflow layers is less clear for partially-mixed and well mixed estuaries. In these systems, the favored approach to address the subtidal salt balance has been the Eulerian framework developed by Pritchard (1954) and popularized by Hansen and Rattray (1965). This approach divides the tidal velocity and salinity fields into three orthogonal components: one that is tidally- and spatially-averaged, a second that is tidally-averaged and spatially-varying, and a third that is tidally- and spatially-varying (Fischer, 1972); for example,

$$u = \langle \overline{u} \rangle + \langle u' \rangle + \widetilde{u}', \tag{3.2}$$

in which $u(x,t)$ is the along-channel velocity, bars indicate spatially-averaged quantities, primes indicate spatial anomalies, brackets indicate tidally-averaged quantities, and tildes indicate tidal anomalies. As shown by Lerczak et al. (2006), this decomposition produces three orthogonal terms on the right side of the steady-state Eulerian salt balance:

$$0 = \underbrace{-Q_r\langle\overline{s}\rangle}_{1} + \underbrace{\int\langle u'\rangle\langle s'\rangle\, d\langle A\rangle}_{2} + \underbrace{\Big\langle\int\widetilde{u}'\widetilde{s}'dA\Big\rangle}_{3}, \tag{3.3}$$

in which $Q_r(t)$ is the river discharge, $s(x,t)$ is salinity, and $A(x,t)$ is the cross-sectional area.

In equation 3.3, term 1 is written as the advection of the tidally- and spatially-averaged salinity by river flow, as $-Q_r$ is equal to $\langle\overline{u}\rangle$ in steady-state (MacCready & Geyer, 2010). Term 2 (the residual salt flux) describes the advection of salt by the residual estuarine circulation. This tidally-averaged circulation is often described as a result of the along-channel density gradient (Hansen & Rattray, 1965), though it can also be generated by nonlinear advective processes such as eddy viscosity–shear covariance (Dijkstra et al., 2017) or advection (C. Li & O'Donnell, 1997; Burchard & Schuttelaars, 2012). Term 3 (the tidal oscillatory salt flux) describes the transport of salt by tidal dispersive processes, such as shear dispersion (Bowden, 1965), tidal trapping in side embayments (Okubo, 1973), and tidal inlet dynamics (Stommel & Farmer, 1952). Because of the complexity of these processes, term 3 is often parameterized by along-channel diffusion, using a dispersion coefficient K (Fischer, 1976):

$$\Big\langle\int\widetilde{u}'\widetilde{s}'dA\Big\rangle = AK\frac{-\partial s}{\partial x}. \tag{3.4}$$

K can be scaled by U_{tide}^2/ω, in which U_{tide} is the tidal velocity amplitude and ω is the tidal frequency, to estimate the effective efficiency of tidal mixing (Fischer et al., 1979). Fischer et al. (1979) found this ratio (α) to be between 0.005 and 0.02 for shear dispersion in a straight, unstratified channel. Okubo (1973) found dispersion by tidal trapping to be a maximum when the timescale of the trap exchange is equivalent to the tidal timescale; this corresponds to a maximum α of 0.05 for a ratio of the embayment to channel volume between 0 and 1. Zimmerman (1986)'s investigation of chaotic stirring in the Dutch Wadden Sea suggests that the maximum α for chaotic stirring is similarly 0.05. For jet-sink dynamics at tidal inlets (Stommel & Farmer, 1952), however, α can be as much as 0.5–0.7 (Chen et al., 2012).

One of the essential aspects of the Eulerian decomposition (Eq. 3.3) is the distinction

of the tidal oscillatory and residual salt fluxes. Hansen and Rattray (1966) defined the parameter ν as the fraction of the landward salt flux that is due to tidal oscillatory processes:

$$\nu = \frac{\left\langle \int \widetilde{u}'\widetilde{s}' dA \right\rangle}{\int \langle u' \rangle \langle s' \rangle \, d\langle A \rangle + \left\langle \int \widetilde{u}'\widetilde{s}' dA \right\rangle}. \tag{3.5}$$

ν was used by Hansen and Rattray (1966) to elucidate the relative importance of tidal to residual salt flux in different estuaries. Chen et al. (2012) described the dynamical differences between the Hudson River estuary and the Merrimack River estuary in part by differences in ν. Chen et al. (2012) found that within the Hudson estuary, ν varied considerably as a function of along-estuary position, with a mean value of 0.2, indicating the substantial contribution of tidal residual processes to the subtidal salt balance. The mean ν in the Merrimack River was found to be 0.8, indicating that the subtidal salt balance is primarily influenced by tidal oscillatory processes (Chen et al., 2012). Banas et al. (2004) used ν to examine the temporal response of the dynamics of Willapa Bay to fluctuations in river discharge, finding that the landward salt flux is largely driven by residual processes during high flow and by tidal processes during low flow. Ralston et al. (2010) found ν to be helpful in examining along-channel changes in the dominant mechanism of salt flux in the Merrimack River, revealing that the contribution of tidal oscillatory processes to the subtidal salt balance peaks at both the mouth and the head of the estuary.

Unlike the Eulerian framework, the Knudsen framework does not address the contribution of tidal oscillatory fluxes. To account for tidal oscillatory fluxes within the Knudsen framework, MacCready (2011) proposed that the exchange flow should be calculated in isohaline coordinates from the time-varying flow. This approach computes the total volume of water that is exchanged between salinities over a tidal cycle, accounting for both tidal and residual salt fluxes (Burchard et al., 2018), by tracking the time-varying volume flux as a function of salinity. Following MacCready (2011), the total exchange flow is defined as follows:

$$-\frac{dQ(s)}{ds} \equiv -\frac{d}{ds}\Big\langle \int_{A_s} u \, dA \Big\rangle, \tag{3.6}$$

in which A_s is the tidally-varying cross-sectional area with a salinity greater than s, Q is defined for all salinities, and $-dQ(s)/ds$ is the exchange flow for a specific salinity. This total exchange flow (TEF) framework reveals the net volume and salinity of water that is transported landward by both tidal oscillatory and residual processes, as well as the net

volume and salinity of water that is transported seaward; the characteristics of the inflow and outflow satisfy the time-dependent Knudsen relation (Eq. 3.3; MacCready, 2011). In equation 3.6, positive exchange flow values are associated with inflow, and negative exchange flow values are associated with outflow (MacCready, 2011). Wang et al. (2017) noted that the TEF approach also reveals the amount of water that is transformed due to mixing of salt over a tidal cycle. This transformation of water from one salinity to another is related to mixing through the salinity variance budget; MacCready et al. (2018) and Burchard et al. (2019) found that volume-integrated mixing, defined in these studies by the rate of destruction of salinity variance, can be estimated directly from the characteristics of the total exchange flow.

Both the Knudsen/TEF approach and the Eulerian approach quantify the subtidal salt balance. However, the Knudsen/TEF approach does not distinguish between subtidal salt fluxes due to residual processes and tidal oscillatory processes, whereas the Eulerian approach does not quantify the exchange flow. In an estuary without stratification, for example, the residual circulation may transport water of a given salinity both landward and seaward; this portion of the residual circulation would not contribute to the exchange flow. This chapter will explore new methodologies to directly compare TEF and Eulerian approaches to the subtidal salt balance, in which the individual contributions of tidal and residual processes can be explicitly described.

The Newark Bay estuarine network provides an interesting test case to compare Eulerian and TEF versions of the subtidal salt balance. This set of interconnected reaches is characterized by a robust residual circulation (Chant et al., 2018), with significant contributions to the salt flux due to both tidal oscillatory and residual processes (Chant et al., 2011). Corlett and Geyer (2018) observed substantial tidal variability throughout the system in the form of tidal salinity fronts at channel junctions (cf. Chapter 2). Does this tidal variability substantially contribute to the exchange flow? The comparison between TEF and Eulerian frameworks in Newark Bay presents an opportunity to examine the relative contribution of the residual circulation to the exchange flow within a system characterized by substantial tidal salinity variability.

The geometry of the Newark Bay estuarine network also introduces new issues that need to be addressed within the TEF framework. Multiple sources of fresh water are present within the estuarine network, introducing the possibility of landward advection of low salin-

ity water in some reaches. Long (1977) found that the consistent presence of fresh water at the mouth of the Baltimore Harbor generates a three-layered residual circulation. Some reaches within the Newark Bay estuarine network may similarly contain multi-layered exchange flows. The estuarine network is also characterized by a mean barotropic circulation through the multiple outlets of Newark Bay to the ocean (Suszkowski, 1978; Blumberg et al., 1999). Lee et al. (2019) addressed the effects of a throughflow on the Eulerian volume and salt balance in an examination of Mobile Bay, but the effect of a throughflow on the total exchange flow has not yet been examined.

This study derives a form of the TEF salt balance (Eq. 3.1) that enables a direct comparison of terms with the Eulerian salt balance (Eq. 3.3), and compares the two approaches by using moored hydrographic observations at four cross-sections within the Newark Bay estuarine network. The methods used to estimate the terms within the TEF and Eulerian salt balances are described in section 3.3; the TEF and Eulerian salt balances at each cross-section in the estuarine network are presented in section 3.4; and the implications of this study are presented in section 3.5.

3.3 Methods

This chapter uses data obtained during two studies of the Newark Bay system, the first by Chant and colleagues in 2008 (Chant et al., 2018), and the second that was conducted in 2016 and was described in detail in Chapter 2. Between the two studies, data from six mooring locations were used to resolve the along-estuary variability of the subtidal salt balance in the Newark Bay estuarine network. From south to north, these mooring locations are labelled Kill van Kull (KK), Arthur Kill (AK), Newark Bay shoal (NBs), Newark Bay channel (NBc), Hackensack River (HR), and Passaic River (PR; Fig. 3-1). The first deployment occurred from May through July 2008, and included moorings KK, AK, HR, and PR (Chant et al., 2018). The second deployment occurred from March through July 2016, and included moorings NBs and NBc (Corlett & Geyer, 2018). The 2016 deployment also included moorings in Kill van Kull and the Passaic River; however, the data at these moorings are incomplete, due to logistical issues. The 2016 mooring in the Passaic lacks velocity measurements. The 2016 mooring in Kill van Kull was not paired with a mooring in Arthur Kill, making it difficult to constrain salt and mass balances at the mouth of Newark

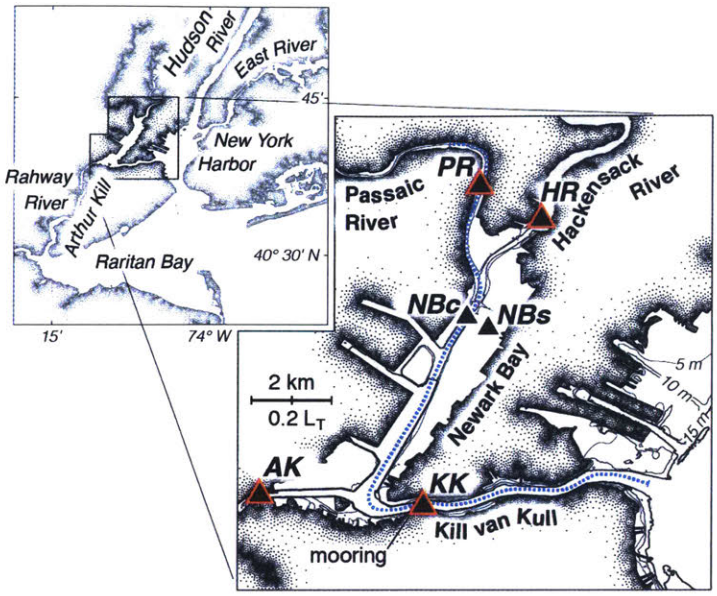

Figure 3-1: Locations of moorings deployed within the Newark Bay estuarine network in 2008 and 2016. Moorings deployed in 2008 are shown with red trim, and moorings deployed in 2016 are shown with white trim. The blue dotted line indicates the main channel of the estuarine network.

Bay. So, data from the 2016 PR and KK moorings are not used in this chapter. Shipboard hydrographic measurements during the 2016 mooring deployment revealed that the lateral structures of salinity and velocity are relatively uniform throughout the estuarine network, supporting the use of individual moorings to describe along-channel fluxes. Because of substantial lateral changes in depth in Newark Bay, salt and volume fluxes at mooring NBc are combined with fluxes at mooring NBs to estimate the local exchange flow and subtidal salt balance. Salt and volume fluxes at moorings KK and AK are also combined to estimate the characteristics of the effective "mouth" of the estuarine network.

3.3.1 Measurements

Each mooring was equipped with Conductivity-Temperature (CT) sensors to measure near-bed (0.5 m above the bed) and near-surface (1 m below the surface) salinity and temperature. Each mooring was also equipped with a bottom-mounted acoustic Doppler current profiler (ADCP) to measure vertical profiles of horizontal velocities. In Kill van Kull, horizontal velocities were measured once every ten minutes in 0.5 m depth-bins by an upward-facing 600 kHz RDI ADCP; the center of the bottom bin was located 0.7 m above the bed. Horizontal

water velocities in Arthur Kill were measured every ten minutes in 0.25 m depth-bins by an upward-facing 1200 kHz RDI ADCP; the center of the bottom bin was located 0.8 m above the bed. In both Kill van Kull and Arthur Kill, near-bed salinities were measured once every ten minutes by a Seabird 16 CT sensor, and near-surface salinities were measured once every five minutes by a Seabird 37 CT sensor. In Newark Bay, near-bed and near-surface salinities were measured once per minute by RBR Conductivity-Temperature-Depth (CTD) sensors. Mooring NBs was equipped with a 2 MHz Nortek Aquadopp ADCP, which measured horizontal velocities in 0.25 m depth bins once every 15 minutes; the center of the bottom bin was located 0.9 m above the bed. Mooring NBc was equipped with a bottom-mounted 1 MHz Nortek Acoustic Wave and Current (AWAC) profiler, which measured horizontal velocities in 0.5 m depth-bins once every ten minutes; the center of the bottom bin was located roughly 1.75 m above the bed. In the Hackensack River, horizontal velocities were measured in 0.25 m depth-bins once every 20 minutes by a bottom mounted Nortek AWAC profiler; the center of the bottom bin was located 0.8 m above the bed. The near-bed salinity was measured by a Seabird 16 CT sensor, and the near-surface salinity was measured by a Seabird 37 CT sensor; salinities were measured once every five minutes. In the Passaic River, horizontal velocities were measured in 0.5 m depth-bins by a bottom-mounted RDI ADCP once every 10 minutes; the center of the bottom bin was located 0.9 m above the bed. The near-bed and near-surface salinity and temperature were measured by Seabird 37 CT sensors; the near-bed salinity was measured once every 10 minutes, and the near-surface salinity was measured once every five minutes. Data at each mooring were interpolated onto common ten-minute sampling intervals for analyses. All moorings exhibited biofouling during the deployments; consequently, the records used to calculate the exchange flow and the subtidal salt balance are truncated versions of the full measurement record.

Shipboard hydrographic measurements, using a downward-facing 1200 kHz RDI ADCP and continuously profiling RBR CTDs, were made over semidiurnal tidal periods in 2016 to capture the spatial characteristics of the estuarine network. The ADCP measured horizontal water velocities in 0.25 m depth-bins once per second, which was roughly equivalent to one profile every 2.5 horizontal meters. CTDs measured salinity, temperature, and depth at a rate of 12 Hz; this produced salinity measurements with a vertical resolution of 0.1 m and a horizontal resolution of 70 m. The results from these hydrographic sections are discussed in detail in Chapter 2.

3.3.2 Salt balance calculation

The subtidal salt balance estimates the amount of salt landward of a cross-section, and is generally divided into landward and seaward salt fluxes in both Eulerian and TEF approaches. In the Eulerian approach, the residual salt flux and tidal oscillatory salt flux tend to be directed landward (Pritchard, 1954); we refer to the combination of these salt fluxes as the Eulerian estuarine salt flux (QS_{Eul}):

$$QS_{Eul} = \int \langle u' \rangle \langle s' \rangle \, d\langle A \rangle + \left\langle \int \widetilde{u}' \widetilde{s}' dA \right\rangle . \tag{3.7}$$

We refer to the residual salt flux as QS_{RC}:

$$QS_{RC} = \int \langle u' \rangle \langle s' \rangle \, d\langle A \rangle . \tag{3.8}$$

Neither the estuarine salt flux (QS_{Eul}; the portion of the salt flux not due to seaward riverine transport) nor the division between tidal oscillatory and residual salt fluxes are explicitly defined within the TEF approach (MacCready, 2011). In the following subsection, we derive expressions that provide TEF equivalents of the estuarine salt flux and the ν parameter, i.e. the ratio of tidal to estuarine salt flux.

Derivation of components of the TEF subtidal salt balance

The TEF and Eulerian versions of the subtidal salt balance (Eq. 3.1 and 3.3) are exactly equal (MacCready, 2011):

$$Q_{\text{in}} S_{\text{in}} - Q_{\text{out}} S_{\text{out}} = -Q_r \, \langle \overline{s} \rangle + \int \langle u' \rangle \langle s' \rangle \, d\langle A \rangle + \left\langle \int \widetilde{u}' \widetilde{s}' dA \right\rangle . \tag{3.9}$$

However, the TEF approach does not explicitly include the spatially- and tidally-averaged contribution of riverine transport, from which the estuarine salt flux can be determined. To find the TEF equivalent of the estuarine salt flux, we follow MacCready (2011) in noting that:

$$-Q_r = Q_{\text{in}} - Q_{\text{out}} . \tag{3.10}$$

The residual spatially-averaged salinity ($\langle \overline{s} \rangle$) does not have a TEF equivalent, but it can

be approximated by the average of the TEF inflow and outflow salinities:

$$\langle \overline{s} \rangle \simeq \frac{S_{\text{in}} + S_{\text{out}}}{2}. \tag{3.11}$$

We refer to the average TEF salinity, calculated on the right side of equation 3.11, as $\overline{S}$. Combining equations 3.9 through 3.11 yields the following form of the estuarine salt flux:

$$\frac{Q_{\text{in}} - Q_{\text{out}}}{2} (S_{\text{in}} - S_{\text{out}}) \simeq QS_{Eul}, \tag{3.12}$$

in which the approximation is only due to the TEF approximation of $\langle \overline{s} \rangle$. Following MacCready (2011):

$$(S_{\text{in}} - S_{\text{out}}) \equiv \Delta S_E. \tag{3.13}$$

We define the estuarine exchange flow, or portion of the exchange flow not due to riverine transport, as the following:

$$\frac{Q_{\text{in}} - Q_{\text{out}}}{2} \equiv Q_E. \tag{3.14}$$

This simplifies the TEF estuarine salt flux to the following form:

$$Q_E \Delta S_E \equiv QS_E. \tag{3.15}$$

This paper will examine to what extent the TEF estuarine salt flux (QS_E) is equivalent to QS_{Eul}.

QS_E can be divided into tidal and residual components, similar to QS_{Eul} (Eq. 3.7). Following MacCready (2011), Chen et al. (2012), and Burchard et al. (2018), we calculate the residual component of the total exchange flow using the same TEF approach as in equation 3.6, but with tidally-averaged values of salinity, velocity, and cross-sectional area:

$$-\frac{dQ_R(s)}{ds} = -\frac{d}{ds} \int_{\langle A(\langle s \rangle, t) \rangle} \langle u \rangle \, d\langle A \rangle. \tag{3.16}$$

We follow Pritchard (1954) and Lerczak et al. (2006)'s division of Eulerian variables into tidal and residual components to define the tidal component of the exchange flow, $Q_T(s)$, as the difference between the total exchange flow and the residual exchange flow in salinity

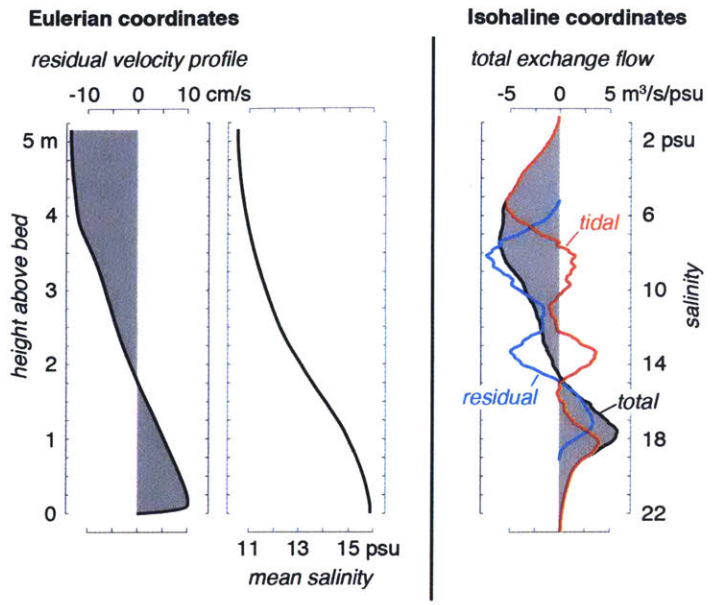

Figure 3-2: Comparison of the record-mean Eulerian residual velocity profile with the record-mean isohaline total exchange flow at the Passaic River cross-section. The record-mean salinity profile is shown to visualize the range of salinities over which the residual circulation contributes to the salt balance. The tidal component of the average total exchange flow is shown in red, the residual component is shown in blue, and the total is outlined in black. All profiles are averaged over the observation record.

coordinates:

$$-\frac{dQ(s)}{ds} + \frac{dQ_R(s)}{ds} \equiv -\frac{dQ_T(s)}{ds}. \tag{3.17}$$

As an example, the record-average tidal and residual components of the total exchange flow in the Passaic River are shown in figure 3-2. These profiles demonstrate that the tidal and residual components of the exchange flow do not need to have the same direction as the total exchange flow, and that these individual components may only cover subsets of the total salinity range.

To calculate the contributions of tidal and residual processes to the estuarine exchange flow (Q_E), the salinity-coordinate profiles of the tidal and residual components of the exchange flow are divided into inflow and outflow layers based on the direction of the *total* exchange flow, such that:

$$Q_{\text{in}} = Q_{\text{in, Tidal}} + Q_{\text{in, Residual}}, \tag{3.18}$$

and,

$$Q_{\text{out}} = Q_{\text{out, Tidal}} + Q_{\text{out, Residual}}. \tag{3.19}$$

So, Q_E is equal to the sum of the tidal (Q_{TE}) and residual (Q_{RE}) components of the total exchange flow:

$$Q_E = Q_{TE} + Q_{RE}, \tag{3.20}$$

where Q_{TE} and Q_{RE} are the average magnitudes of inflow and outflow; e.g.:

$$Q_{RE} \equiv \frac{Q_{\text{in, Residual}} + Q_{\text{out, Residual}}}{2}. \tag{3.21}$$

This is consistent with the method of determining Q_E (Eq. 3.14). The decomposition of Q_E into tidal and residual components in equation 3.20 shows that the residual component of the exchange flow (Q_{RE}) may encompass a significantly smaller volume transport than Q_E because it does not include the tidally-varying contributions of the exchange flow. In the Passaic River (Fig. 3-2), for example, the average Q_{RE} is 20 m^3/s, whereas the average Q_E is 50 m^3/s.

The contributions of tidal and residual processes to the TEF estuarine salt flux (QS_E) are also determined from the division of the tidal and residual salinity-coordinate exchange flow profiles into inflow and outflow layers based on the direction of the *total* exchange flow. By recognizing that TEF layer-specific salinities are flux-weighted averages, the definition of QS_E in equation 3.15 can be expanded to the following form:

$$QS_E = QS_{\text{in}} - QS_{\text{out}} - Q_{\text{in}}\overline{S} + Q_{\text{out}}\overline{S}, \tag{3.22}$$

in which $\overline{S}$ is the average salinity of the TEF inflow and outflow (Eq. 3.11) and salt fluxes are determined by integrating over the salinities associated with inflow or outflow, e.g.:

$$QS_{\text{in}} \equiv \int_{\text{in}} s\left(-\frac{dQ(s)}{ds}\right)ds. \tag{3.23}$$

Because the salt flux of each layer is a function of the salinity-coordinate profile of the exchange flow, equations 3.18 and 3.19 can be rewritten as divisions of layer-specific salt fluxes such that:

$$QS_{\text{in}} = QS_{\text{in, Tidal}} + QS_{\text{in, Residual}}, \tag{3.24}$$

and,

$$QS_{\text{out}} = QS_{\text{out, Tidal}} + QS_{\text{out, Residual}}. \tag{3.25}$$

Applying equations 3.24 and 3.25 to the expanded definition of QS_E yields the following form of the estuarine salt flux:

$$\begin{aligned} QS_E &= QS_{\text{in, Tidal}} - QS_{\text{out, Tidal}} - Q_{\text{in, Tidal}}\overline{S} + Q_{\text{out, Tidal}}\overline{S} \\ &\quad + QS_{\text{in, Residual}} - QS_{\text{out, Residual}} - Q_{\text{in, Residual}}\overline{S} + Q_{\text{out, Residual}}\overline{S}. \end{aligned} \quad (3.26)$$

This can be rewritten as the sum of tidal (QS_{TE}) and residual (QS_{RE}) salt fluxes:

$$QS_E = QS_{TE} + QS_{RE}, \quad (3.27)$$

where, defining TEF layer-specific salinities as flux-weighted averages following MacCready (2011),

$$QS_{RE} \equiv Q_{\text{in, Residual}}\left(S_{\text{in, Residual}} - \overline{S}\right) - Q_{\text{out, Residual}}\left(S_{\text{out, Residual}} - \overline{S}\right), \quad (3.28)$$

and QS_{TE} is similarly defined using tidal components of the total exchange flow. This permits the calculation of TEF tidal and residual salt fluxes which differ from Eulerian quantities only in the TEF approximation of the Eulerian $\langle \overline{s} \rangle$ (cf. Eq. 3.11). The discretized form of this method is available on the Woods Hole Open Access Server (Appendix A; Corlett et al., 2019).

Returning now to Eulerian quantities, we can obtain an Eulerian counterpart to Q_{RE} which is the volumetric circulation associated with what we will call the residual circulation (Q_{RC}). In the classical view of estuaries (Pritchard, 1954), in which the residual circulation is hypothesized to be driven by the along-estuary density gradient, this would be referred to as the "estuarine circulation". But to avoid false attribution of forcing mechanisms, we will simply call it the residual circulation. This is defined by the cross-sectional integral of the outgoing or incoming Eulerian tidally-averaged velocity less the river flow. This is not the exchange flow, because the tidally-averaged incoming and outgoing flows may or may not differ in salinity. For example, the average Q_{RC} in the Passaic River is 27 m^3/s (Fig. 3-2), whereas the average Q_{RE} is 20 m^3/s.

We also recall the fundamental Eulerian quantity ν (Eq. 3.5) that represents the ratio of the tidal component of Eulerian salt flux (2^{nd} term in Eq. 3.3) to the total Eulerian salt flux (Eq. 3.7). An equivalent expression for ν can be obtained in the TEF framework from

equation 3.27, using the TEF tidal salt flux (QS_{TE}) to obtain the tidal fraction of total salt flux, or ν_E:

$$\nu_E = \frac{QS_{TE}}{QS_E}. \tag{3.29}$$

Application to mooring-based observations

Calculating the subtidal salt balance requires tidally resolved, cross-sectional estimates of salinity and horizontal velocity. The shipboard hydrography in 2016 revealed that the lateral structures of salinity and velocity are relatively uniform throughout the Newark Bay estuarine network, these fields were assumed to be laterally homogeneous in the calculation of the subtidal salt balance at each mooring. Vertical profiles of horizontal velocities at each mooring contained two gaps: one at the bed due to the elevation and blanking-distance of the bottom-mounted ADCP, and another at the surface due to the truncation of near-surface velocities for quality control. To minimize estimation errors, velocities near the bed were extrapolated by assuming a cubic near-bed velocity profile with a no-slip bottom boundary. Velocity measurements near the surface were extrapolated by assuming a quadratic surface velocity profile with a free-slip surface boundary. Salinities at each mooring were measured at two points: roughly 0.5 m above the bed and 1 m below the water surface. The tidally-varying vertical salinity structure at each mooring was estimated from normalized shipboard salinity profiles measured within 500 m of the mooring in 2016. This tidally-varying structure was fit to the near-bed and near-surface salinity measurements to provide a best-estimate of the full vertical salinity profile. Shipboard hydrography during the 2016 deployment did not approach the locations of moorings HR and AK. The salinity profile at these moorings was estimated from the vertical structure of the nearest mooring with similar stratification characteristics, though the choice of salinity structure does not change salt flux estimates by more than 10%. The shape of the salinity profile at mooring HR was assumed to be similar to that measured near mooring NBs, and the shape of the salinity profile at mooring AK was assumed to be similar to that measured near mooring KK. The resulting full salinity and velocity profiles at each mooring were then used to calculate salt fluxes in both Eulerian and isohaline coordinates.

Approximations were required to account for spatial salinity and velocity variability that was not measured at each mooring. The conservation of volume and salt within the estuarine network occurs on long timescales—days with respect to volume, and weeks with respect to

salt, based on estimates of the response timescales of these quantities by Caplow et al. (2003). Consequently, approximations for salinity and velocity variability were determined such that all mooring-based estimates of the subtidal salt budget conserve salt and volume over the course of the mooring deployment. Approximations for tidal velocity heterogeneity were determined first at each mooring. The tidal approximations for spatial velocity heterogeneity are less than or equal to 2% of the barotropic tidal velocity at all locations other than mooring PR. At mooring PR, the approximation for tidal velocity heterogeneity suggests that flood tide velocities are underestimated by 6% and ebb tide velocities are overestimated by 6%; this is likely due to large tidal variations in the lateral structure of the along-channel velocity. The velocity field, including the approximations for tidal spatial heterogeneity, was then used to determine approximations for both tidal and residual spatial salinity heterogeneity. These approximations amount to less than 5% of the mean salinity at all cross-sections other than Newark Bay. In Newark Bay, approximations for tidally-averaged spatial salinity heterogeneity suggest that the depth averaged salinity is underestimated by 8%, likely due to persistent lateral variability on the wide shoal; approximations for tidal salinity heterogeneity amount to less than 1% of the mean salinity. The approximations for lateral salinity and velocity variability are small throughout the estuarine network, which either suggests that salinity and velocity fields are almost laterally homogeneous, or that the lateral variability at each location is cancelled by cross-sectional averaging. The small adjustments required to conserve volume and salt indicate that the moorings can be used to accurately depict the tidally-averaged salt and volume fluxes within the Newark Bay estuarine network.

Salt and volume fluxes were calculated from salinity and velocity fields over discrete tidal cycles, using the Eulerian approach described by Lerczak et al. (2006) and the TEF approach described by Wang et al. (2017). Tidal cycles were determined from local depth-averaged velocities, extending from slack water at the start of flood tide to slack water at the end of ebb tide. Cross-sectional areas were calculated from the observed water depth and regional bathymetric surveys (Halonen, 2011). Eulerian salt fluxes were estimated in depth-normalized coordinates (Lerczak et al., 2006; Chen et al., 2012). TEF salt fluxes were calculated in isohaline coordinates following the methods of MacCready (2011) and Wang et al. (2017), using a resolution of 0.1 psu. The TEF values are stable despite this salinity resolution, as inflow and outflow layers were defined by the extrema of the isohaline-integrated transport (cf. Wang et al., 2017) rather than the direction of the exchange flow

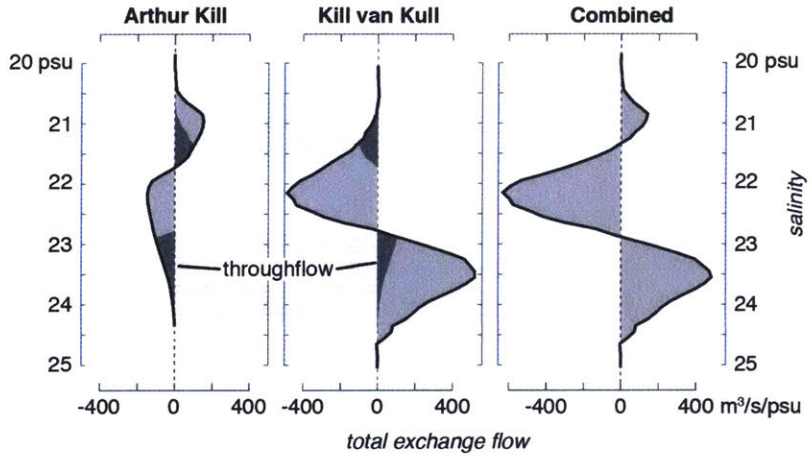

Figure 3-3: Average TEF profiles at the mouth of the Newark Bay estuarine network from June 3–7, 2008. Positive volume fluxes are directed toward Newark Bay; this is eastward in Arthur Kill and westward in Kill van Kull. The combined total exchange flow, representing the exchange flow at the mouth of the estuarine network, is shown at right and does not include the contributions of throughflows (shown with darker shading)

(cf. MacCready, 2011). However, coarser salinity resolutions do not resolve tidal salinity variability in well-mixed regions of the estuarine network, producing differences between TEF and Eulerian salt fluxes.

The TEF approach requires adaptations to account for throughflows, or volume and salt fluxes that enter an estuary in one location and exit in another, in estimates of the exchange flow. In Eulerian coordinates, a throughflow is a barotropic flux of unmodified water (Chant et al., 2006; Lee et al., 2019). We define a throughflow similarly in the TEF approach, requiring that the volume flux of a throughflow enters and exits an estuary at the same salinity. Throughflows were removed from estimates of the exchange flow simply by considering all entrances to an estuary as part of the same cross-section. This is a generalization of MacCready (2011)'s treatment of a subtidal recirculation eddy with constant salinity, as a throughflow can be thought of as an eddy that rotates through the plane defined by the estuary mouth. As an example, the exchange flow at the mouth of the Newark Bay estuarine network, as the sum of the exchange flows in Kill van Kull and Arthur Kill, is shown in figure 3-3. In Kill van Kull, high salinity water is transported into Newark Bay and low salinity water is transported out of Newark Bay. In Arthur Kill, on the other hand, high salinity water is transported out of Newark Bay and low salinity water is transported into Newark Bay. Because of the reversed circulation of Arthur Kill relative to Newark Bay, a

portion of the high salinity inflow in Kill van Kull exits the estuary through Arthur Kill as throughflow. The portion of low salinity inflow in Arthur Kill that exits the estuary through Kill van Kull is similarly categorized as throughflow. Consequently, both throughflows do not affect the exchange flow or the TEF salt balance.

The TEF approach, as described by Wang et al. (2017) and others, also requires modifications to account for multiple layers of the total exchange flow. The persistent presence of low salinity anomalies at the seaward end of an estuary can generate a three-layered exchange flow (Long, 1977). This is shown in figure 3-3 for the mouth of the Newark Bay estuarine network. The Rahway River is the primary source of fresh water for Arthur Kill; consequently, Arthur Kill transports water into Newark Bay that is fresher than the salinity of water that is exported through Kill van Kull. The local extrema of the isohaline-integrated transport (using a window of 0.5 psu) were used to objectively divide the TEF profile into inflow and outflow layers. Lorenz et al. (2019) applied a similar methodology to identify multiple inflow and outflow layers in the Baltic Sea. However, the method used in this chapter differs from that of Lorenz et al. (2019), in that Lorenz et al. determined the boundaries between inflow and outflow layers by specifying a minimum extrema value rather than the size of the window over which the extrema is observed. Both methodologies require the specification of values that reflect the characteristics of the estuary in question, and are expected to yield similar results although the two methods have not been quantitatively compared. The relatively small extrema window used in this chapter was required to accurately capture the multiple exchange flow layers that are observed in the Newark Bay reach (cf. §3.4.2); this reach is characterized by relatively weak salinity gradients. Fluxes were integrated between extrema to produce bulk flux estimates that are independent of the salinity bin resolution of each layer, following Wang et al. (2017). Bulk salt and volume fluxes in the same direction were summed together to represent the characteristics of effective inflow and outflow of the total exchange flow. The salinity of the effective outflow "layer" was determined by dividing the total outflow salt flux by the total outflow volume flux, following the methods of MacCready (2011); the same method was also used to determine the inflow salinity.

3.4 Results and analysis

During the 2008 mooring deployment, the mean combined freshwater discharge from the Passaic and Hackensack rivers was close to the historically-average discharge rate (25 m^3/s; USGS gages 01389890 and 01378500). Although the mean combined discharge was lower during the 2016 deployment (19 m^3/s), both deployments captured similar ranges of discharge. The combined freshwater discharge from the Passaic and Hackensack rivers ranged from 7 to 64 m^3/s during the 2008 deployment (Fig. 3-4, top panel), and from 4 to 53 m^3/s during the 2016 deployment (Fig. 3-5, top panel). Both deployments also contained large tidal ranges; spring tides aligned with lunar perigee to create larger-than-average perigean spring tides. From neap tides to spring tides, the tidal water level amplitude ranged from 0.5 m to 1.0 m, and the depth-averaged tidal velocity amplitude ranged from 0.5 to 0.9 m/s. The similar range of tidal variability and freshwater discharge during both deployments enables the spatial comparison of temporal responses of the salt balance and exchange flow to environmental variability to shed light on the overall characteristics of the estuary.

3.4.1 Overall conditions

Salinity measurements at each mooring during the 2008 (Fig. 3-4) and 2016 (Fig. 3-5) deployments show fluctuations associated with freshwater discharge, the fortnightly spring-neap cycle, and the semidiurnal tide. The influence of fluctuations in freshwater discharge is most evident in near-surface salinity variations. The surface salinity in the Passaic River (Fig. 3-4, panel PR), for example, decreases by 8 psu during periods of high discharge. Fluctuations in freshwater discharge also influence the near-bed salinity; however, this response weakens toward the mouth of the estuarine network (panels AK and KK). At the mouth of the estuarine network, the near-bed salinity is jointly influenced by fluctuations in freshwater discharge and the fortnightly spring-neap cycle; both high discharge and spring tides decrease the near-bed salinity at mooring KK by roughly 3 psu. The fortnightly spring-neap cycle in the Passaic and Hackensack rivers, on the other hand, primarily modifies the range of tidal salinity variability. The tidal salinity ranges at moorings PR and HR roughly double during spring tides. All moorings exhibit rapid tidal salinity fluctuations (Fig. 3-4 and 3-5), which suggests that there are significant horizontal salinity variations at the scale of the tidal excursion.

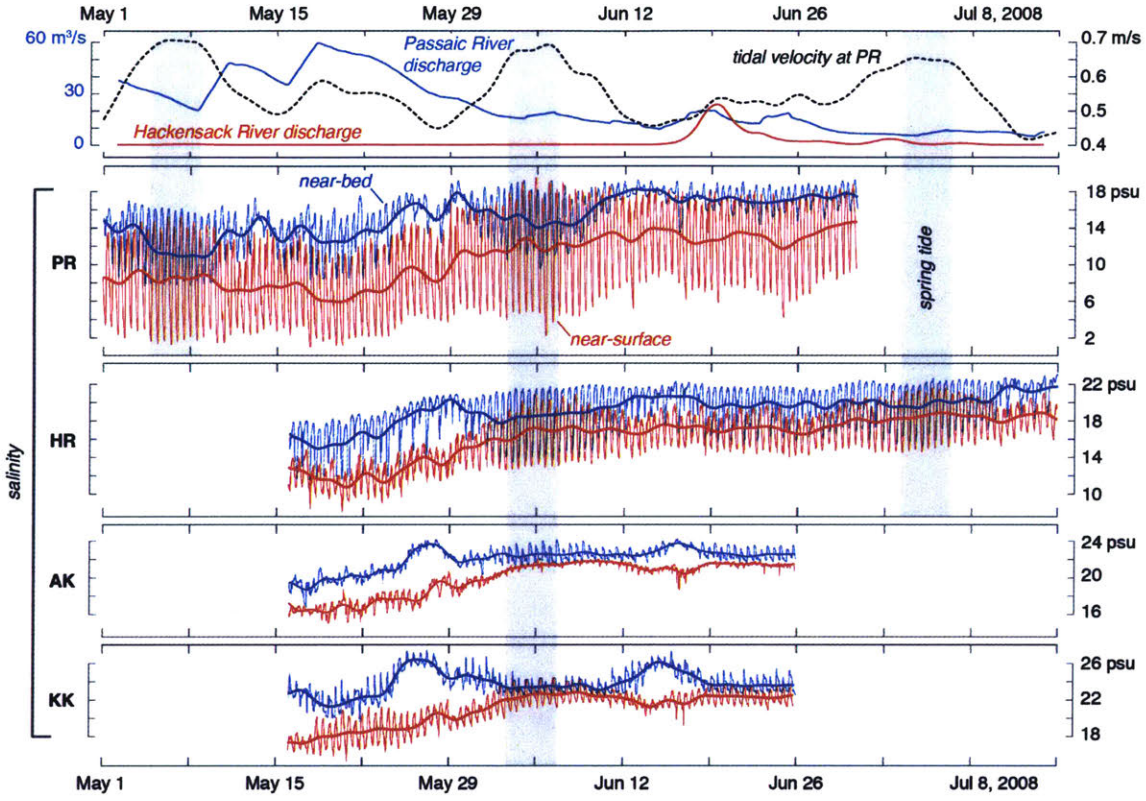

Figure 3-4: Environmental conditions and salinity measured during the 2008 mooring deployment. Perigean spring tides are shaded in grey. Near-bed and near-surface salinities measured every ten minutes are shown with thin lines, and the tidally-averaged salinities (using a 55-hour low-pass filter) are shown with thick lines. All salinity measurements are shown with the same vertical scale. Missing data at the end of a record is due to biofouling; missing data at the start of a record is due to a late deployment relative to mooring PR.

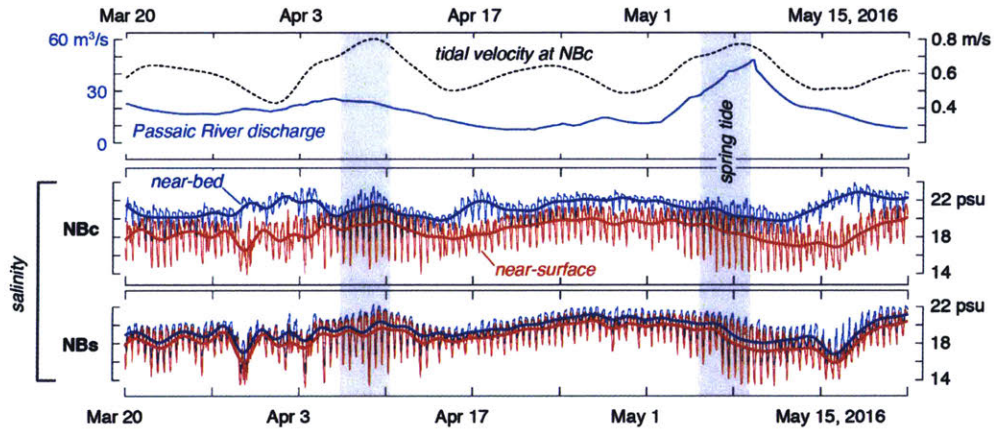

Figure 3-5: Environmental conditions and salinity measured in Newark Bay during the 2016 mooring deployment. Perigean spring tides are shaded in grey. Thin lines are used to show salinities measured every ten minutes, and thick lines are used to show subtidal salinity variability (using a 55-hour low-pass filter). All salinity measurements are shown with the same vertical scale.

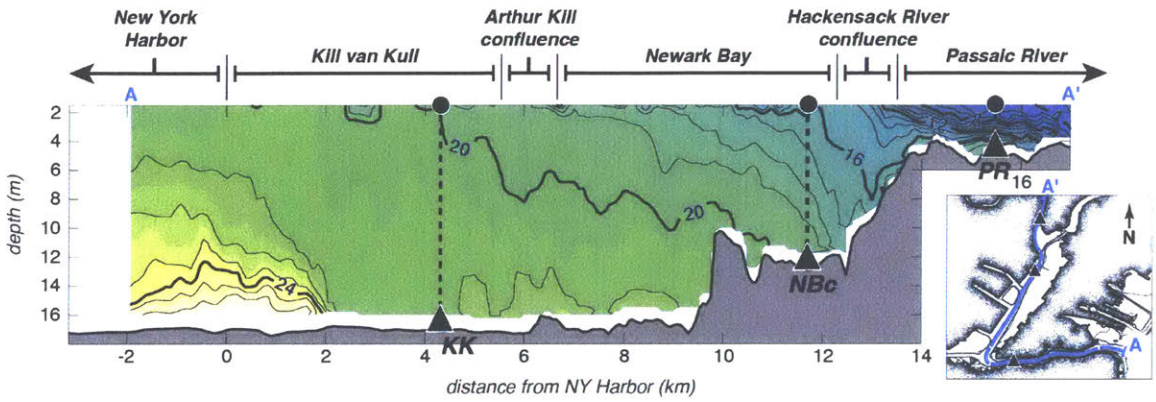

Figure 3-6: Hydrographic section captured during a spring tide in 2016, showing the along-channel salinity structure of the Newark Bay estuarine network at the end of ebb tide. Salinity is indicated with both color shading and 1 psu contour lines.

An along-channel hydrographic section captured during a spring tide in 2016 (Fig. 3-6) confirms the spatial heterogeneity of salinity within the estuarine network. Saline water in New York Harbor is separated from Kill van Kull by a bottom salinity front at 2 km. Low-salinity water in the Passaic River, often referred to in this chapter as "fresh" water, is similarly separated from saline water in the Hackensack River by a surface salinity front at 13 km. Corlett and Geyer (2018) found that the along-channel salinity gradient in Newark Bay is also concentrated in salinity fronts; both a surface front and a bottom front form at 10.5 km. Each of these four fronts forms during ebb tide and propagates landward during flood tide (Corlett & Geyer, 2018). The tidal fronts within the estuarine network may be expected to influence tidal contributions to the estuarine salt flux. This was indeed found to be the case, as the ensuing results and analysis will demonstrate.

3.4.2 Comparison of Eulerian and TEF subtidal salt balances

The mean characteristics of each cross-section within the estuarine network are shown in Table 3.1. On average, the estuarine exchange flow (Q_E) increases toward the mouth of the estuarine network. This is reflected in a general increase in the estuarine salt flux (QS_E and QS_{Eul}) toward the mouth of the estuary. In the Hackensack, however, QS_E, QS_{Eul}, and the TEF salinity difference (ΔS_E) are nearly negligible; this is expected because the Hackensack lacks a significant net freshwater outflow. At all other sites, temporal variations of both QS_E and QS_{Eul} on average reflect the variability of river outflow.

QS_E is similar to QS_{Eul} at all sites within the Newark Bay estuarine network (Table

Table 3.1: Mean record-length characteristics of each cross-section within the Newark Bay estuarine network. Standard errors are roughly ten percent of each value. *Values of ν for the Hackensack use the magnitude of tidal and residual salt fluxes to indicate the relative size of the tidal salt flux. †Values of ν for Newark Bay are median values to more accurately reflect observed conditions.

	Q_E m^3/s	ΔS_E psu	QS_E psu-m^3/s	QS_{Eul} psu-m^3/s	QS_{RE} psu-m^3/s	QS_{RC} psu-m^3/s	ν_E	ν_{Eul}
PR	50	5.7	300	300	90	90	0.7	0.7
HR	110	0.3	25	20	120	110	0.5*	0.5*
NBc/NBs	270	1.2	340	400	240	230	0.2†	0.4†
KK/AK	480	1.8	760	750	430	380	0.4	0.5

3.1); although the values of QS_E and QS_{Eul} are different in Newark Bay, they are within estimates of the standard error. QS_{RE} is also similar to QS_{RC} at all sites within the estuarine network. Throughout much of the estuary, residual salt fluxes are similar in magnitude to tidal salt fluxes ($\nu_{Eul} \sim 0.5$). This is consistent with the substantial tidal and subtidal salinity variability observed at each mooring in figures 3-4 and 3-5. The subtidal salinity variability in figures 3-4 and 3-5 suggests that the characteristics of the system substantially change with variations in environmental conditions.

Temporal variations in the TEF and Eulerian characteristics of each reach are shown in a sequence of figures 3-7, 3-9, 3-11, and 3-12. The top panel of each figure depicts the fresh water discharge and tidal volume flux over the course of the mooring deployment; the tidal volume flux is the tidally-averaged magnitude of the volume fluxes associated with depth-averaged tidal velocities. The second panel depicts the estuarine exchange flow (Q_E; Eq. 3.14), the residual circulation (Q_{RC}), and the residual component of the exchange flow (Q_{RE}; Eq. 3.16) to directly examine the contribution of the residual circulation to the exchange flow. The difference between Q_E and Q_{RE} indicates the contribution of tidal processes to the estuarine exchange flow. The third panel shows the difference between the TEF inflow and outflow salinities (ΔS_E; Eq. 3.13), as well as the Eulerian tidally-averaged stratification (ΔS_V) and depth-averaged tidal salinity range (ΔS_T) for reference. The estuarine salt flux (QS_E), which is the product of Q_E and ΔS_E (Eq. 3.15), is depicted in the fourth panel. The Eulerian estuarine salt flux (QS_{Eul}; Eq. 3.7) is shown in the fourth panel to compare the TEF and Eulerian approaches to the subtidal salt balance. TEF and Eulerian versions of the residual salt flux (QS_{RE} and QS_{RC}) are also depicted to illuminate the relative contributions

of residual processes to the estuarine salt flux. The fifth panel shows estimates of the tidal fraction of the estuarine salt flux (ν_E and ν_{Eul}). The normalized unsteadiness of the salt balance is also shown, which is normalized by the record-mean estuarine salt flux following Banas et al. (2004):

$$\psi_{Eul} = \frac{\frac{d}{dt}\langle \int_V s \, dV \rangle}{\langle\langle QS_{Eul} \rangle\rangle}, \tag{3.30}$$

and

$$\psi_E = \frac{\frac{d}{dt}\langle \int_V s \, dV \rangle}{\langle\langle QS_E \rangle\rangle}. \tag{3.31}$$

Single brackets are used to signify tidally-averaged quantities, and double brackets signify record-average quantities. These non-dimensional values provide context to the contributions of tidal and residual processes to the estuarine salt flux, as well as the overall subtidal salt balance. The unsteadiness of the salt balance is shown on its own in the sixth panel; this term is independent of the framework used to calculate the subtidal salt balance (cf. Eq. 3.1 and 3.3).

Salt balance in the Passaic River

The estuarine exchange flow in the Passaic River (Q_E; Fig. 3-7, second panel) remains nearly constant through the observation period despite significant fluctuations in the spring-neap cycle and freshwater discharge. The residual circulation (Q_{RC}), however, changes substantially in response to the spring-neap cycle. Q_{RC} is nearly three times larger during neap tides as it is during spring tides. Q_{RC} is similar to the residual component of the exchange flow (Q_{RE}) throughout much of the deployment, indicating that much of the residual circulation contributes to the exchange flow. However, Q_{RE} is often much smaller than Q_E, indicating that much of the exchange flow is driven by tidal processes. The tidal fraction of the exchange flow fluctuates substantially in response to the spring-neap cycle. Roughly half of Q_E is driven by tidal processes during neap tides, and nearly all of Q_E is driven by tidal processes during spring tides.

The difference between TEF inflow and outflow salinities (ΔS_E,third panel) remains nearly constant throughout the deployment, and is similar in magnitude to the tidally-averaged stratification (ΔS_V). The tidal salinity range (ΔS_T), however, is much larger than ΔS_V and ΔS_E, and increases substantially during spring tides. Note that ΔS_T results mainly from the horizontal advection of the salinity gradient. Its large value is consistent

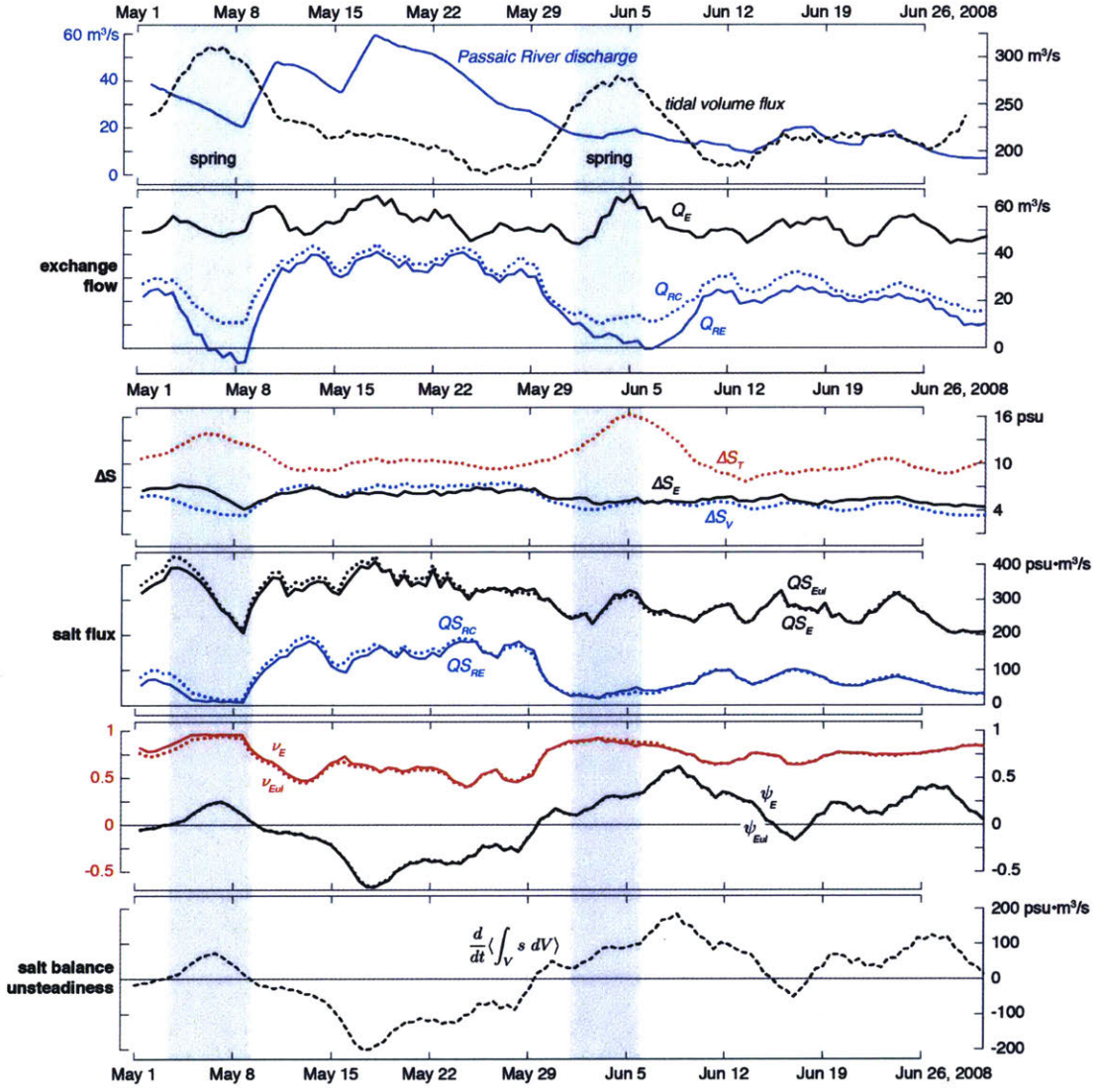

Figure 3-7: Environmental conditions and salt balance terms in the Passaic River during the 2008 deployment. Eulerian values—the residual circulation (Q_{RC}), stratification (ΔS_V), tidal salinity range (ΔS_T), and salt flux components—are shown with dotted lines. The salinity difference between inflow and outflow in isohaline coordinates is indicated by ΔS_E.

with the presence of a salinity front in the vicinity of the mooring, as discussed in Chapter 2.

TEF and Eulerian salt fluxes are nearly identical (fourth panel), as was already verified for the record-length averages in Table 3.1. The estuarine salt flux (QS_E and QS_{Eul}) is always substantially larger than the residual salt flux (QS_{RE} and QS_{RC}). The large tidal component of the estuarine salt flux is reflected in the large value of ν (bottom panel), especially during spring tides, when both ν_E and ν_{Eul} are both nearly one. The large value of ν is not surprising in light of the large value of Q_E relative to Q_{RE} (second panel). What is surprising is that ΔS_E is so similar to ΔS_V, even when virtually all of the salt flux is accomplished by tidal variability. This result indicates, in effect, that the tidal variations of salinity responsible for the net salt flux have the same magnitude as the tidally-averaged vertical salinity difference. This suggests that the tidal distortion of the vertical salinity gradient may be a key process leading to the tidal oscillatory salt flux. Such tidal distortions can be caused by the vertical heaving of a pycnocline, described by Geyer and Nepf (1996) and Wang et al. (2015) in the Hudson River, as well as by tidal asymmetries in shear and/or stratification (e.g., J. H. Simpson et al., 1990).

Although the estuarine salt flux is nearly constant, the tendency of the salt content within the Passaic fluctuates in response to the freshwater discharge rate (ψ, fifth panel). ψ_E and ψ_{Eul} are nearly identical, and reveal that the Passaic River loses salt during high discharge and gains salt during low discharge. Because QS_E and QS_{Eul} only change slightly throughout the deployment, these fluctuations are due to changes in the seaward riverine transport (Eq. 3.3; term 1). During much of the deployment, however, ψ less than 0.5. While not steady-state, the relative variability is smaller than other parts of the system, as will be seen in the ensuing discussion.

Salt balance in the Hackensack River

The primary source of fresh water for the Hackensack River is the Passaic River; fresh water from the Passaic is transported landward into the Hackensack from the Passaic-Hackensack confluence. This seaward source of fresh water often generates three distinct layers of the exchange flow within the Hackensack (Fig. 3-8, left panel), in which the landward flux of both low and high salinity water is compensated by the seaward flux of mid-salinity water. Because the inflow contains both high and low salinity water, the salinity difference

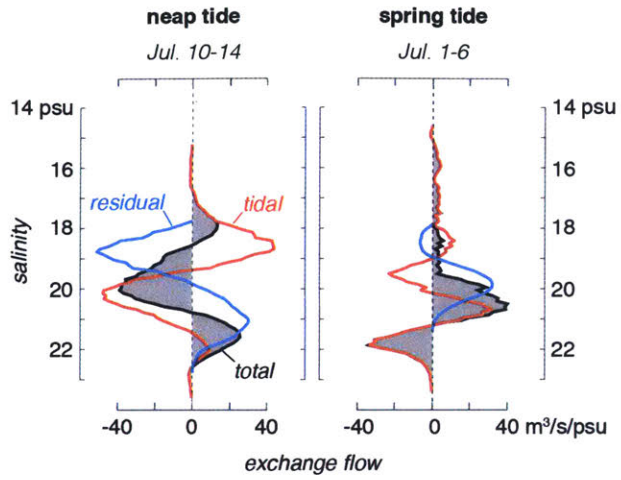

Figure 3-8: Exchange flow in the Hackensack River during the neap tide in mid-July 2008 and the spring tide in early July 2008. The total exchange flow is shown in black and with grey shading, the residual exchange flow is shown in blue, and the tidal oscillatory exchange flow is shown in red.

between TEF inflow and outflow (ΔS_E) can be positive, negligible, or even negative, despite a substantial exchange flow. In the Hackensack, the exchange flow (Q_E) is quantified as the average of the outflowing layer and the sum of the two inflowing layers (cf. §3.3.2):

$$Q_E = 0.5 \times \left(\frac{Q_{\text{in, saline}} + Q_{\text{in, fresh}}}{2} - Q_{\text{out}} \right). \tag{3.32}$$

ΔS_E in the Hackensack is similarly calculated from the average of the outflow salinity and the flux-weighted average inflow salinity:

$$\Delta S_E = 0.5 \times \left(\frac{QS_{\text{in, saline}} + QS_{\text{in, fresh}}}{Q_{\text{in, saline}} + Q_{\text{in, fresh}}} - S_{\text{out}} \right). \tag{3.33}$$

The exchange flow in the Hackensack (Q_E; Fig. 3-9, second panel) remains nearly constant throughout the deployment, similar to the Passaic, however it is roughly twice as large. The residual circulation (Q_{RC}) fluctuates in response to the spring-neap cycle, similar to the Passaic. However, much of Q_{RC} does not contribute to the exchange flow; Q_{RE} is often much smaller than Q_{RC}. This means that while there is a robust residual circulation in the Hackensack, it is only weakly correlated with salinity variations, so it generates little exchange flow. Moreover, Q_{RE} is much smaller than Q_E, accounting for only 20% of the exchange flow on average. During neap tides, roughly two-thirds of the exchange flow is due

to tidal processes; as shown in the left panel of figure 3-8, these processes drive the landward transport of fresh water from the Passaic as well as much of the seaward transport of mixed water. During spring tides, on the other hand, nearly all of the exchange flow is associated with tidal processes. The right panel of figure 3-8 reveals that the residual exchange flow does not contribute to the bulk measure of the total exchange flow during these periods because it is entirely confined to salinities associated with the exchange flow inflow.

ΔS_E in the Hackensack River is small and fluctuates in response to the spring-neap cycle; ΔS_E is positive during neap tides and negative during spring tides. Recall that ΔS_E in this three-layer regime does not have the simple meaning that it has in the two-layer regime, and its small and variable value reflects the lack of a persistent along-estuary salinity gradient due to the absence of a significant landward source of fresh water. The small ΔS_E during neap tides reflects the landward transport of both high and low salinity water (shown in the left panel of figure 3-8). The negative ΔS_E during spring tides is caused by the reversal of the exchange flow (Fig. 3-8, right panel); tidal processes transport high salinity water seaward and low salinity water landward during these periods.

Eulerian and TEF salt fluxes are nearly identical, and reveal that the small estuarine salt flux (QS_E and QS_{Eul}) is generated by a balance between the positive residual salt flux (QS_{RE} and QS_{RC}) and a negative tidal salt flux (Fig. 3-9, fourth panel). Although the tidal salt flux is negative, it is nearly the same magnitude as the residual salt flux (ν, fifth panel). The TEF profiles in figure 3-8 reveal that much of the negative tidal salt flux is generated by the landward transport of fresh water (left panel), though tidal processes also transport salt water seaward during spring tides (right panel). Both of these aspects of the tidal exchange flow induce a negative tidal salt flux.

Both TEF and Eulerian approaches show that the Hackensack gains salt during spring tides, despite a negative estuarine salt flux due to the reversal of the exchange flow (ψ; Fig. 3-9, fifth panel). During neap tides, the Hackensack loses salt despite a weak positive estuarine salt flux. This indicates that much of the subtidal salt balance is driven by barotropic processes that oscillate in response to the spring-neap cycle. The spring-neap dependence of the Hackensack salt tendency stands in contrast with the Passaic salt tendency, which fluctuates in response to changes in freshwater discharge. This, together with differences in the roles of tidal and residual processes, emphasizes the stark difference in estuarine regime between the Hackensack and Passaic Rivers.

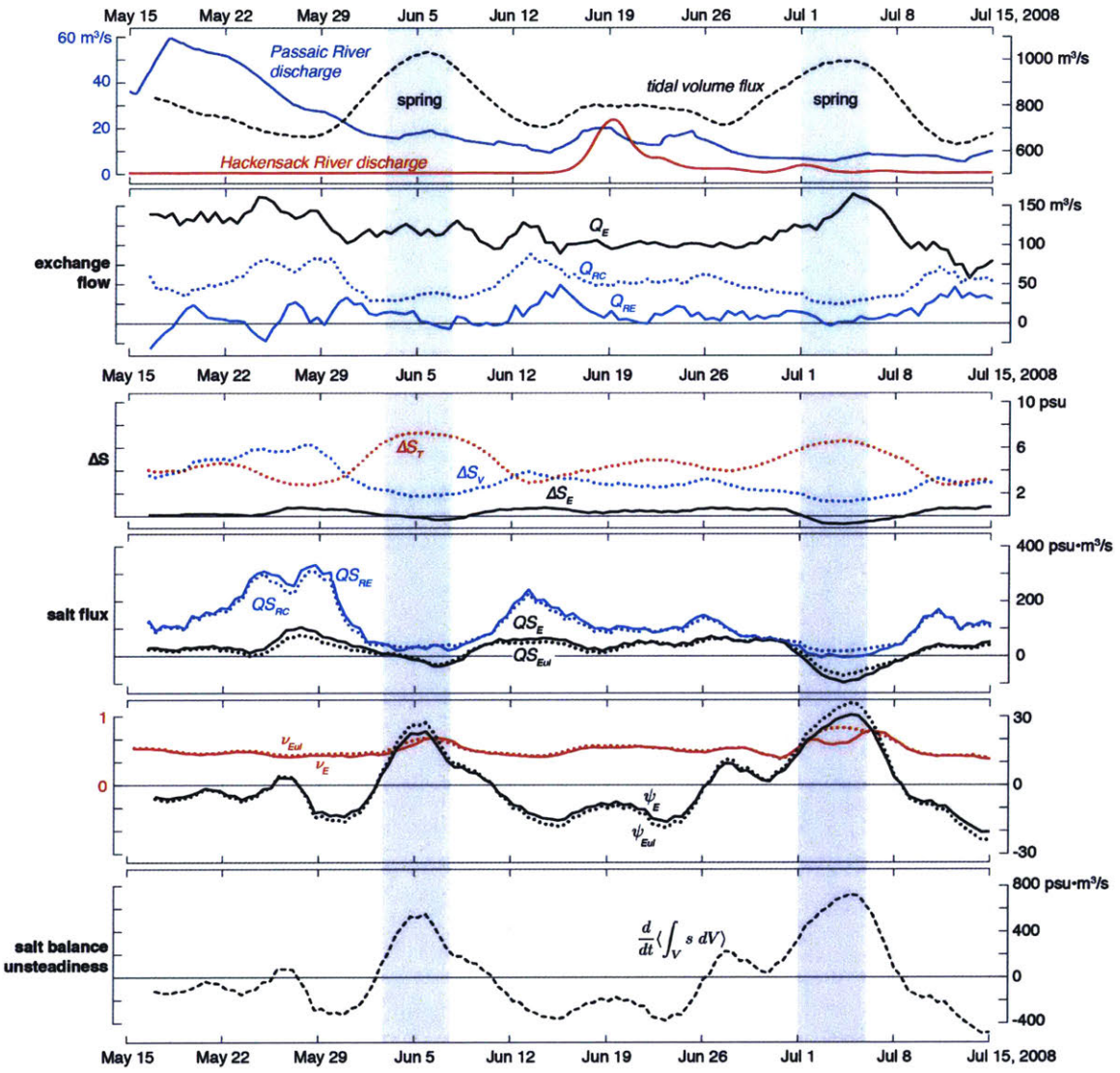

Figure 3-9: Environmental conditions and salt balance terms in the Hackensack River during the 2008 deployment. Eulerian values—the residual circulation (Q_{RC}), stratification (ΔS_V), tidal salinity range (ΔS_T), and salt flux components—are shown with dotted lines. The salinity difference between inflow and outflow in isohaline coordinates is indicated by ΔS_E. *values of ν are shown based on the magnitudes of the tidal and residual salt fluxes to indicate the relative size of the tidal salt flux.

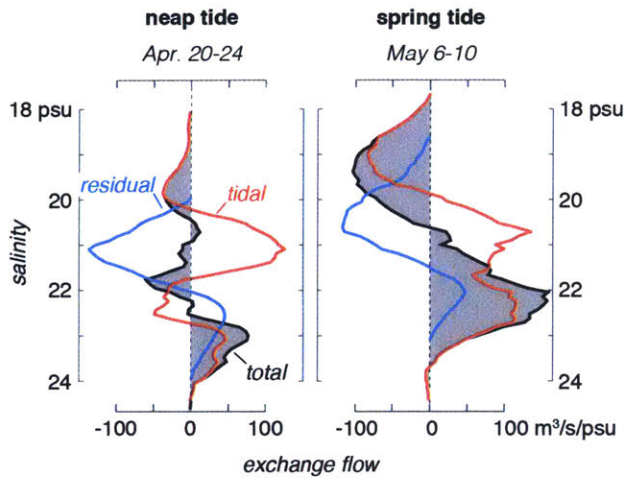

Figure 3-10: Exchange flow in Newark Bay during the neap tide in late April 2016 and the spring tide in early May 2016. The total exchange flow is shown in black and with grey shading, the residual exchange flow is shown in blue, and the tidal oscillatory exchange flow is shown in red.

Salt balance in Newark Bay

Nearly all fresh water enters Newark Bay from its head at the Passaic-Hackensack confluence, so Newark Bay has more persistent upstream freshwater forcing than the Hackensack River. However, the cross-sectional area of Newark Bay is much larger than the Passaic and low salinity water from the Hudson and Rahway rivers sometimes compete with the Passaic outflow, leading to much more time-variability in the salt balance than the Passaic, even including reversals of the estuarine salt flux. Like the Hackensack, the exchange flow is not always two-layered in salinity space (Fig. 3-10)—a consequence of the variability of the freshwater sources in the landward and seaward directions. Because the exchange flow is multi-layered, volumetric exchange flows in Newark Bay may not be commensurate with the corresponding salt fluxes.

First considering the exchange flow, Q_E in Newark Bay substantially changes in response to the spring-neap cycle (Fig. 3-11, second panel). During spring tides, the exchange flow is 50% larger than it is during neap tides. This is due to the spring-neap dependence of the tidal component of the exchange flow. Tidal processes account for 80% of the exchange flow during spring tides, and roughly 60% of the exchange flow during neap tides. The residual component of the exchange flow (Q_{RE}) is weakly influenced by the spring-neap cycle as well, and increases slightly during neap tides. The residual circulation (Q_{RC}), on the other hand,

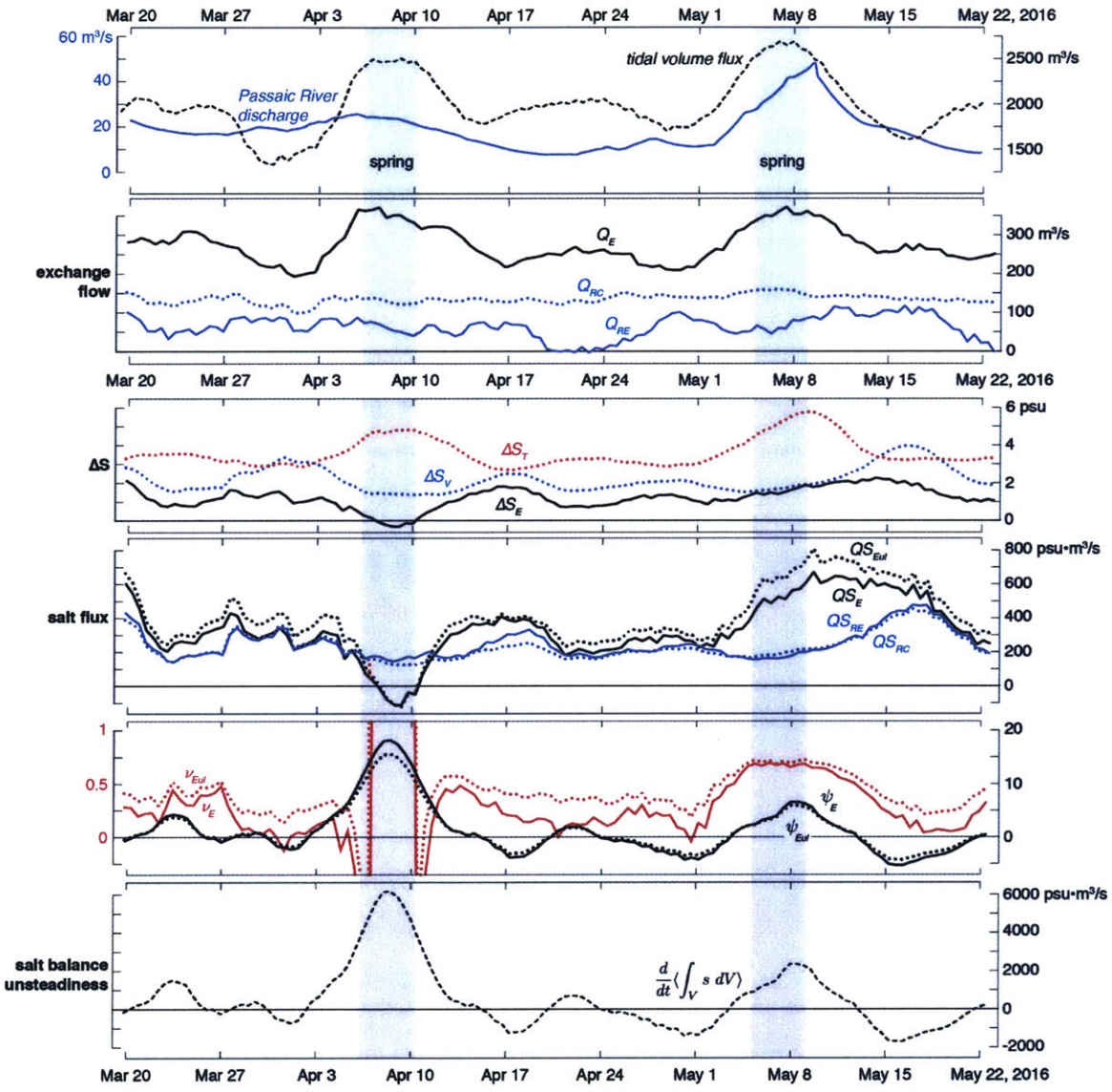

Figure 3-11: Environmental conditions and salt balance terms in Newark Bay during the 2016 deployment. Eulerian values—the residual circulation (Q_{RC}), stratification (ΔS_V), tidal salinity range (ΔS_T), and salt flux components—are shown with dotted lines. The salinity difference between inflow and outflow in isohaline coordinates is indicated by ΔS_E.

remains nearly constant throughout much of the deployment.

ΔS_E shows large variations, even going negative at one point in the record, indicative of the variability of the salt flux relative to the exchange flow. Note that changes in the sign of ΔS_E correspond to changes in sign of the salt flux. The negative tidal salt flux observed during the early April spring tide is due to the landward flux of fresh water, similar to the conditions observed in the Hackensack. The source of this fresh water is likely the Hudson River, as a large fresh water discharge event (on the order of 1000 m^3/s) was measured in the Hudson several days prior, and this discharge event coincided with a period of strong westerly winds over Raritan Bay, which have been shown to enhance the transport of water from New York Harbor into the Newark Bay estuarine network via Kill van Kull (Kaluarachchi et al., 2003; Chant et al., 2006).

The value of ΔS_E generally increases during neap tides and decreases during spring tides; this roughly corresponds to the presence of multiple layers of the exchange flow. During neap tides (Fig. 3-10, left panel), the exchange flow transports multiple water masses landward and multiple water masses seaward, largely due to tidal processes. During spring tides (Fig. 3-10, right panel), on the other hand, the exchange flow exhibits a more classical structure, transporting salt water landward and fresh water seaward. Consequently, the volumetric exchange flow is more commensurate with QS_E during spring tides, whereas the multi-layered exchange flow during neap tides masks relationships between volumetric exchange flows and salt fluxes (i.e. Q_{RE} and QS_{RE}).

ΔS_E also increases during high freshwater discharge, such as during the spring tide in early May 2008 (Fig. 3-11, third panel). This is a general finding for estuarine regimes, in which increases in discharge translate into larger amplitude salinity variations, irrespective of the relative roles of tidal and residual flows (MacCready & Geyer, 2010). This increased ΔS_E with discharge is reflected in the increase in the estuarine salt flux (QS_E and QS_{Eul}) shown in the fourth panel.

While the estuarine salt flux does not appear to be highly variable during the deployment, it is quite variable relative to the mean advective outflow of salt. Both ψ_E and ψ_{Eul} vary markedly through the deployment, with typical values of ± 5 that indicate marked departures from a steady salt flux regime. These departures appear to be larger than can be accounted for by gains and losses of salt in this reach of Newark Bay, suggesting that there may be errors in the flux estimates due to unresolved lateral variability.

Salt balance in Kill van Kull/Arthur Kill

The estuarine exchange flow (Q_E) at the Kill van Kull/Arthur Kill combined section is strongly influenced by the spring-neap cycle (Fig. 3-12, second panel), increasing by a factor of two from neap tide to spring tide. This is driven by an increase in the magnitude of the tidal exchange flow, similar in manner to Newark Bay. In contrast, both the residual circulation (Q_{RC}) and the residual exchange flow (Q_{RE}) in Kill van Kull/Arthur Kill increase during neap tides. On average, half of the residual circulation contributes to the exchange flow. This fraction is largest during neap tides due to enhanced stratification (ΔS_V; third panel), which increases the salinity-correlated portion of the residual circulation. Due to fluctuations in both the tidal and residual components of the exchange flow, Q_{RE} accounts for roughly half of the total exchange flow during neap tides, but only 10% of the exchange flow during spring tides. This indicates that tidal processes dominate the exchange flow during spring tides.

ΔS_E is also strongly influenced by the spring-neap cycle, but its behavior is opposite that of Q_E. ΔS_E substantially increases during neap tides rather than spring tides (third panel). The same spring-neap behavior also characterizes the local stratification (ΔS_V) and tidal salinity range (ΔS_T). The occurrence of weak salinity gradients during spring tides rather than neap tides suggests that the region is characterized by efficient tidal dispersion. This would effectively disperse salt during periods of large tidal velocities, creating a more homogeneous salinity field. The shipboard hydrography shown in figure 3-6, and discussed in Chapter 2, indicates that the region is indeed characterized by a local minimum of the along-channel salinity gradient during spring tides.

Because the spring-neap behavior of ΔS_E is opposite that of Q_E, the estuarine salt flux (QS_E and QS_{Eul}) largely tracks fluctuations in freshwater discharge (Fig. 3-12, fourth panel); TEF and Eulerian salt fluxes are nearly identical. This trend is similar to trends of QS_E in Newark Bay. However, more of the estuarine salt flux in Kill van Kull/Arthur Kill is due to tidal processes; the tidal salt flux accounts for roughly 20% of the estuarine salt flux during neap tides, but at least 60% of the salt flux during even moderate spring tides. Kill van Kull/Arthur Kill also shows much less temporal variability in salt flux than Newark Bay; ψ is roughly an order of magnitude smaller (fifth panel), and ranges from -0.5 to $+0.5$. Unlike the other reaches of the estuarine network, ψ_E and ψ_{Eul} reveal that Kill

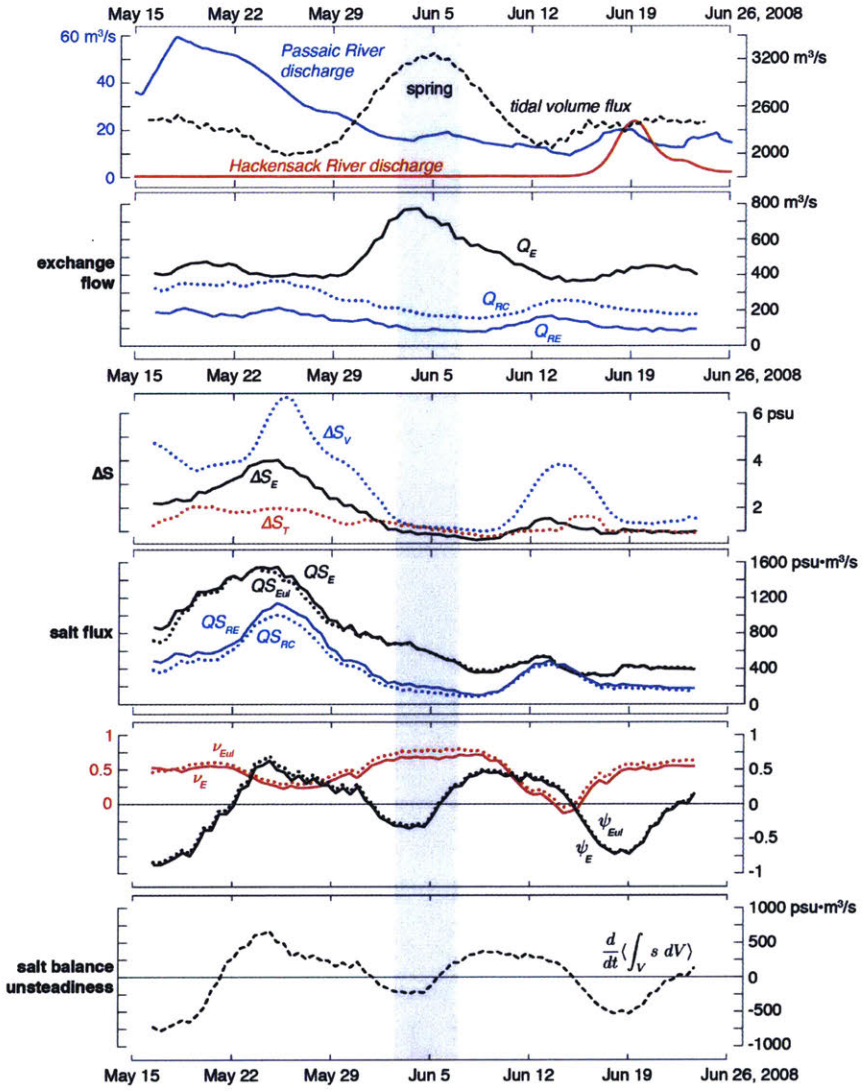

Figure 3-12: Environmental conditions and salt balance terms in Kill van Kull and Arthur Kill during the 2008 deployment. Eulerian values—the residual circulation (Q_{RC}), stratification (ΔS_V), tidal salinity range (ΔS_T), and salt flux components—are shown with dotted lines. The salinity difference between inflow and outflow in isohaline coordinates is indicated by ΔS_E.

van Kull/Arthur Kill loses salt during spring tides and gains salt during neap tides. This is similar to trends of the salt content in the adjacent Hudson River (Lerczak et al., 2006), and suggests that variations in stratification in the Hudson may drive this spring-neap variation in the salt content of the Newark Bay estuarine network.

Mechanisms of tidal salt dispersion

Throughout the Newark Bay estuarine network, both the Eulerian and TEF estuarine salt fluxes are largely driven by tidal processes during spring tides (Fig. 3-7–3-12). The tidal mechanisms that contribute to the estuarine salt flux, however, change from site to site. Following Fischer (1976), we estimate a site-specific tidal dispersion coefficient (K) from the mean tidal salt flux (Q_{TE}; equivalent to $QS_E - QS_{RE}$, cf. Eq. 3.27), tidally-averaged cross-sectional area (A), and along-channel salinity gradient ($\partial s/\partial x$):

$$K \equiv QS_{TE} \Big/ \left(A \frac{-\partial s}{\partial x} \right). \tag{3.34}$$

K varies by a factor of six between sites (Table 3.2), revealing that much of the tidal dispersion of salt occurs in Kill van Kull/Arthur Kill. To suggest mechanisms for this tidal dispersion, K is scaled with U_{tide}^2/ω as a measure of the efficiency of tidal mixing (α, Table 3.2; Fischer et al., 1979). These estimates are generally larger than would be expected for tidal shear dispersion alone; Fischer et al. (1979) found α to be between 0.005 and 0.02 for shear dispersion in a straight, unstratified channel (Fig. 3-13). This suggests that other, more efficient dispersion mechanisms are occurring. In Newark Bay, the average magnitude of α is consistent with tidal trapping. From Okubo (1973)'s investigation of tidal trapping when the ratio of the embayment to channel volume is between 0 and 1, α is estimated to be a maximum of 0.05 for tidal trapping when the timescale of embayment-channel exchange is equivalent to the tidal timescale (Fig. 3-13). Observations of the northern side channel in Newark Bay by Corlett and Geyer (2018) suggest that the two timescales at this side channel may be similar. From equation 3.34, Geyer and Signell (1992) estimated a maximum dispersion coefficient due to tidal trapping from the ratio between the embayment volume and the main channel volume (R), the tidal excursion (L_{tide}), and the average tidal velocity (U_{tide}):

$$K_{\text{trapping}} \leq \frac{1}{4} R L_{\text{tide}} U_{\text{tide}}. \tag{3.35}$$

Table 3.2: Mean tidal dispersion characteristics of each cross-section within the Newark Bay estuarine network. *Negative values in the Hackensack River are due to the tidal dispersion of fresh water from the Passaic River. †ν is modified in the Hackensack to reflect the relative magnitude of the tidal salt flux, and is calculated from the combined magnitudes of the tidal and residual salt fluxes. ‡The median value of ν is given in Newark Bay to more accurately reflect the observed conditions.

	ν_{Eul}	QS_{TE} psu-m^3/s	Area m^2	$\partial s/\partial x$ psu/km	K m^2/s	U_{tide} m/s	α
PR	0.7	210	750	-1.3	230	0.5	0.13
HR	0.5†	-90*	2000	-0.4	-150*	0.6	-0.08*
NBc/NBs	0.4‡	90	6000	-0.4	50	0.5	0.03
KK/AK	0.5	350	8400	-0.1	300	0.5	0.21

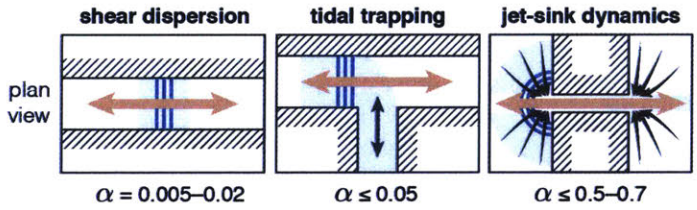

Figure 3-13: Channel geometries associated with tidal salt dispersion by tidal shear, tidal trapping, and jet-sink dynamics. Blue lines indicate the initial along-channel salinity gradient, and blue shading indicates the spread of salt after dispersion. Arrows indicate the tidal oscillatory flow field. Ranges of the tidal mixing efficiency (α) are provided for each mechanism: tidal shear dispersion (Fischer et al., 1979), tidal trapping (Okubo, 1973), and jet-sink dynamics (Chen et al., 2012).

Assuming that tidal trapping generates the frontal processes observed by Corlett and Geyer (2018) at the northern side channel in Newark Bay, $R \sim$ 0.09; using appropriate values for the tidal excursion ($L_{\mathrm{tide}} \sim$ 7 km) and tidal velocity, the maximum dispersion coefficient is estimated to be 80 m^2/s, which is consistent with the observed tidal dispersion coefficient. The higher tidal mixing efficiencies observed elsewhere in the estuarine network suggest that more complex processes contribute to tidal dispersion at the mouth and head of the estuary. In Kill van Kull/Arthur Kill, the relatively high tidal mixing efficiency suggests that tidal dispersion occurs due to jet-sink dynamics (Fig. 3-13; Stommel & Farmer, 1952), as Chen et al. (2012) observed that α can be as much as 0.5–0.7 due to inlet dynamics at the mouth of the Merrimack. At the mouth of the Newark Bay estuarine network, these jet-sink dynamics likely occur at the entrance of Kill van Kull in New York Harbor, as well as at the head of Kill van Kull in Newark Bay. Similar dynamics may also occur at the confluence

between the Passaic and Hackensack rivers; the hydrographic sections shown in Chapter 2 indicate that the region is characterized by intense tidal mixing during ebb tide, and the TEF analysis in the Hackensack River (§3.4.2) revealed that tidal processes are responsible for transporting fresh water from the Passaic landward.

3.5 Summary and implications

This chapter compares Eulerian and isohaline estimates of terms in the subtidal salt balance using data collected from a series of hydrographic moorings within a partially-mixed estuarine network. A new form of the isohaline salt balance is derived that explicitly includes contributions from tidal oscillatory and residual processes. The results at multiple cross-sections within the estuarine network reveal that Eulerian and isohaline estimates of tidal and residual salt fluxes are similar. However, the estuarine exchange flow, as the portion of the total exchange flow driven by non-riverine processes, does not have an equivalent in Eulerian coordinates. The Eulerian residual circulation *is* similar to isohaline estimates of the residual exchange flow, but only in some cases, such as in highly-stratified regions. In regions with multiple sources of fresh water, the use of isohaline coordinates also reveals multi-layered exchange flows, which are largely generated by tidal oscillatory processes.

The Eulerian and isohaline salt balances presented in this chapter can be similar because they are based upon the same salinity and velocity measurements. The ability of these fields to represent the physical salt balance of the estuary was assessed by calculating the necessary approximations for unresolved tidal and spatial variability to conserve salt and volume landward of each cross-section over the course of the mooring deployment (cf. §3.3.2). Although these approximations were small (<5–10%) at all sites, the salt balance in Newark Bay was found to be highly unsteady (Fig. 3-11). Estimates of the amount of salt stored landward of the Newark Bay cross-section over the course of a spring-neap cycle exceed the magnitude of observed salinity variability in the estuary. This suggests that the salt balance in Newark Bay is modified on timescales shorter than the mooring deployment, likely by unresolved lateral variability. At the other cross-sections, the salt balance unsteadiness is within reasonable bounds, indicating that Eulerian and isohaline salt balances are good approximations of the physical salt balance.

The comparison of Eulerian and isohaline estimates of terms in the subtidal salt balance

builds upon previous studies by Burchard et al. (2018), Chen et al. (2012), and others by directly comparing the two methods, and by including comparisons of the individual contributions of tidal and residual processes to Eulerian and isohaline salt and volume balances. These comparisons reveal that the approaches are consistently similar, despite different definitions of the salinity advected by subtidal barotropic processes (cf. Eq. 3.11). This chapter uses the average of the inflow and outflow salinities ($\overline{S}$) to provide an isohaline-native estimate of the Eulerian quantity $\langle \overline{s} \rangle$. $\overline{S}$ was defined from quantities commonly used in isohaline calculations (e.g., Wang et al., 2015; Burchard et al., 2018), as the isohaline TEF framework does not specify an isohaline-native version of $\langle \overline{s} \rangle$ (MacCready, 2011). We note that MacCready (2011) defined the TEF inflow and outflow salinities as flux-weighted averages, which suggests that $\overline{S}$ could be calculated as a flux-weighted average as well. However, we found that flux-weighted estimates of $\overline{S}$ differ more from the Eulerian $\langle \overline{s} \rangle$ than the simplified version of $\overline{S}$ used in this study. This was most evident during periods of high freshwater discharge, during which the flux-averaged $\overline{S}$ was less saline than both the average of the inflow and outflow salinities and the Eulerian $\langle \overline{s} \rangle$. The consistent similarity between $\langle \overline{s} \rangle$ and the simplified version of $\overline{S}$ indicates that the isohaline approximation of $\langle \overline{s} \rangle$ described in this chapter works well. Perhaps the flux-weighted salinity more accurately reflects the salinity of water transported seaward by river flow, but this line of research is beyond the scope of this thesis.

Bulk values are used to characterize the TEF inflow and outflow in both two-layer (e.g., MacCready, 2011) and multi-layer (e.g., Lorenz et al., 2019) exchange flows; however, we note that multi-layered exchange flows limit the dynamical insight that can be gained from bulk terms, especially when examining the individual effects of tidal and residual processes. The difference between bulk TEF inflow and outflow salinities (ΔS_E) in a multi-layered exchange flow, for example, reflects the sign of the estuarine salt flux but masks the characteristics of the individual circulation cells within the exchange flow. In addition, the presence of a multi-layered exchange flow masks relationships between volumetric exchange flows associated with tidal or residual processes and the corresponding salt fluxes. In both the Hackensack River and Newark Bay, for example, the bulk residual exchange flow can be negligible despite a substantial residual salt flux. In these cases, although the subtidal salt balance is effectively represented by bulk parameterizations, the examination of TEF profiles is often required to illuminate the detailed effects of tidal and residual processes on

the subtidal salt balance.

The Eulerian residual circulation was often observed to be similar in variability to the residual component of the exchange flow. However, the residual circulation and residual exchange flow were only similar in magnitude during periods of high stratification. This residual exchange flow was often less than half of the total exchange flow at many locations within the estuarine network. Consequently, the magnitude and variability of the estuarine exchange flow was often substantially different from the Eulerian residual circulation. This builds on previous studies, which have primarily focussed on the variability of the inflow portion of the total exchange flow (Wang et al., 2017; Burchard et al., 2018). The decomposition presented here indicates that, as the inflow and outflow of the total exchange flow are the generated by the sum of barotropic, baroclinic, and tidal oscillatory processes, the exchange flow can fluctuate independently of fluctuations in freshwater discharge in regions characterized by tidal processes. This is evident within the Newark Bay estuarine network. The residual circulation at the mouth of the estuarine network responds to fluctuations in freshwater discharge in a manner that is consistent with the classical scaling (Chant et al., 2018). We find that this residual circulation is often similar in variability to the residual exchange flow, but the residual exchange flow is roughly half as large. The tidal oscillatory exchange flow at the Kill van Kull/Arthur Kill cross-section is often three times larger than the residual exchange flow, and increases when the residual exchange flow decreases. Consequently, the total exchange flow is governed by fluctuations in the magnitude of the tidal oscillatory exchange flow.

This chapter also revealed the rich heterogeneity of estuarine characteristics within an estuarine network, as each of the sites examined in this chapter contains very different characteristics despite being within a tidal excursion of the other sites. In the Passaic and Hackensack rivers, both the estuarine salt flux and exchange flow are largely influenced by tidal processes during spring tides, and residual processes during neap tides (Fig. 3-7 and 3-9). A similar temporal oscillation between tidal- and residual-driven dynamics was observed by Jay and Smith (1990) in the Columbia, suggesting that these conditions occur in estuaries characterized by large horizontal salinity gradients and strong tidal variability. In Kill van Kull/Arthur Kill, the estuarine salt flux is driven by fluctuations in freshwater discharge (Fig. 3-12), which is similar to the variability in the estuarine salt flux that is observed in estuaries that are long relative to the tidal excursion, such as the Hudson River (Lerczak

et al., 2006). Unlike the Hudson, however, the exchange flow in Kill van Kull/Arthur Kill increases during spring tides instead of neap tides. This is more similar to shorter estuaries, such as the Merrimack River (Ralston et al., 2010), which are often influenced by tidal inlet processes (Chen et al., 2012). Newark Bay exhibits modes of variability for the estuarine exchange flow that are similar to Kill van Kull/Arthur Kill, but the tidal component of the salt flux is muted (Fig. 3-11). This range of estuarine dynamics over a relatively short along-channel distance suggests that estuarine networks may provide helpful case studies in which to observationally examine the characteristics of estuarine parameter space.

Chapter 4

Evaluating estuarine parameter space

A comparison of the Newark Bay estuarine network with other estuaries

4.1 Abstract

Estuaries are often described by the characteristics of a single location despite inherent spatial and temporal variability in the mechanisms that influence the exchange flow and subtidal salt balance. This variability in estuarine dynamics is often large in estuarine networks, which are characterized by multiple connecting channels, and may also contain multiple sources of fresh water or connections to the ocean. Recent hydrographic observations in Newark Bay, an estuarine network at the mouth of the Hudson River estuary, provide an interesting case in which to examine the capability of existing estuarine classification schemes in describing the characteristics of a complex estuarine network. This chapter investigates similarities of estuarine dynamics through the Hansen and Rattray (1966) and Geyer and MacCready (2014) parameter spaces, in light of the complex characteristics of the Newark Bay estuarine network. The estuarine network is represented by a wide scatter of regions in both classification schemes, ranging from time-dependent salt wedge estuary to fjord. The characteristics of regions that are influenced by both large freshwater and tidal forcings are well predicted in parameter space. Regions characterized by abrupt changes in bathymetry, however, are not, due to the large influence of local processes, such as salinity

front formation or jet-sink inlet dynamics. This study suggests that an additional parameter, describing the length-scale of local processes, is required to account for the observed variability in parameter space.

4.2 Introduction

Estuarine classification serves to group estuaries into categories, either qualitatively or quantitatively, in order to make inferences about processes in one estuary based on the characteristics of other estuaries in the same category. Stommel and Farmer (1952) were the first to quantitatively classify estuaries. They applied a one-dimensional parameter space based on the normalized stratification of an estuary, creating a range of estuarine classes between stratified, density-driven estuaries and well-mixed, tide-driven estuaries. Hansen and Rattray (1966) recognized that estuaries with weak stratification may also have a distinct residual circulation, prompting them to construct a two-dimensional estuarine parameter space that includes both stratification and circulation as parameters (Fig. 4-1). Based on an analytical model of the subtidal salt balance in a partially-mixed estuary (Hansen & Rattray, 1965), Hansen and Rattray (1966) estimated the steady-state salt balance based on the location of estuaries within their two-dimensional estuarine parameter space. One important aspect of estuarine dynamics revealed by this analysis is the relative strength of tidal dispersion processes compared to the residual, estuarine circulation in the context of the subtidal salt balance. They defined the parameter ν as the "diffusive fraction" of the salt flux, where "diffusive" represents what we now call the tidal oscillatory salt flux (Ralston et al., 2010). Their analysis indicated that the relative importance of tidal processes to the estuarine exchange flow is not simply a function of stratification. Their analysis does show a general tendency for the estuarine circulation to become more important with increasing stratification; some highly stratified estuaries (i.e., salt wedges), however, may be dominated by tides, and some weakly stratified fjords may be dominated by exchange flow.

Geyer and MacCready (2014) attempted a different classification approach that was based on key forcing variables—the freshwater discharge and magnitude of tidal mixing—to predict the characteristics of an estuary (Fig. 4-2). This prognostic approach stands in contrast to the diagnostic approach of Hansen-Rattray. In the Geyer-MacCready classification, the effect of river discharge on estuarine dynamics is parameterized by a freshwater Froude

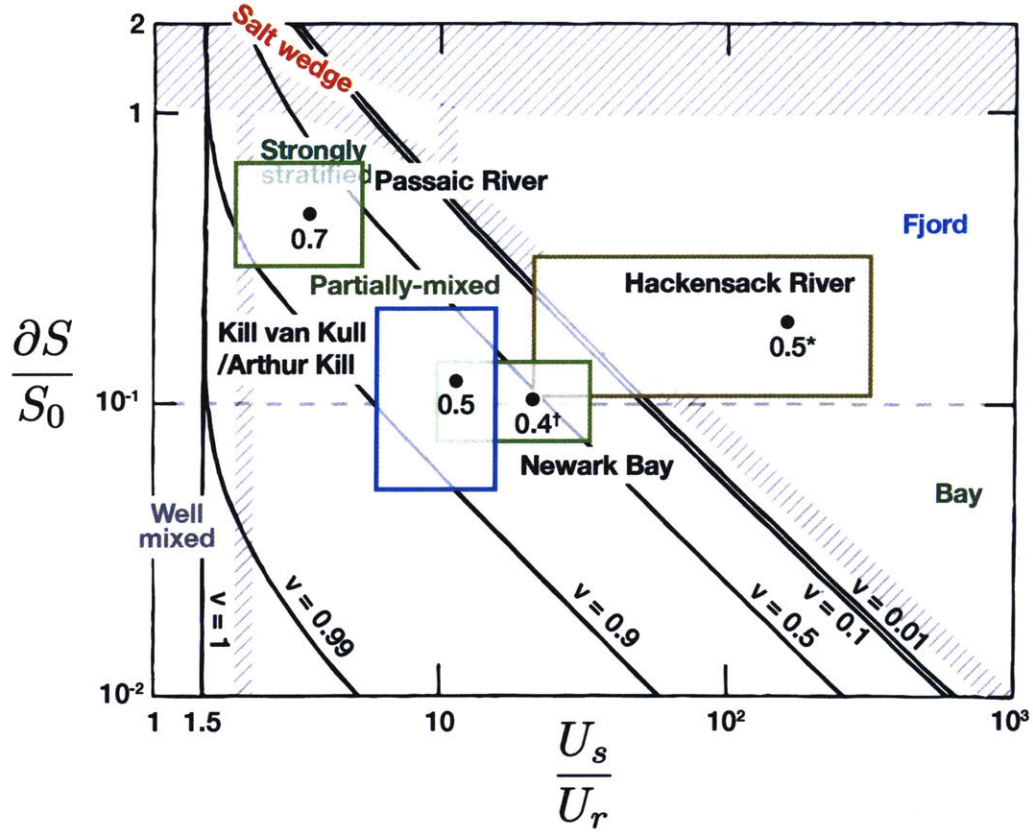

Figure 4-1: Hansen-Rattray stratification-circulation diagram, relating the tidal fraction of the estuarine salt flux (ν) to parameter space using results from the analytical model of a coastal plain estuary described by Hansen and Rattray (1965). Mean locations of reaches within the Newark Bay estuarine network are shown with black dots; the encompassing boxes represent two standard deviations of variability. Mean values of ν are given for each reach. $^{*}\nu$ in the Hackensack River is calculated as the magnitude of the tidal salt flux relative to the sum of the magnitudes of the tidal and residual salt fluxes, as the tidal and residual salt fluxes are nearly the same magnitude and consistently of opposite sign (Chapter 3). $^{\dagger}\nu$ for Newark Bay is the median value to more accurately reflect observed conditions (Chapter 3).

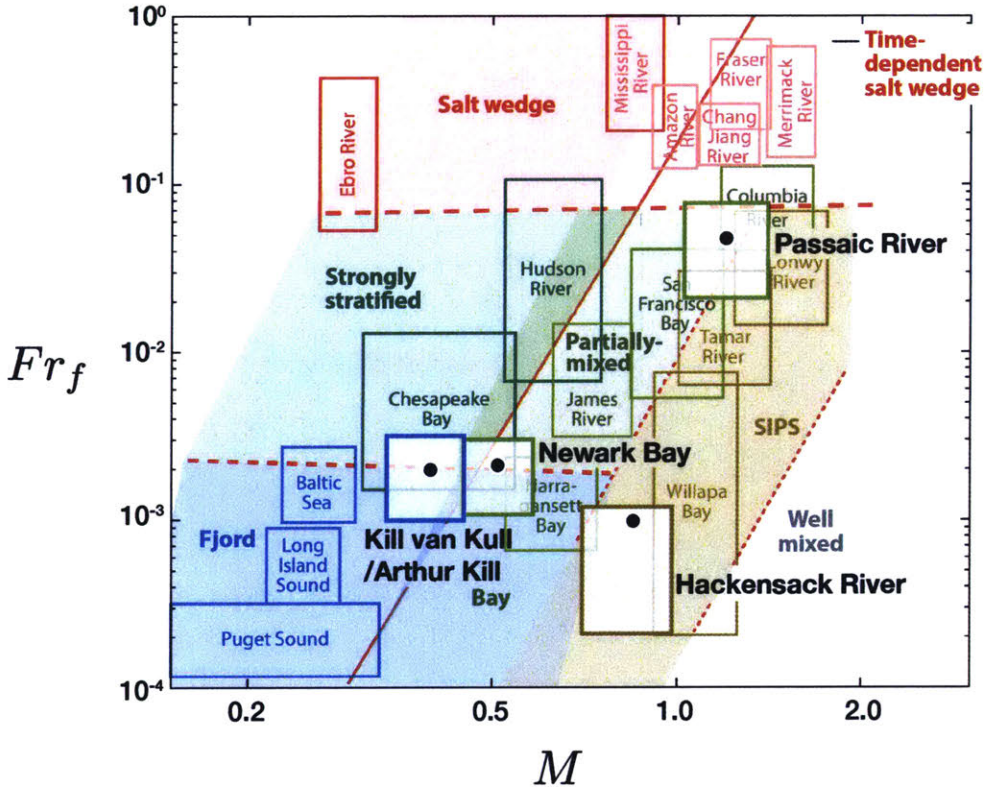

Figure 4-2: Geyer-MacCready predictive estuarine parameter space, relating the strength of the local freshwater discharge to tidal mixing. The mean locations of reaches within the Newark Bay estuarine network are shown with black dots; the surrounding rectangles represent two standard deviations of variability in both Fr_f and M over the course of hydrographic observations in 2008 and 2016.

number (Fr_f), which scales the tidally-averaged river discharge velocity by a densimetric velocity:

$$Fr_f = \frac{U_r}{\sqrt{g'H}}, \tag{4.1}$$

in which $g' = \beta g S_{\text{ocean}}$. Tidal mixing is parameterized by M, which provides a measure of the effectiveness of tide-induced bottom stress in destroying estuarine stratification:

$$M = \sqrt{\frac{C_D U_t^2}{\omega N_0 H^2}}, \tag{4.2}$$

in which ω is the tidal frequency, U_t is the amplitude of the depth-averaged tidal velocity, C_D is a drag coefficient, and $N_0 = \sqrt{\beta g S_{\text{ocean}} H^{-1}}$. As M increases, the water column of the estuary is expected to be increasingly mixed. One problem with this classification approach is that these parameters vary within an estuary over time due to variations in freshwater discharge (Fr_f), as well as changes in tidal velocity over the course of the spring-neap cycle (M). While this variability is a significant obstacle to applying the Geyer-MacCready approach to a particular estuary, the parameter space may still provide insights about how different estuaries behave in context with the strength of external forcing agents.

There is some indication that estuaries in similar locations in the Geyer-MacCready diagram share common characteristics. For example, the estuaries in the upper right quadrant are characterized by high river discharge and large tidal velocities; these include such estuaries as the Merrimack River (Chen et al., 2012) and Fraser River (Geyer & Farmer, 1989). They would be classified as salt wedges based on their stratification and strong horizontal salinity gradient, but they also exhibit strong tidal variability, consistent with the high ν categorization of salt wedges in the upper left corner of Hansen-Rattray diagram. Partially-mixed estuaries are in the middle of the Geyer-MacCready diagram, and are also in the middle of the Hansen-Rattray diagram. Interestingly, this is the part of the Hansen-Rattray diagram with strong variability in ν. The lower left quadrant of the Geyer-MacCready parameter space, which is characterized by low freshwater discharge and weak tidal velocities, includes large embayments such as Puget Sound and the Baltic Sea. This corresponds to the right side of the Hansen-Rattray diagram, which suggests small values of ν, i.e., dominance of the residual exchange flow. These estuaries tend to have long residence times, and so their exchange processes may extend over many spring-neap cycles and multiple discharge events. The lower right quadrant of the Geyer-MacCready diagram includes the strong tidal

regimes with weak river inflow. These are the high ν regimes in the lower left corner of the Hansen-Rattray parameter space.

Although temporal variability was discussed above as a challenge in the classification of estuaries, spatial variability within an estuary may present an even greater challenge. Many estuaries, such as Puget Sound (Banas et al., 2014), Narragansett Bay (Spaulding & Swanson, 2008), and Chesapeake Bay (Hayward et al., 1982), have multiple branches and/or tributaries, with considerable variation in depth and width, and sometimes have multiple connections to the ocean and/or multiple sources of fresh water. In this study, these estuaries are referred to as estuarine networks. Within estuarine networks, the mechanisms that drive the exchange flow or subtidal salt balance often substantially change from location to location. In Puget Sound, for example, the exchange flow is driven by tidal processes over the shallow sills, and by density-driven flow within the adjacent deep basins (Sutherland et al., 2011). Similar spatial variability is observed in Narragansett Bay; the salt flux within the deep Eastern Passage is primarily influenced by density-driven flow (Hess, 1976), whereas the salt flux within the adjacent shallow Sakonnet River passage is largely tidal (Pilson, 1985). Despite this spatial heterogeneity of the processes that drive the exchange flow and subtidal salt balance, estuarine networks are often compared with other estuaries in parameter space (Hansen & Rattray, 1966; Geyer & MacCready, 2014).

Recent hydrographic observations in the Newark Bay estuarine network present an opportunity to examine how to evaluate an estuarine network in context with estuarine classification parameterizations. Newark Bay is connected to the ocean through two tidal straits, and is fed by multiple internal and external sources of fresh water (Fig. 4-3; Blumberg et al., 1999). In addition, the estuarine network is segmented into a series of reaches, with significant variations in cross-sectional geometry, tidal conditions and hydrography, as noted in Chapters 2 and 3. Can the Geyer-MacCready parameter space provide insight about the overall characteristics of an estuarine network such as Newark Bay? Can estuarine parameterization capture the characteristics of individual reaches?

This chapter compares the characteristics of the overall Newark Bay estuarine network, as well as the individual reaches, to similar estuaries in order to shed light on the applicability of estuarine parameterizations. Section 4.3 contains a description of the dynamical characteristics of Newark Bay. Section 4.4 describes the methods used to determine the parameter space locations of individual reaches of the Newark Bay estuarine network. Section

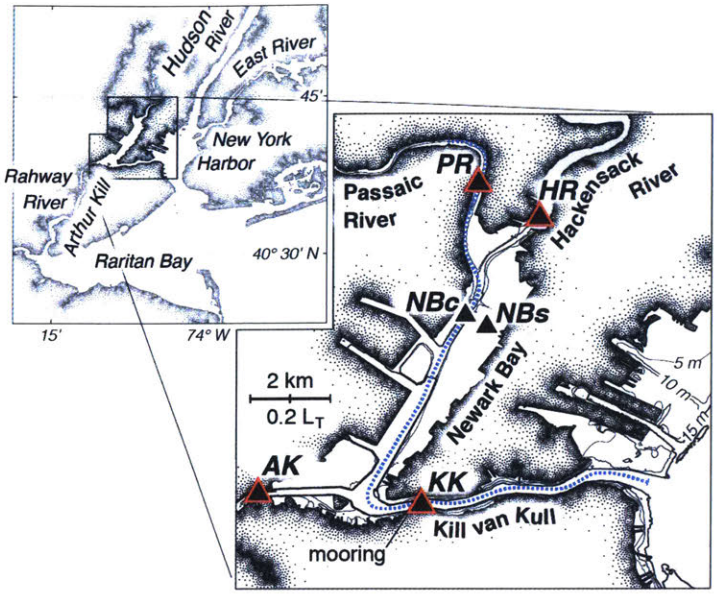

Figure 4-3: Map of Newark Bay and the surrounding environs, showing the locations of moorings used in this chapter. Moorings deployed in 2008 are shown with red trim, and moorings deployed in 2016 are shown with white trim. The blue dotted line indicates the main channel of the estuarine network.

4.5 investigates the parameter space regime of the estuarine network, both as an overall system and as individual locations within parameter space, comparing conditions between this estuarine network and others. Section 4.6 discusses the utility of estuarine parameter space in diagnosing conditions within estuaries, and suggests additional aspects of an estuary that should be included in future frameworks. The chapter concludes in Section 4.7 with the implications of this investigation for future comparative studies.

4.3 Site description

Each reach of the Newark Bay estuarine network—Kill van Kull/Arthur Kill, Newark Bay, Hackensack River, and Passaic River—is characterized by a distinct cross-sectional geometry (Fig. 4-3; cf. Chapter 1). Along-channel salinity sections analyzed in Chapter 2 indicate that each reach also contains different characteristics. As shown in figure 4-4, Kill van Kull is largely well-mixed, and is characterized by the landward propagation of a bottom salinity front during flood tide. Newark Bay is partially-mixed; Corlett and Geyer (2018) found that two fronts form at the entrance of the northern side channel during ebb tide and propagate landward during flood (Chapter 2). Mixing between the Hackensack and Passaic

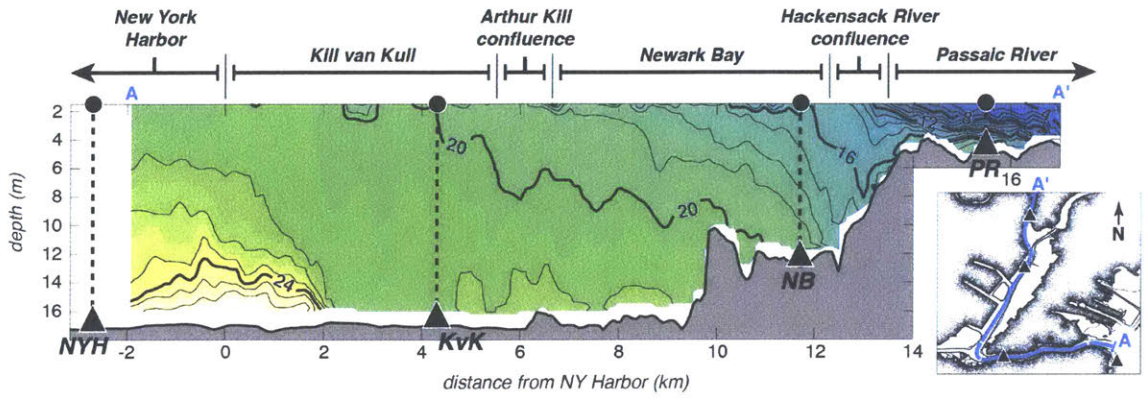

Figure 4-4: Hydrographic section captured during a spring tide in 2016, showing the along-channel salinity structure of the Newark Bay estuarine network at the end of ebb tide. Salinity is indicated with both color shading and 1 psu contour lines.

Table 4.1: Mean record-length characteristics of individual reaches within the Newark Bay estuarine network determined from mooring-based observations in 2008 and 2016. ν_Q is the tidal fraction of the estuarine exchange flow (the exchange flow not associated with river discharge; cf. Chapter 3). $^*\nu$ in the Hackensack River is calculated as the magnitude of the tidal salt flux relative to the sum of the magnitudes of the tidal and residual salt fluxes, as the tidal and residual salt fluxes are nearly the same magnitude and consistently of opposite sign (Chapter 3). †Values of ν for Newark Bay are median values to more accurately reflect observed conditions (Chapter 3).

	U_r	U_t	U_s	H	δS	ν	ν_Q
	m/s	m/s	m/s	m	psu		
Passaic River	0.035	0.52	0.10	5	5.3	0.7	0.6
Hackensack River	0.001	0.62	0.05	10	3.1	0.5^*	0.9
Newark Bay	0.003	0.49	0.05	13	2.2	$0.4^\dagger$	0.8
Kill van Kull/Arthur Kill	0.003	0.47	0.03	17	2.9	0.5	0.7

rivers during ebb tide generates a surface salinity front at the confluence, which propagates landward into the stratified Passaic during flood tide (Chapter 2).

The steady-state characteristics of each reach are shown in Table 4.1; these values are determined from moored hydrographic observations in 2008 and 2016 (Chapter 3). The riverine velocity (river discharge divided by cross-sectional area; U_r) increases toward the head of the estuarine network due to a steady decrease in cross-sectional area; the velocity is a minimum in the Hackensack due to the negligible local supply of fresh water. Depth-averaged tidal velocities (U_t) and tidally-averaged stratification (δS) also increase toward the head of the estuary. The tidally-averaged surface velocity (U_s), as a measure of the strength of the estuarine circulation, is largest in the Passaic River.

Tidal processes substantially contribute to both the subtidal salt balance and the exchange flow throughout the estuarine network. The tidal oscillatory salt flux is similar in magnitude to the residual salt flux throughout much of Newark Bay ($\nu \sim 0.5$). In addition, tidal processes account for more than half of the exchange flow; the tidal fraction of the exchange flow (ν_Q) is consistently larger than 0.6. The substantial influence of tidal processes on both the subtidal salt balance and the exchange flow was explained in Chapter 3 by the prevalence of tidal salinity fronts, which were described in Chapter 2. Each front forms at a channel junction during ebb tide and propagates landward during flood tide, contributing substantially to the tidal salinity signal (cf. Chapter 2). The presence of fronts results in a significant correlation between salinity and velocity at tidal timescales, often leading to an enhanced tidal salt flux and thus large ν. The details of these frontal transport mechanisms vary from site to site (see Chapter 3), but the values of ν are similar.

4.4 Methods

Both the Hansen-Rattray and Geyer-MacCready classification schemes were used to categorize the observed conditions in Newark Bay. The time-averaged conditions as well as the observed range through the period of the deployment were considered. To assess the dependence on location, independent estimates of the parameters were used for each of the reaches: the Passaic River, Hackensack River, Newark Bay, and Kill van Kull/Arthur Kill. The conditions in Newark Bay were nominally considered as the overall characterization of the system, although it was recognized a priori that the local Newark Bay properties would not necessarily represent the mean conditions over the domain.

The tidally-averaged stratification (δS) and depth-averaged salinity (S_0) for the Hansen-Rattray classification scheme were determined at each mooring for the period of the deployment. The tidally-averaged surface velocity (U_s) was extrapolated from moored velocity observations by assuming a quadratic surface velocity profile with a free-slip surface boundary. The tidally-averaged riverine velocity (U_r) was calculated by dividing the observed discharge in the Passaic River (USGS gage 01389890) and/or Hackensack River (USGS gage 01378500) by the relevant tidally-averaged cross-sectional area.

The values of U_r at each mooring over the course of the deployment were also used in the Geyer-MacCready classification scheme. The tidally-averaged depth of the channel was

used for H, and C_D was assumed equivalent to 3.3×10^{-3}. The choice of a canonical value for the drag coefficient was required as no information was available regarding bottom drag within the Newark Bay estuarine network; the chosen value is based on studies of bottom drag by Soulsby (1990), and is similar to values of C_D estimated in the Hudson River by Geyer et al. (2000). The amplitude of the depth-averaged tidal velocity (U_t) was calculated as the average amplitude of peak depth-averaged flood and ebb velocities. To include sites within the Newark Bay estuarine network in the Geyer-MacCready parameter space, the parameter S_{ocean} was assumed to be equivalent to the inflow salinity of the exchange flow, calculated using the isohaline TEF framework (MacCready, 2011, see Chapter 3).

The locations of the different reaches of the estuarine network in parameter space were determined by the mean values of each parameter and the observed range of parameter variability; two standard deviations of variability were represented by the 17^{th} and 83^{rd} percentiles of each parameter over the period of moored observations. Once the locations of the reaches in parameter space were determined, the characteristics of those sub-estuarine environments, most notably the mechanisms of salt flux in consideration of the parameter ν, were evaluated in context with the Hansen-Rattray predictions and in comparisons with other estuaries in the same part of parameter space. This analysis was used to provide insights into the estuarine mechanisms of the different reaches of Newark Bay as well as to provide an assessment of the utility of these classification schemes.

4.5 Results

4.5.1 Parameterization of the Newark Bay sub-domains

The mean parameterization of each reach is shown as a black dot in both the Hansen-Rattray and Geyer-MacCready parameterization schemes (Fig. 4-1 and 4-2). In both schemes, the Newark Bay reach is found in the "partially-mixed" estuary portion of parameter space, consistent with previous descriptions of the estuary (Suszkowski, 1978). Regarding the parameterizations of the other reaches, the local Newark Bay categorization clearly does not reflect the range of conditions observed throughout the rest of the estuarine network. The Passaic River has substantially greater freshwater forcing than the other segments, and its parameterization resides close to the "salt wedge" category in both parameterization schemes. Kill van Kull is close to Newark Bay in both classification approaches. Slightly weaker tidal

weaker tidal forcing moves it to the left of Newark Bay in the Geyer-MacCready scheme; however, a comparable shift to the left is also observed in the Hansen-Rattray scheme, indicating an increased role of tidal processes relative to the estuarine circulation. The Hackensack is on the far right in both the Hansen-Rattray and Geyer-MacCready schemes. The very low freshwater forcing and significant tidal forcing explains its position in the Geyer-MacCready scheme. The large exchange flow relative to the very low riverine forcing explains its far right position in the Hansen-Rattray scheme. Whether or not these relative positions in parameter space reveal useful information about the processes in these estuarine reaches is discussed in the next subsection.

4.5.2 Comparisons with neighboring estuaries in parameter space

Passaic River

The Passaic River, located in the upper-right quadrant of parameter space, has some features in common with other estuaries close to it in parameter space, including the Columbia River. While the Columbia is much bigger, with a river discharge that is more than two orders of magnitude greater than the discharge of the Passaic (Sherwood et al., 1990), it shares some similar characteristics with the Passaic. The subtidal salt balance in both estuaries is largely driven by tidal processes during spring tides ($\nu \simeq 1$). During neap tides, however, the salt balance in the Columbia is largely driven by the residual circulation (Hughes & Rattray, 1980; Jay & Smith, 1990), whereas the salt balance in the Passaic is still influenced by tidal processes ($\nu \simeq 0.5$; Chapter 3). The persistent influence of tidal processes in the Passaic River is likely due to the landward propagation of the salinity front during nearly every flood tide (Chapter 2). The recurring presence of a tidal front is similar to the characteristics of another neighbor in parameter space—the Fraser River—that is substantially influenced by tidal processes during both spring and neap tides (Geyer & Farmer, 1989). This category of time-dependent salt wedge has the interesting characteristic of being forced by both strong density gradients and tidal processes. In the Hansen-Rattray parameterization, that combination is indicated by the high value of stratification combined with a relatively high value of the ν parameter, indicating the significant contribution of tidal processes. The potential mechanisms responsible for this combination are explored in the Discussion section.

Hackensack

The location of the Hackensack in the lower-right quadrant of the Geyer-MacCready parameter space—"tide-dominated bay"—is based on the local freshwater discharge (Fig. 4-2). The Passaic discharge does influence the Hackensack via transport from the mouth, so an alternative would be to include the Passaic discharge in the classification, which would move the classification to the "partially-mixed estuary" category. However, neither designation represents the dynamics of the Hackensack, because the freshwater forcing at the mouth is a key defining characteristic that is not included in either the Hansen-Rattray or Geyer-MacCready classification. Baltimore Harbor is perhaps the most familiar example of an estuary in which the freshwater influence comes from the mouth (Stroup et al., 1961; Long, 1977). Long (1977) described the three-layer circulation that results from this regime, in which low-salinity and high salinity water enter in the upper and lower layers, and mixed water leaves in the middle layer. The persistent three-layer exchange flow that characterizes the Hackensack River (Chapter 3) is consistent with this category of estuary. This type of circulation is a likely occurrence within an estuarine network that has multiple branches with different strength freshwater sources. Carr Inlet (Edwards et al., 2007) and Hood Canal (Sutherland et al., 2011), within the estuarine network of Puget Sound, provide additional examples in which a three-layer circulation develops under conditions when the mouth has stronger freshwater forcing than the interior. Willapa Bay intermittently experiences similar landward fluxes of freshwater from the Columbia River plume (Hickey et al., 2002). In this case, the large discharge of the Columbia provides such a large freshwater anomaly to the Pacific Ocean that in effect, Willapa Bay becomes subsumed into the estuarine network of the Columbia. To conclude this assessment of the Hackensack, there are analogous regimes in the estuarine literature, but they do not map onto the existing, two-dimensional parameterization schemes.

Newark Bay

The stratification of Newark Bay is reasonably well predicted by the Geyer-MacCready parameter space. Tidal mixing in Newark Bay reduces the local stratification during peak flood and ebb tides (Chapter 2), consistent with the location of the reach along the line of that separates partially-mixed from strongly-stratified estuaries in the Geyer-MacCready

diagram. As to the dynamics of Newark Bay—which contains an exchange flow that is largely driven by tidal processes, and is characterized by large variability in ν due to multi-layered exchange flows during neap tides—the Geyer-MacCready diagram does not provide any useful insight. The problem is that other estuaries in this category, such as the James River and the Hudson, also have significant variability in ν. The value of ν in the James is roughly 0.1, according to Hansen and Rattray (1966). Its value in the Hudson is highly variable, based on analyses by Chen et al. (2012), ranging from 0.6 to -0.4 along a 50-km stretch of the estuary, and averaging approximately 0.2 (based on moderate discharge conditions). It is conceivable that the James also has similar variability, but it would require a detailed model analysis similar to that performed by Chen et al. (2012) to resolve it. More insight about the Hudson comes from a model study of frontogenesis by Geyer and Ralston (2015), which revealed the formation of multiple fronts along the stretch in which Chen et al. (2012) found the large variations in ν. The study by Wang et al. (2015) on the influence of topographically-induced hydraulic transitions on ν in the Hudson estuary also helps explain the large variability of ν. These studies suggest that ν may be expected to be highly variable in partially-mixed estuaries, due to topographic variability and the associated formation of fronts. So, the moderate value of ν in Newark Bay is consistent with the observed association of partially-mixed estuaries with frontal processes.

Kill van Kull/Arthur Kill

The Kill van Kull/Arthur Kill segment lies close to Newark Bay in both the Hansen-Rattray and the Geyer-MacCready parameter space, near the partially-mixed category. The Geyer-MacCready mixing parameter for Kill van Kull is weaker than Newark Bay, mainly because of its greater depth. This should be reflected in slightly greater stratification, which is consistent with the higher stratification indicated in the Hansen-Rattray diagram. However, the proximity of Newark Bay and Kill van Kull in parameter space belies the key difference in the dynamics of these two environments that was identified in Chapter 3: Kill van Kull has much more efficient tidal transport of salt than Newark Bay, especially during spring tides ($\nu \simeq 0.8$, $\nu_Q \simeq 0.9$; Chapter 3). This is similar to conditions both over shallow sills in fjords (Sutherland et al., 2011), and in "short" energetic estuaries such as the Merrimack River (Ralston et al., 2010). The mouths of both Kill van Kull and the Merrimack River are constricted inlets, and much of the tidal dispersion in both systems is attributed to

Stommel and Farmer (1952)-type jet-sink flow interactions at this constriction (Chen et al., 2012). The presence of a constricted inlet is not a feature represented by these two-parameter classification schemes, so these dynamics are not illuminated in either the Hansen-Rattray or Geyer-MacCready diagrams. What *is* revealed in the Hansen-Rattray classification of these spatially and temporally complex regimes is the tremendous variability of the stratification and circulation parameters as a function of time, which indicate the richness and variability of salt exchange mechanisms.

The discrepancies between observed and predicted characteristics of Kill van Kull/Arthur Kill, Newark Bay, and the Hackensack and Passaic rivers are due to the influence of local processes. The large influence of local processes is likely due to the prevalence of tidal salinity fronts within the estuarine network. In both Kill van Kull and Newark Bay, for example, most of the tidal salinity range is associated with the passage of a salinity front during flood tide (Chapter 2). The range of characteristics observed in other estuaries are similarly produced by local processes. The prevalence of tidal mixing over shallow sills in Puget Sound creates local regions of well-mixed conditions adjacent to deep stratified basins (Farmer & Freeland, 1983). Tidal processes also drive the characteristics of shallow reaches in Narragansett Bay, whereas the characteristics of deep reaches are driven by tidal-residual processes (Hess, 1976). Spatial changes in salt flux mechanisms are even observed within "classical" estuaries such as the Hudson River, as Wang et al. (2015) found that the magnitude and sign of the tidal salt flux substantially changes between sites of different cross-sectional geometry in the Hudson.

4.6 Discussion

These estuarine classification schemes attempt to describe the large-scale characteristics of an estuary, even though the mechanisms that influence the subtidal salt balance or the exchange flow at a particular location within an estuary are inherently local. Hansen and Rattray (1966) argued that spatial and temporal variability within an estuary are represented as a single diagonal line in their parameter space, stating that a temporal change in river flow produces the same effect as a spatial shift toward the head of the estuary. Bowden and Gilligan (1971), however, demonstrated that conditions within the Mersey estuary are represented by multiple lines in parameter space by examining multiple sites within the estu-

ary. The time- and space-varying conditions of Newark Bay similarly produce a tremendous scatter in the Hansen-Rattray diagram, as shown in figure 4-1. This variability indicates that the steady-state assumptions on which the underlying analytic solution of Hansen and Rattray (1965) are not valid, so the predictive ability of this framework, such as for estimating ν, is not expected to be of quantitative value.

In the Geyer and MacCready (2014) parameter space, the temporal and spatial variability of estuarine dynamics is addressed by assigning rectangles to encompass the range of variation of the forcing parameters. These ranges provide some indication of the non-stationarity of an estuary, which is often large in "long" estuaries such as Chesapeake Bay (Xu et al., 2012) or Willapa Bay (Banas et al., 2004). However, the application of the Geyer-MacCready scheme to Newark Bay reveals that, as in the case of the Hansen-Rattray application, characterizing an estuary as a single region of parameter space is insufficient when considering its temporal and spatial variability.

The results of this study suggest that an additional parameter is needed in these classification schemes to represent the spatial variability observed in the Newark Bay estuarine network. This parameter would represent the degree of spatial heterogeneity of an estuary. Estuaries with a high degree of heterogeneity would be expected to be influenced by local processes rather than estuary-scale processes. This characteristic is evident in the importance of tidal processes within the reaches of the Newark Bay estuarine network, and in the spatial shifts between tidal and subtidal processes in driving the exchange flow and salt flux within fjords such as Puget Sound (Sutherland et al., 2011), or other estuarine networks such as Narragansett Bay (Weisberg, 1976; Kincaid, 2006). Ralston et al. (2008) similarly noted the importance of local dynamics in modifying the length of the salt intrusion in San Francisco Bay.

The main motivation for the identification of heterogeneity as an important estuarine parameter arises from (1) the observation of tidal-timescale salinity fronts, described in Chapter 2, and (2) the important role of tidal-timescale salt fluxes, described in Chapter 3. Therefore, heterogeneity may be quantitatively described through the comparison of a cross-front salinity difference to the tidal salinity range. On average, this fraction is roughly 0.4 in Kill van Kull, 0.3 in Newark Bay, and 0.2 in the Passaic River (Fig. 4-5). The spatial decrease of the frontal salinity fraction toward the Passaic occurs throughout much of the moored record, and is strongest during spring tides. This persistent spatial trend is

consistent with the smaller discrepancies between observed and predicted characteristics at the head of the estuarine network.

As shown by Geyer and Ralston (2015) in the Hudson River, and Corlett and Geyer (2018) in the sub-estuaries of the Newark Bay estuarine network, tidal salinity fronts form in regions in which the cross-sectional geometry of an estuary abruptly changes. This suggests that a geometric length scale, such as the along-channel correlation-scale of the cross-sectional area of an estuary, could be used to predict the overall heterogeneity of an estuary. Estuaries that are much longer than the tidal excursion, such as those in the lower-left quadrant of the Geyer-MacCready parameter space, would be expected to have a higher likelihood of containing multiple abrupt changes in cross-sectional geometry. This suggests that the characteristics of these "long" estuaries may substantially change from site to site due to local processes that are not predicted by the two-dimensional parameter space.

The dominant length scale of local processes is expected to approach the length of the estuary in the "time-dependent salt wedge" estuaries in the upper-right quadrant of the Geyer-MacCready parameter space. In these "short" estuaries, strong river discharge concentrates the along-channel and vertical density gradients during ebb tide, creating a salt wedge that is transported landward by tidal velocities during flood tide; this leads to relatively high values of the ν parameter. As the length of the estuary approaches the tidal excursion, we expect that the dominant physics of an estuary are better resolved in parameter space. In the Passaic, for example, the average tidal excursion is 9 km, and the length of the estuary is estimated to be roughly 5 km for the average discharge during the hydrographic observations (cf. Chant et al., 2011). The characteristics of the Passaic River were also found to be well-represented by parameter space. In the Passaic, which was often nearly in steady-state (Chapter 3), fluctuations in parameter space account for nearly 80% of the variability in both the tidal fraction of the estuarine salt flux and the exchange flow; both ν and ν_Q increase with decreasing Fr_f and increasing M.

The presence of heterogeneous characteristics within both "long" estuaries, such as the Hudson River (Geyer & Ralston, 2015), and estuarine networks introduces the need for further clarification regarding the definition of an estuarine network. An estuarine network is defined in Chapter 1 to have multiple sources of fresh water and/or multiple connections to the ocean. We interpret this to include estuaries that contain side channels or embayments that may not have a local source of freshwater, as these reaches may be effective sources of

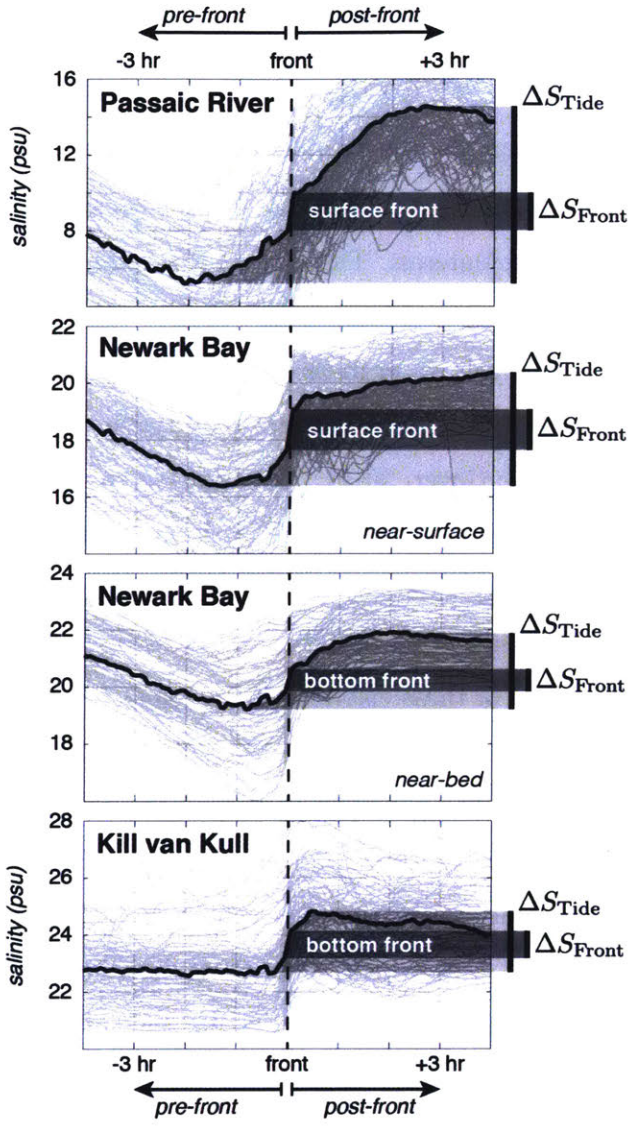

Figure 4-5: Comparisons between frontal salinity difference (ΔS_{Front}) and tidal salinity range (ΔS_{Tide}) at moorings within the Newark Bay estuarine network, adapted from figure 2-4. The comparison suggests that the frontal salinity fraction can be used as a metric to describe the relative influence of local processes rather than estuary-wide processes in estuarine dynamics.

low salinity water for the main channel due to tidal phase-shifts. The junctions between the multiple channels of an estuarine network are often characterized by barotropic and/or baroclinic tidal phase-shifts, and can both generate and modify tidal salinity fronts (cf. Chapter 2). Consequently, fronts may be common within estuarine networks, but they are not defining features of an estuarine network. Similarly, estuarine networks may contain reaches with drastically different characteristics, but this may also occur within "long" classical estuaries due to segmentation by abrupt changes in cross-sectional geometry.

Within "long" estuaries, the ability of parameter space to capture the characteristics of an estuary depends on the scale of interest. The Hudson River, for example, is largely influenced by a single source of fresh water and has a single channel that extends over multiple tidal excursions from the source of salt water to the primary source of fresh water (Abood, 1974). At the scale of the estuary, the Hudson is a stratified system that is largely influenced by residual processes (Ralston & Geyer, 2019). At scales less than a tidal excursion, however, the Hudson can be characterized by tidal mixing, front formation, and large values of ν (Chen et al., 2012). The Hansen-Rattray and Geyer-MacCready classification schemes do not capture this local-scale variability, but they do describe the large-scale characteristics of the estuary. The inability of these classification schemes to describe the dynamics of an estuarine network such as Newark Bay, therefore, is due to the lack of general characteristics within an estuarine network. The processes that drive the exchange flow and salt balance in one reach of an estuarine network can be independent of the processes that drive the exchange flow and salt balance within an adjacent reach, despite both reaches containing similar features (e.g., fronts). Consequently, the characteristics of an estuarine network are inherently local, and likely cannot be described at the scale of the estuary.

The inability of existing estuarine classification schemes to describe local dynamics is emphasized by both schemes being unable to distinguish the exchange flow regime of estuaries in which freshwater inflow comes from the mouth. The commonality between the Hackensack River regime and other "three-layer" estuaries, such as Baltimore Harbor, suggests that this "class" of estuarine regime needs to be defined within an estuarine classification scheme. However, that cannot be done with either of the two-dimensional schemes that were evaluated, and it is unlikely that this category could be accommodated within two dimensions.

The ability of local processes to determine the characteristics of an estuary suggests

that, in some cases, anthropogenic modifications may substantially modify the dynamical regime of an estuary. Estuary modifications, such as the construction of a side embayment or deepening of the main channel, are largely local perturbations. These modifications have previously been found to modify local dynamics. van Maren et al. (2009), for example, found that the length of a side channel substantially modifies local sediment trapping. Hetland and MacDonald (2008) similarly attributed some of the efficiency of tidal dispersion at the mouth of the Merrimack River to the presence of rock jetties. Do these local anthropogenic modifications also modify the characteristics of the larger estuary? Ralston et al. (2018) argue that the deepening of the main channel in the Hudson River has had little effect on the location of the estuary in parameter space; however, channel deepening may have substantially modified the characteristics of regions characterized by fronts by reducing the influence of tidal processes.

4.7 Conclusions

This examination of the characteristics of the Newark Bay estuarine network in context with the Hansen-Rattray and Geyer-MacCready estuarine classification schemes indicates that neither of these schemes distinguishes the variations in processes among the sub-estuaries of Newark Bay. Some of these discrepancies between observed and predicted characteristics arise because local tidal dynamics drive much of the exchange flow and subtidal salt balance within the estuarine network. Similar discrepancies occur in other estuarine networks, and in other estuaries that contain abrupt changes in cross-sectional geometry. This suggests that an additional geometry-dependent parameter is necessary to provide an indication of the heterogeneity of dynamics within an estuary. The heterogeneity of an estuary, or dominant influence of local processes, likely increases in larger estuaries, represented by the lower-left quadrant of the Geyer-MacCready parameter space, as these estuaries tend to be longer than the tidal excursion and often consist of multiple reaches, sources of fresh water, and/or connections to the ocean. Heterogeneity likely decreases toward the upper-right quadrant of the Geyer-MacCready parameter space as the length of the estuary and the length scale of local processes converge. Within these energetic "short" estuaries, the same processes are expected to drive both local and estuary-wide characteristics.

We echo Pritchard (1989)'s conclusions in his evaluation of estuarine classification:

> "...despite the new knowledge of the complexity of estuaries, there is still value in using some of the simpler tools which have been available to us for some time. We must of course use them with caution, and not extend their use to problems which require greater spatial and temporal detail than can be represented by these tools."

The Hansen-Rattray and Geyer-MacCready classification schemes are useful in examining the characteristics of "short" energetic estuaries, or regions of larger estuaries that have similar characteristics. However, additional parameters are required to account for the range of processes that drive the salt balance or exchange flow within complex estuarine networks. This study suggests that future attempts to construct a dynamical estuarine parameter space consider the range of variability within an estuary through the inclusion of local dynamically-important length scales, such as the along-channel geometry of the system or the inherent along-channel salinity variability.

Chapter 5

Conclusions and implications

5.1 Summary and conclusions

Estuarine networks are a distinct and important class of estuarine environments, characterized by multiple channels and tributaries, as well as multiple sources of fresh water and/or multiple connections to the ocean. Many estuarine networks are also associated with globally significant ports; the Port of New York and New Jersey, for example, is largely contained within the Newark Bay estuarine network (Chant et al., 2018). Within urban estuarine networks, the shape and depth of the estuary are often substantially modified to enable the safe passage of ships (Jiang et al., 2012; van Maren, van Kessel, et al., 2015). Because of feedback processes between the shape of an estuary and estuarine dynamics (Winterwerp & Wang, 2013), anthropogenic modifications have the potential to substantially modify the dynamics of urban estuaries. This thesis uses hydrographic observations in the Newark Bay estuarine network to investigate the hydrographic variability and exchange flow of estuarine networks in light of both natural and man-made aspects of the estuarine geometry. Newark Bay is connected to the ocean through two tidal straits, and is fed by multiple internal and external sources of fresh water. Dredging within the estuarine network has deepened the main channel by 300% throughout much of the estuary over the past 150 years, and has created two side channels in Newark Bay to support port activities (Marshall, 2004). The natural geometry of the estuarine network divides the estuary into a series of reaches that are each characterized by a different cross-sectional geometry, with varying amounts of anthropogenic influence. Hydrographic observations within each reach were examined to provide insight into both the local and estuary-wide dynamics of an estuarine network, with

implications for ecology, sediment trapping, and anthropogenic estuary modifications.

Hydrographic observations of the Newark Bay estuarine network reveal that the system is characterized by multiple tidal salinity fronts (Chapter 2). The relevant frontogenesis mechanisms have in many cases been described by previous studies (Best, 1987; van Maren et al., 2009; Geyer & Ralston, 2015); however, the dynamics at junctions within Newark Bay substantially modify fronts such that this study reveals important variations on classical ideas of frontogenesis. For example, a bottom lift-off front forms where Kill van Kull meets New York Harbor. This front forms through the hydraulic response of ebb flow to the seaward channel expansion, similar to other lift-off fronts (Luketina & Imberger, 1987; Geyer & Ralston, 2015). However, this front is substantially modified by the 90-minute tidal phase shift between Kill van Kull and New York Harbor (Corlett & Geyer, 2018). The phase-shift initially strengthens the front, allowing the bottom front to form earlier in ebb tide than would otherwise occur. During flood tide, on the other hand, the phase-shift weakens the landward-propagating front by removing its source of salt water. The fronts observed in Newark Bay are also influenced by a tidal phase shift. This phase shift is between the main channel and a side channel, and generates a lateral density-driven circulation similar to previous observations at the entrances of harbors (e.g., Roelfzema & van Os, 1978; Langendoen & Karelse, 1990). However, instead of forming a bottom front within the side channel (van Maren et al., 2009), this circulation forms both a bottom front and a surface front in the main channel during ebb tide. The bottom front is a modified version of a lift-off front. The surface front is distinctive in that it is associated with the lateral divergence in the main channel. This front, as well as the confluence front that forms at the junction between the Passaic and Hackensack rivers, is also distinctive in that the front maintains its position while the water within the front persistently decreases in salinity. The frontal dynamics responsible for this phenomenon involve a combination of horizontal convergence and spatial variation of mixing, as described in an oceanic context by Rudnick and Davis (1988). Each of the fronts documented in the Newark Bay estuarine network propagates landward during flood tide, substantially influencing the along-channel salinity distribution and contributing to tidal oscillatory salt flux, as described next.

The effect of tidal processes on the kinematics of the estuarine network was examined in Chapter 3 through a combination of isohaline (e.g., MacCready, 2011) and Eulerian (e.g., Lerczak et al., 2006) estimates of the subtidal salt balance in individual reaches of

the estuarine network. The comparison of isohaline and Eulerian estimates of tidal and residual salt fluxes revealed that the two coordinate systems produce near-identical values—this was previously known for the overall salt balance (MacCready, 2011), but had not been investigated for individual terms. The comparison further emphasized the value of using the isohaline framework to resolve the magnitude and variability of the exchange flow, as neither is resolved by the Eulerian residual circulation. This was shown previously by Sutherland et al. (2011) and Wang et al. (2015), but deserves reemphasizing in light of the direct comparison between isohaline and Eulerian versions of the salt balance. On average, the exchange flow throughout the Newark Bay estuarine network is largely driven by tidal processes. In addition, the tidal oscillatory salt flux is at least as large as the residual salt flux throughout much of the estuarine network. From the geometry of the different reaches and scalings of the magnitude of salt flux relative to forcing variables, potential mechanisms of tidal dispersion were identified. These include tidal trapping (Okubo, 1973) in Newark Bay and jet-sink exchange (Stommel & Farmer, 1952) at the mouth of Kill van Kull. Both of these potential dispersion mechanisms are likely associated with the dynamics of the tidal salinity fronts identified in Chapter 2; however, we stress that these are only *potential* mechanisms, as more information is needed regarding the spatial structure of flow within the estuarine network before the tidal dispersion mechanisms can be definitively identified.

In Chapter 4, the hydrographic structure and salt-flux mechanisms of the Newark Bay estuarine network were considered in light of two estuarine classification schemes: Hansen and Rattray (1966) and Geyer and MacCready (2014). Both of these approaches were effective at characterizing the conditions in the Passaic River, in light of comparison with other estuaries in the same part of parameter space as well as consideration of the mechanisms of salt flux. The classification of the Newark Bay and Kill van Kull reaches near the "partially-mixed" category provides a reasonable representation of the hydrographic conditions, but the roles of the tidal salt flux and exchange flow could not be discerned from either classification approach. The Hackensack did not fit into either scheme, due to the special circumstance of having the dominant low-salinity water source at the mouth of the river. The problems with these classification schemes are due in part to their attempt to describe an entire estuarine system with one region in parameter space, without taking into account the inherent spatial variability of estuarine dynamics. This analysis suggests a way forward that would quantify the relative importance of local processes by defining a "heterogeneity" parameter. This

parameter could compare the scale of frontal salinity variability to the tidal salinity range to describe the importance of local tidal dispersion processes. This frontal salinity fraction would elucidates the tidal dispersion in Kill van Kull; however, it would not shed light on the special regime of the Hackensack River. Future advances in estuarine classification will need to recognize the rich variation of forcing conditions and geometric configurations in estuarine networks which require categories and parameterizations that extend beyond the two dimensions of the Hansen-Rattray and Geyer-MacCready schemes.

5.2 Implications

The relevance of tidal processes, such as the formation of salinity fronts, within estuarine networks has wide-reaching implications for the ecological characteristics of such estuaries. The along-channel velocity convergences that often generate surface salinity fronts, for example, also gather together phytoplankton and larvae (Dustan & Pinckney, 1989; Wolanski & Hamner, 1988). Consequently, salinity fronts are biological hotspots for higher trophic levels as well (Kingsford & Suthers, 1996; Skov & Prins, 2001). Salinity fronts are also boundaries between distinct ecological habitats (Holligan et al., 1984). The ecological characteristics on either side of a frontal region are often substantially different because of species' preferences for different salinities (Kirst, 1989), contributing to the biological diversity of an estuary (Meire et al., 2005; Sharpe & Baldwin, 2009). Nekton often take advantage of the tidal propagation of fronts as well; Epifanio et al. (1984) found that crab larvae use the landward propagation of bottom fronts to preferentially migrate into Delaware Bay. The prevalence of tidal surface and bottom fronts at junctions within Newark Bay suggests that estuarine networks are biological hotspots due to the complex mixing of waters and concentration of biology at fronts.

Tidal salinity fronts may also substantially influence the transport and trapping of suspended sediments within estuarine networks. Traykovski et al. (2004) found that propagating bottom fronts in the Hudson River trap suspended sediments, and deposit thin layers of sediment on the bed. The sediment that is trapped within fronts may also propagate landward with the front (Shellenbarger et al., 2015). These sediments, however, may also propagate into quiescent side embayments with bottom fronts (Yellen et al., 2017), resulting in extremely high trapping efficiencies. de Nijs et al. (2009), for example, found that

the trapping efficiency of a side channel in the Rotterdam waterway estuarine network approached 100%. These regions of enhanced trapping concentrate estuarine pollutants, such as methylmercury (Brunk et al., 1997; Geyer & Ralston, 2018), that are often associated with fine sediment. Within estuaries with gradual along-channel transitions in cross-sectional area, much of the suspended sediment is trapped at the head of the salt intrusion (Migniot, 1971). Within an estuarine network, sediment and pollutants are instead likely concentrated in local regions of sediment trapping, such as within side channels or at sites of front formation.

Anthropogenic modifications to an estuary may trap sediment by constructing side channels (Parchure & Teeter, 2002), shift the location of the head of salt landward by deepening the main channel (Ralston & Geyer, 2019), or change the mechanisms that drive the local salt balance and the exchange flow by modifying the cross-sectional geometry. Chant et al. (2018), for example, found that the deepening of the main channel in the Newark Bay estuarine network over the past decade has doubled the magnitude of the residual circulation in Kill van Kull. This suggests a substantial dynamical shift toward a regime largely influenced by residual processes, and yet the characteristics of the estuarine network are largely influenced by *tidal* processes (Chapter 3). This is likely due to the recurring presence of fronts. In the Hudson River, dredging has increased the depths of sites of front formation (Ralston & Geyer, 2019), likely weakening fronts and creating a more uniform estuary. In Newark Bay, however, the construction of side channels has created recurring bottom and surface salinity fronts, which likely contribute to tidal salt dispersion.

The substantial contribution of tidal processes to the exchange flow and salt balance throughout much of the Newark Bay estuarine network despite channel deepening emphasizes the importance of understanding local dynamics before predicting the effects of anthropogenic modifications. Regions initially driven by tidal processes (e.g., Kill van Kull), for example, may actually experience a reduction in the total exchange flow with channel deepening, as deepening often produces a decrease in tidal energy (Chant et al., 2018). Changes in the subtidal salt balance are similarly difficult to predict without knowledge of local processes. Although channel deepening often increases the salt flux associated with residual processes and decreases that associated with tidal processes (Ralston & Geyer, 2019), the initial magnitudes of these fluxes are in many cases unknown. So, it is often difficult to say whether deepening will increase or decrease the magnitude of the combined "estuarine" salt

flux (cf. Chapter 3) without prior knowledge of local dynamics.

By containing a spectrum of characteristics, estuarine networks are important test sites in which to further investigate estuarine dynamics and to illuminate the complex cascade of estuarine characteristics from local tidal phenomena to the overall regime of an estuary. By examining the range of tidal and residual dynamics within Newark Bay, this thesis provides an important step toward resolving fundamental questions of estuarine physics, and prompts such questions as how much of the exchange flow at a site of active frontogenesis is due to the formation and propagation of the front? And how many dimensions are required to construct a predictive parameter space that accounts for the local variability of estuarine processes? More data, and perhaps a model, are required.

Appendix A

Data and numerical methods

Data and numerical methods that were created for this thesis have been placed on the Woods Hole Open Access Server, and should be cited as follows:

> Corlett, W. B., Geyer, W. R., Chant, R. J., Ralston, D. K., & Sommerfield, C. K. (2019). *Data and numerical methods for determining the dynamics and kinematics of Newark Bay, NJ* [Data set]. Woods Hole Open Access Server. Retrieved from `https://hdl.handle.net/1912/24371` doi: 10.26025/1912/24371

This data set contains the following materials:

1. raw data for the moorings described in Chapters 2 and 3;
2. processed data for the moorings described in Chapters 2 and 3;
3. numerical methods* for calculating the total exchange flow at individual moorings (Chapter 3); and,
4. numerical methods* for calculating Eulerian and isohaline salt balance terms (Chapter 3).

*Numerical methods are written in the MATLAB® programming language; MATLAB is a registered trademark of The MathWorks, Inc.

THIS PAGE INTENTIONALLY LEFT BLANK

References

Abood, K. A. (1974). Circulation in the Hudson estuary. *Annals of the New York Academy of Sciences*, *250*(1), 39–111. doi: 10.1111/j.1749-6632.1974.tb43895.x

Alebregtse, N. C., de Swart, H. E., & Schuttelaars, H. M. (2013). Resonance characteristics of tides in branching channels. *Journal of Fluid Mechanics*, *728*, R3. doi: 10.1017/jfm.2013.319

Allen, F. H., & Price, W. A. (1959). Density currents and siltation in docks and tidal basins. *The Dock and Harbour Authority*, *40*(465), 72–76.

Armi, L., & Farmer, D. M. (1986). Maximal two-layer exchange through a contraction with barotropic net flow. *Journal of Fluid Mechanics*, *164*, 27–51. doi: 10.1017/S0022112086002458

Aubrey, D. G., & Speer, P. E. (1985). A study of non-linear tidal propagation in shallow inlet/estuarine systems Part I: Observations. *Estuarine, Coastal and Shelf Science*, *21*(2), 185–205. doi: 10.1016/0272-7714(85)90096-4

Balcom, P. H., Hammerschmidt, C. R., Fitzgerald, W. F., Lamborg, C. H., & O'Connor, J. S. (2008). Seasonal distributions and cycling of mercury and methylmercury in the waters of New York/New Jersey Harbor Estuary. *Marine Chemistry*, *109*(1–2), 1–17. doi: 10.1016/j.marchem.2007.09.005

Banas, N. S., Conway-Cranos, L., Sutherland, D. A., MacCready, P., Kiffney, P., & Plummer, M. (2014). Patterns of River Influence and Connectivity Among Subbasins of Puget Sound, with Application to Bacterial and Nutrient Loading. *Estuaries and Coasts*, *38*(3), 735–753. doi: 10.1007/s12237-014-9853-y

Banas, N. S., Hickey, B. M., & MacCready, P. (2004). Dynamics of Willapa Bay, Washington: A highly unsteady, partially mixed estuary. *Journal of Physical Oceanography*, *34*, 2413–2427. doi: 10.1175/JPO2637.1

Beerenhout, B. (1994). Velsen-1: Indications for water-pollution in the harbour of a Roman castellum in the Netherlands. *Archaeofauna*, *3*, 127—130.

Benjamin, T. B. (1968). Gravity currents and related phenomena. *Journal of Fluid Mechanics*, *31*(2), 209–248. doi: 10.1017/S0022112068000133

Best, J. L. (1987). Flow dynamics at river channel confluences: implications for sediment transport and bed morphology. In F. G. Ethridge, R. M. Flores, & M. D. Harvey (Eds.), *Recent Developments in Fluvial Sedimentology* (Vol. SP39, pp. 27–35). Tulsa, OK: SEPM Society for Sedimentary Geology. doi: 10.2110/pec.87.39.0027

Blumberg, A. F., Khan, L. A., & St John, J. P. (1999). Three-Dimensional Hydrodynamic Model of New York Harbor Region . *Journal of Hydraulic Engineering*, *125*(8), 799–816. doi: 10.1061/(ASCE)0733-9429(1999)125:8(799)

Bœuf, G., & Payan, P. (2001). How should salinity influence fish growth? *Comparative Biochemistry and Physiology Part C: Toxicology & Pharmacology*, *130*(4), 411–423. doi: 10.1016/S1532-0456(01)00268-X

Bowden, K. F. (1965). Horizontal mixing in the sea due to a shearing current. *Journal of Fluid Mechanics*, *21*(1), 83–95. doi: 10.1017/S0022112065000058

Bowden, K. F., & Gilligan, R. M. (1971). Characteristic features of estuarine circulation as represented in the Mersey Estuary. *Limnology and Oceanography*, *16*(3), 490–502. doi: 10.4319/lo.1971.16.3.0490

Brubaker, J. M., & Simpson, J. H. (1999). Flow convergence and stability at a tidal estuarine front: Acoustic Doppler current observations. *Journal of Geophysical Research: Oceans*, *104*(C8), 18257–18268. doi: 10.1029/1999JC900117

Brunk, B. K., Jirka, G. H., & Lion, L. W. (1997). Effects of Salinity Changes and the Formation of Dissolved Organic Matter Coatings on the Sorption of Phenanthrene: Implications for Pollutant Trapping in Estuaries. *Environmental Science & Technology*, *31*(1), 119–125. doi: 10.1021/es9602051

Burchard, H., Bolding, K., Feistel, R., Gräwe, U., Klingbeil, K., MacCready, P., ... van der Lee, E. M. (2018). The Knudsen theorem and the Total Exchange Flow analysis framework applied to the Baltic Sea. *Progress in Oceanography*, *165*, 268–286. doi: 10.1016/j.pocean.2018.04.004

Burchard, H., Lange, X., Klingbeil, K., & MacCready, P. (2019). Mixing estimates for estuaries. *Journal of Physical Oceanography*, *49*, 631–648. doi: 10.1175/JPO-D-18-0147.1

Burchard, H., & Schuttelaars, H. M. (2012). Analysis of Tidal Straining as Driver for Estuarine Circulation in Well-Mixed Estuaries. *Journal of Physical Oceanography*, *42*, 261–271. doi: 10.1175/JPO-D-11-0110.1

Caplow, T., Schlosser, P., Ho, D. T., & Santella, N. (2003). Transport Dynamics in a Sheltered Estuary and Connecting Tidal Straits: SF_6 Tracer Study in New York Harbor. *Environmental Science & Technology*, *37*(22), 5116–5126. doi: 10.1021/es034198+

Chant, R. J., Fugate, D. C., & Garvey, E. (2011). The Shaping of An Estuarine Superfund Site: Roles of Evolving Dynamics and Geomorphology. *Estuaries and Coasts*, *34*(1), 90–105. doi: 10.1007/s12237-010-9324-z

Chant, R. J., Glenn, S., Styles, R., Hunter, E., Haldeman, C., Creed, L., ... Herrington, T. (2006). *Hydrodynamics of the Newark Bay/Kill System* (Tech. Rep. No. I-E). New Brunswick, NJ: New Jersey Department of Environmental Protection. doi: 10.7282/T36H4GMH

Chant, R. J., Sommerfield, C. K., & Talke, S. A. (2018). Impact of channel deepening on tidal and gravitational circulation in a highly engineered estuarine basin. *Estuaries and Coasts*, *41*(6), 1587–1600. doi: 10.1007/s12237-018-0379-6

Chao, S.-Y., Boicourt, W. C., & Wang, H. V. (1996). Three-layered circulation in reverse estuaries. *Continental Shelf Research*, *16*(10), 1379–1397. doi: 10.1016/0278-4343(95)00072-0

Chen, S.-N., Geyer, W. R., Ralston, D. K., & Lerczak, J. A. (2012). Estuarine Exchange Flow Quantified with Isohaline Coordinates: Contrasting Long and Short Estuaries. *Journal of Physical Oceanography*, *42*, 748–763. doi: 10.1175/JPO-D-11-086.1

Cloern, J. E. (1987). Turbidity as a control on phytoplankton biomass and productivity in estuaries. *Continental Shelf Research*, *7*(11–12), 1367–1381. doi: 10.1016/0278-4343(87)90042-2

Cokelet, E. D., & Stewart, R. J. (1985). The exchange of water in fjords: The efflux/reflux theory of advective reaches separated by mixing zones. *Journal of Geophysical Research: Oceans*, *90*(C4), 7287–7306. doi: 10.1029/JC090iC04p07287

Corlett, W. B., & Geyer, W. R. (2018). *Coupled Dynamics and Sediment Transport in a Human-modified Estuarine Network* (Tech. Rep. No. GF/01/17). New York, NY: Hudson River Foundation. doi: 10.13140/RG.2.2.21234.35529

Corlett, W. B., Geyer, W. R., Chant, R. J., Ralston, D. K., & Sommerfield, C. K. (2019). *Data and numerical methods for determining the dynamics and kinematics of Newark Bay, NJ* [Data set]. Woods Hole Open Access Server. Retrieved from `https://hdl.handle.net/1912/24371` doi: 10.26025/1912/24371

Crawford, D., Bonnevie, N., & Wenning, R. (1995). Sources of Pollution and Sediment Contamination in Newark Bay, New Jersey. *Ecotoxicology and Environmental Safety*, *30*, 85–100.

de Jonge, V. N., Schuttelaars, H. M., van Beusekom, J. E. E., Talke, S. A., & de Swart, H. E. (2014). The influence of channel deepening on estuarine turbidity levels and dynamics, as exemplified by the Ems estuary. *Estuarine, Coastal and Shelf Science*, *139*, 46–59. doi: 10.1016/j.ecss.2013.12.030

de Kok, J. M. (2002). The influence of fresh water distribution on SPM transport in the Dutch coastal zone. In J. C. Winterwerp & C. Kranenburg (Eds.), *Fine Sediment Dynamics in the Marine Environment* (Vol. 5, pp. 563–576). doi: 10.1016/S1568-2692(02)80040-7

Delile, H., Goiran, J., & Blichert-Toft, J. (2018). The contribution of geochemistry to ancient harbor geoarcheology: The example of Ostia Antica. *Quaternary Science Reviews*, *193*, 170–187. doi: 10.1016/j.quascirev.2018.06.019

de Nijs, M. A. J., Winterwerp, J. C., & Pietrzak, J. D. (2009). On harbour siltation in the fresh-salt water mixing region. *Continental Shelf Research*, *29*(1), 175–193. doi: 10.1016/j.csr.2008.01.019

De Serres, B., Roy, A. G., Biron, P. M., & Best, J. L. (1999). Three-dimensional structure of flow at a confluence of river channels with discordant beds. *Geomorphology*, *26*(4), 313–335. doi: 10.1016/S0169-555X(98)00064-6

Di Donato, V., Ruello, M. R., Liuzza, V., Carsana, V., Giampaola, D., Vito, M. A. D., ... Ermolli, E. R. (2018). Development and decline of the ancient harbor of Neapolis. *Geoarchaeology*, *33*(5), 542–557. doi: 10.1002/gea.21673

Dijkstra, Y. M., Schuttelaars, H. M., & Burchard, H. (2017). Generation of exchange flows in estuaries by tidal and gravitational eddy viscosity-shear covariance (ESCO). *Journal of Geophysical Research: Oceans*, *122*(5), 4217–4237. doi: 10.1002/2016JC012379

Dustan, P., & Pinckney, J. L. (1989). Tidally induced estuarine phytoplankton patchiness. *Limnology and Oceanography*, *34*(2), 410–419. doi: 10.4319/lo.1989.34.2.0410

Ebbesmeyer, C. C., & Barnes, C. A. (1980). Control of a fjord basin's dynamics by tidal mixing in embracing sill zones. *Estuarine and Coastal Marine Science*, *11*(3), 311–330. doi: 10.1016/S0302-3524(80)80086-7

Edwards, K. A., Kawase, M., & Sarason, C. P. (2007). Circulation in Carr Inlet, Puget Sound, during Spring 2003. *Estuaries and Coasts*, *30*(6), 945–958. doi: 10.1007/BF02841387

Epifanio, C., Valenti, C., & Pembroke, A. (1984). Dispersal and recruitment of blue crab larvae in Delaware Bay, U.S.A. *Estuarine, Coastal and Shelf Science*, *18*(1), 1–12. doi: 10.1016/0272-7714(84)90002-7

Farmer, D. M., D'Asaro, E. A., Trevorrow, M. V., & Dairiki, G. T. (1995). Three-dimensional structure in a tidal convergence front. *Continental Shelf Research*, *15*(13), 1649–1673. doi: 10.1016/0278-4343(94)00084-Z

Farmer, D. M., & Freeland, H. J. (1983). The physical oceanography of Fjords. *Progress in Oceanography*, *12*(2), 147–219. doi: 10.1016/0079-6611(83)90004-6

Festa, J. F., & Hansen, D. V. (1978). Turbidity maxima in partially mixed estuaries: A two-dimensional numerical model. *Estuarine and Coastal Marine Science*, *7*(4), 347–359. doi: 10.1016/0302-3524(78)90087-7

Fischer, H. B. (1972). Mass transport mechanisms in partially stratified estuaries. *Journal of Fluid Mechanics*, *53*(4), 671–687. doi: 10.1017/S0022112072000412

Fischer, H. B. (1976). Mixing and dispersion in estuaries. *Annual review of fluid mechanics*, *8*, 107–133. doi: 10.1146/annurev.fl.08.010176.000543

Fischer, H. B., List, J. E., Koh, C. R., Imberger, J., & Brooks, N. H. (1979). *Mixing in Inland and Coastal Waters*. San Diego, CA: Academic Press.

Friedrichs, C. T. (2009). York River Physical Oceanography and Sediment Transport. *Journal of Coastal Research*, *2009*(10057), 17–22. doi: 10.2112/1551-5036-57.sp1.17

Friedrichs, C. T., & Aubrey, D. G. (1994). Tidal propagation in strongly convergent channels. *Journal of Geophysical Research*, *99*(C2), 3321–3336. doi: 10.1029/93JC03219

Frittelli, J. (2008). *Ship Navigation in Harbors: Safety Issues* (Tech. Rep. No. RL34365). Washington, DC: Congressional Research Service.

Garvine, R. W. (1977). Observations of the motion field of the Connecticut River plume. *Journal of Geophysical Research: Oceans*, *82*(3), 441–454. doi: 10.1029/JC082i003p00441

Geyer, W. R., & Farmer, D. M. (1989). Tide-Induced Variation of the Dynamics of a Salt Wedge Estuary. *Journal of Physical Oceanography*, *19*(8), 1060–1072. doi: 10.1175/1520-0485(1989)019<1060:TIVOTD>2.0.CO;2

Geyer, W. R., & MacCready, P. (2014). The Estuarine Circulation. *Annual Review of Fluid Mechanics*, *46*, 175–197. doi: 10.1146/annurev-fluid-010313-141302

Geyer, W. R., & Nepf, H. M. (1996). Tidal pumping of salt in a moderately stratified estuary. In D. G. Aubrey & C. T. Friedrichs (Eds.), *Buoyancy Effects on Coastal and Estuarine Dynamics* (Vol. 53, pp. 213–226). Washington, DC: American Geophysical Union. doi: 10.1029/CE053p0213

Geyer, W. R., & Ralston, D. K. (2015). Estuarine Frontogenesis. *Journal of Physical Oceanography*, *45*(2), 546–561. doi: 10.1175/JPO-D-14-0082.1

Geyer, W. R., & Ralston, D. K. (2018). A mobile pool of contaminated sediment in the Penobscot Estuary, Maine, USA. *Science of the Total Environment*, *612*, 694–707. doi: 10.1016/j.scitotenv.2017.07.195

Geyer, W. R., & Signell, R. P. (1992). A Reassessment of the Role of Tidal Dispersion in Estuaries and Bays. *Estuaries*, *15*(2), 97–108. doi: 10.2307/1352684

Geyer, W. R., Trowbridge, J. H., & Bowen, M. M. (2000). The Dynamics of a Partially Mixed Estuary*. *Journal of Physical Oceanography*, *30*(8), 2035–2048. doi: 10.1175/1520-0485(2000)030<2035:TDOAPM>2.0.CO;2

Giddings, S. N., Fong, D. A., Monismith, S. G., Chickadel, C. C., Edwards, K. A., Plant, W. J., ... Jessup, A. T. (2012). Frontogenesis and Frontal Progression of a Trapping-Generated Estuarine Convergence Front and Its Influence on Mixing and Stratification. *Estuaries and Coasts*, *35*(2), 665–681. doi: 10.1007/s12237-011-9453-z

Haas, L. W. (1977). The effect of the spring-neap tidal cycle on the vertical salinity structure of the James, York and Rappahannock Rivers, Virginia, USA. *Estuarine and Coastal Marine Science*, *5*(4), 485–496. doi: 10.1016/0302-3524(77)90096-2

Halonen, J. R. (2011). *Effects of Historical Morphologic Change on Sediment Accumulation in Newark Bay, New Jersey* (Master's thesis). Newark, DE.

Hansen, D. V., & Rattray, M., Jr. (1965). Gravitational circulation in straits and estuaries. *Journal of Marine Research*, *23*(2), 104–122.

Hansen, D. V., & Rattray, M., Jr. (1966). New dimensions in estuarine classification. *Limnology and Oceanography*, *11*(3), 319–326. doi: 10.4319/lo.1966.11.3.0319

Hayward, D., Welch, C. S., & Haas, L. W. (1982). York River Destratification: An Estuary-Subestuary Interaction. *Science*, *216*(4553), 1413–1414. doi: 10.1126/science.216.4553.1413

He, Q., Silliman, B. R., & Cui, B. (2017). Incorporating thresholds into understanding salinity tolerance: A study using salt-tolerant plants in salt marshes. *Ecology and Evolution*, *7*(16), 6326–6333. doi: 10.1002/ece3.3209

Hess, K. W. (1976). A three-dimensional numerical model of the estuary circulation and salinity in Narragansett Bay. *Estuarine and Coastal Marine Science*, *4*(3), 325–338. doi: 10.1016/0302-3524(76)90064-5

Hetland, R. D., & MacDonald, D. G. (2008). Spreading in the near-field Merrimack River plume. *Ocean Modelling*, *21*(1–2), 12–21. doi: 10.1016/j.ocemod.2007.11.001

Hickey, B. M., Zhang, X., & Banas, N. (2002). Coupling between the California Current System and a coastal plain estuary in low riverflow conditions. *Journal of Geophysical Research: Earth Surface*, *107*(C10), 3166. doi: 10.1029/1999JC000160

Holligan, P. M., Williams, P. J. l., Purdie, D., & Harris, R. (1984). Photosynthesis, respiration and nitrogen supply of plankton populations in stratified, frontal and tidally mixed shelf waters. *Marine Ecology Progress Series*, *17*, 201–213. doi: 10.3354/meps017201

Horner-Devine, A. R., Hetland, R. D., & MacDonald, D. G. (2015). Mixing and Transport in Coastal River Plumes. *Annual review of fluid mechanics*, *47*(1), 569–594. doi: 10.1146/annurev-fluid-010313-141408

Hughes, F., & Rattray, M., Jr. (1980). Salt flux and mixing in the Columbia River Estuary. *Estuarine and Coastal Marine Science*, *10*(5), 479–493. doi: 10.1016/S0302-3524(80)80070-3

Huzzey, L. M. (1982). The dynamics of a bathymetrically arrested estuarine front. *Estuarine, Coastal and Shelf Science*, *15*(5), 537–552. doi: 10.1016/0272-7714(82)90005-1

Jay, D. A., & Musiak, J. D. (1994). Particle trapping in estuarine tidal flows. *Journal of Geophysical Research: Oceans*, *99*(C10), 20445–20461. doi: 10.1029/94JC00971

Jay, D. A., & Smith, J. D. (1990). Circulation, density distribution and neap-spring transitions in the Columbia River Estuary. *Progress in Oceanography*, *25*(1–4), 81–112. doi: 10.1016/0079-6611(90)90004-L

Jiang, C., Li, J., & Swart, H. E. d. (2012). Effects of navigational works on morphological changes in the bar area of the Yangtze Estuary. *Geomorphology*, *139–140*, 205–219. doi: 10.1016/j.geomorph.2011.10.020

Kaluarachchi, I. D., Bruno, M. S., Ahsan, Q., Blumberg, A. F., & Li, H. (2003). Estimating the Volume and Salt Fluxes Through Arthur Kill and the Kill van Kull. In *World Water Environmental Resources Congress 2003* (p. 10). Philadelphia, PA: American Society of Civil Engineers. doi: 10.1061/40685(2003)225

Kincaid, C. (2006). The Exchange of Water through Multiple Entrances to the Mount Hope Bay Estuary. *Northeastern Naturalist*, *13*(SP4), 117–144. doi: 10.1656/1092-6194(2006)13[117:TEOWTM]2.0.CO;2

Kingsford, M., & Suthers, I. (1996). The Influence of Tidal Phase on Patterns of Ichthyoplankton Abundance in the Vicinity of an Estuarine Front, Botany Bay, Australia. *Estuarine, Coastal and Shelf Science*, *43*(1), 33–54. doi: 10.1006/ecss.1996.0056

Kirst, G. O. (1989). Salinity Tolerance of Eukaryotic Marine Algae. *Annual Review of Plant Physiology and Plant Molecular Biology*, *41*, 21–53. doi: 10.1146/annurev.pp.41.060190.000321

Knudsen, M. (1900). Ein hydrographischer Lehrsatz. *Annalen der Hydrographie und Maritimen Meteorologie*, *28*(7), 316–320.

Langendoen, E. J., & Karelse, M. (1990). *Laboratory observations of velocity and density fields in the entrance of a harbor on a stratified tidal river.* (Tech. Rep. No. 1-90). Delft, NL: TU Delft, Department of Hydraulic Engineering.

Largier, J. L. (1992). Tidal intrusion fronts. *Estuaries*, *15*(1), 26–39. doi: 10.2307/1352707

Largier, J. L. (1993). Estuarine fronts: How important are they? *Estuaries*, *16*(1), 1–11. doi: 10.2307/1352760

Lavelle, J. W., Cokelet, E. D., & Cannon, G. A. (1991). A model study of density intrusions into and circulation within a deep, silled estuary: Puget Sound. *Journal of Geophysical Research*, *96*(C9), 16779–16800. doi: 10.1029/91JC01450

Lee, J., Webb, B. M., Dzwonkowski, B., Valle-Levinson, A., & Lee, J. (2019). Characteristics of exchange flow in a multiple inlet diurnal estuary: Mobile Bay, Alabama. *Journal of Marine Systems*, *191*, 38–50. doi: 10.1016/j.jmarsys.2018.12.004

Lerczak, J. A., Geyer, W. R., & Chant, R. J. (2006). Mechanisms driving the time-dependent salt flux in a partially stratified estuary*. *Journal of Physical Oceanography*, *36*, 2296–2311. doi: 10.1175/JPO2959.1

Levings, C. D., Foreman, R. E., & Tunnicliffe, V. J. (1983). Review of the Benthos of the Strait of Georgia and Contiguous Fjords. *Canadian Journal of Fisheries and Aquatic Sciences*, *40*(7), 1120–1141. doi: 10.1139/f83-131

Levinton, J., Doall, M., Ralston, D., Starke, A., & Allam, B. (2011). Climate Change, Precipitation and Impacts on an Estuarine Refuge from Disease. *PLoS ONE*, *6*(4), e18849. doi: 10.1371/journal.pone.0018849

Li, C., & O'Donnell, J. (1997). Tidally driven residual circulation in shallow estuaries with lateral depth variation. *Journal of Geophysical Research: Oceans*, *102*(C13), 27915–27929. doi: 10.1029/97JC02330

Li, W.-h., Cheng, H.-q., Li, J.-f., Li, M.-t., Chen, J.-y., & Fu, G. (2007). Estimated Effect of Bed Sediments and Sand Waves During Dry Season on the Safe Nautical Depth in the South Channel of the Changjiang River Estuary. *Hydrographic Surveying and Charting*.

Long, R. R. (1977). Three-layer circulations in estuaries and harbors. *Journal of Physical Oceanography*, *7*, 415–421.

Lorenz, M., Klingbeil, K., MacCready, P., & Burchard, H. (2019). Numerical issues of the Total Exchange Flow (TEF) analysis framework for quantifying estuarine circulation. *Ocean Science*, *15*, 601–614. doi: 10.5194/os-15-601-2019

Luketina, D. A., & Imberger, J. (1987). Characteristics of a surface buoyant jet. *Journal of Geophysical Research: Earth Surface*, *92*(C5), 5435–5447. doi: 10.1029/JC092iC05p05435

MacCready, P. (2011). Calculating Estuarine Exchange Flow Using Isohaline Coordinates*. *Journal of Physical Oceanography*, *41*, 1116–1124. doi: 10.1175/2011JPO4517.1

MacCready, P., & Geyer, W. R. (2010). Advances in Estuarine Physics. *Annual Review of Marine Science*, *2*(1), 35–58. doi: 10.1146/annurev-marine-120308-081015

MacCready, P., Geyer, W. R., & Burchard, H. (2018). Estuarine Exchange Flow Is Related to Mixing through the Salinity Variance Budget. *Journal of Physical Oceanography*, *48*, 1375–1384. doi: 10.1175/JPO-D-17-0266.1

MacDonald, D. G., & Geyer, W. R. (2005). Hydraulic control of a highly stratified estuarine front. *Journal of Physical Oceanography*, *35*(3), 374–387. doi: 10.1175/jpo-2692.1

Mackas, D. L., & Harrison, P. J. (1997). Nitrogenous Nutrient Sources and Sinks in the Juan de Fuca Strait/Strait of Georgia/Puget Sound Estuarine System: Assessing the Potential for Eutrophication. *Estuarine, Coastal and Shelf Science*, *44*(1), 1–21. doi: 10.1006/ecss.1996.0110

MacVean, L. J., & Stacey, M. T. (2010). Estuarine Dispersion from Tidal Trapping: A New Analytical Framework. *Estuaries and Coasts*, *34*(1), 45–59. doi: 10.1007/s12237-010-9298-x

Mallin, M., Paerl, H., Rudek, J., & Bates, P. (1993). Regulation of estuarine primary production by watershed rainfall and river flow. *Marine Ecology Progress Series*, *93*, 199—203. doi: 10.3354/meps093199

Marmorino, G. O., & Trump, C. L. (1996). High-resolution measurements made across a tidal intrusion front. *Journal of Geophysical Research: Oceans*, *101*(C11), 25661–25674. doi: 10.1029/96jc02384

Marshall, S. (2004). The Meadowlands Before the Commission: Three Centuries of Human Use and Alteration of the Newark and Hackensack Meadows. *Urban Habitats*, *2*(1), 4—27.

Marsili, L. F. (1681). *Osservazioni intorno al Bosforo Tracio overo canale di Constantinopoli rappresentate in lettera alla sacra real maesta di Cristina regina die Svezia.* Rome, IT.

Mathew, R., & Winterwerp, J. C. (2017). Surficial sediment erodibility from time-series measurements of suspended sediment concentrations: development and validation. *Ocean Dynamics*, *67*(6), 691–712. doi: 10.1007/s10236-017-1055-2

Meire, P., Ysebaert, T., Damme, S. V., Bergh, E. V. d., Maris, T., & Struyf, E. (2005). The Scheldt estuary: a description of a changing ecosystem. *Hydrobiologia*, *540*(1–3), 1–11. doi: 10.1007/s10750-005-0896-8

Migniot, C. (1971). L'évolution de la Gironde au cours des temps. *Bulletin del'Institut de Geologie du Bassin d'Aquitaine*, *11*, 221–281.

Morhange, C., & Marriner, N. (2008). Mind the (stratigraphic) gap: Roman dredging in ancient Mediterranean harbours. *Bollettino di Archeologia*, *B7*, 23–32.

Nepf, H. M., & Geyer, W. R. (1996). Intratidal variations in stratification and mixing in the Hudson estuary. *Journal of Geophysical Research: Oceans*, *101*(C5), 12079–12086. doi: 10.1029/96JC00630

Nunes, R. A. (1982). *The dynamics of small-scale fronts in estuaries* (Doctoral dissertation). University of Wales, Anglesey, UK.

O'Donnell, J. (1990). The formation and fate of a river plume: A numerical model. *Journal of Physical Oceanography*, *20*, 551–569. doi: 10.1175/1520-0485(1990)020<0551:TFAFOA>2.0.CO;2

O'Donnell, J. (1993). Surface fronts in estuaries: A review. *Estuaries*, *16*(1), 12–39. doi: 10.2307/1352761

Okubo, A. (1973). Effect of shoreline irregularities on streamwise dispersion in estuaries and other embayments. *Netherlands Journal of Sea Research*, *6*(1-2), 213–224.

Parchure, T. M., & Teeter, A. M. (2002). *Lessons Learned from Existing Projects on Shoaling in Harbors and Navigation Channels* (Tech. Rep. No. ERDC/CHL CHETN-XIV-5). Vicksburg, MS: US Army Engineer Research and Development Center, Coastal and Hydraulics Laboratory.

Pelegri, J. L. (1988). Tidal fronts in estuaries. *Estuarine, Coastal and Shelf Science*, *27*(1), 45–60. doi: 10.1016/0272-7714(88)90031-5

Pilson, M. E. Q. (1985). On the residence time of water in Narragansett Bay. *Estuaries*, *8*(1), 2–14. doi: 10.2307/1352116

Pinardi, N., Özsoy, E., Latif, M. A., Moroni, F., Grandi, A., Manzella, G., ... Lyubartsev, V. (2018). Measuring the sea: Marsili's oceanographic cruise (1679–1680) and the roots of oceanography. *Journal of Physical Oceanography*, *48*(4), 845–860. doi: 10.1175/JPO-D-17-0168.1

Postma, H. (1961). Transport and accumulation of suspended matter in the Dutch Wadden Sea. *Netherlands Journal of Sea Research*, *1*(1–2), 148–190. doi: 10.1016/0077-7579(61)90004-7

Pritchard, D. W. (1952a). Estuarine Hydrography. In H. E. Landsberg (Ed.), *Advances in geophysics* (Vol. 1, pp. 243–280). New York, NY: Academic Press.

Pritchard, D. W. (1952b). Salinity Distribution and Circulation in the Chesapeake Bay Estuarine System. *Journal of Marine Research*, *11*(2), 106–123.

Pritchard, D. W. (1954). A study of the salt balance in a coastal plain estuary. *Journal of Marine Research*, *13*(1), 133–144.

Pritchard, D. W. (1967). What is an estuary: physical viewpoint. In G. H. Lauff (Ed.), *Estuaries* (pp. 3–5). Washington, DC: American Association for the Advancement of Science.

Pritchard, D. W. (1989). Estuarine Classification—A Help or a Hindrance. In B. Neilson, A. Kuo, & J. Brubaker (Eds.), *Estuarine circulation* (pp. 1–38). Totowa, NJ: Humana Press. doi: 10.1007/978-1-4612-4562-9_1

Pritchard, D. W., & Bunce, R. E. (1959). *Physical and Chemical Hydrography of the Magothy River* (Tech. Rep. No. 17). Baltimore, MD: Johns Hopkins University.

Procopius. (1928). *History of the Wars* (Vol. VIII; H. B. Dewing, Trans.). Cambridge, MA: Harvard University Press.

Ralston, D. K., & Geyer, W. R. (2019). Response to channel deepening of the salinity intrusion, estuarine circulation, and stratification in an urbanized estuary. *Journal of Geophysical Research: Oceans*, *124*. doi: 10.1029/2019JC015006

Ralston, D. K., Geyer, W. R., & Lerczak, J. A. (2008). Subtidal Salinity and Velocity in the Hudson River Estuary: Observations and Modeling. *Journal of Physical Oceanography*, *38*, 753–770. doi: 10.1175/2007JPO3808.1

Ralston, D. K., Geyer, W. R., & Lerczak, J. A. (2010). Structure, variability, and salt flux in a strongly forced salt wedge estuary. *Journal of Geophysical Research: Oceans*, *115*(C6), C06005. doi: 10.1029/2009JC005806

Ralston, D. K., Geyer, W. R., & Warner, J. C. (2012). Bathymetric controls on sediment transport in the Hudson River estuary: Lateral asymmetry and frontal trapping. *Journal of Geophysical Research: Oceans*, *117*(C10), C10013. doi: 10.1029/2012JC008124

Ralston, D. K., Talke, S. A., Geyer, W. R., Al-Zubadaei, H., & Sommerfield, C. K. (2018). Bigger tides, less flooding: Effects of dredging on barotropic dynamics in a highly modified estuary. *Journal of Geophysical Research: Oceans*, *124*(1), 196–211. doi: 10.1029/2018JC014313

Redbourn, L. J. (1996). *The structure and dynamics of a convergent estuarine front* (Doctoral dissertation). University of Plymouth, Plymouth, UK.

Rhoads, B. L., & Kenworthy, S. T. (1995). Flow structure at an asymmetrical stream confluence. *Geomorphology*, *11*(4), 273–293. doi: 10.1016/0169-555x(94)00069-4

Rhoads, B. L., & Sukhodolov, A. N. (2001). Field investigation of three-dimensional flow structure at stream confluences: 1. Thermal mixing and time-averaged velocities. *Water Resources Research*, *37*(9), 2393–2410. doi: 10.1029/2001wr000316

Riley, J. D., Rhoads, B. L., Parsons, D. R., & Johnson, K. K. (2014). Influence of junction angle on three-dimensional flow structure and bed morphology at confluent meander bends during different hydrological conditions. *Earth Surface Processes and Landforms*, *40*(2), 252–271. doi: 10.1002/esp.3624

Roelfzema, A., & van Os, A. G. (1978). Effect of Harbours on Salt Intrusion in Estuaries. In *Coastal Engineering 1978* (pp. 2810–2826). Reston, VA: American Society of Civil Engineers. doi: 10.1061/9780872621909.174

Roos, P. C., & Schuttelaars, H. M. (2015). Resonance properties of tidal channels with multiple retention basins: role of adjacent sea. *Ocean Dynamics*, *65*(3), 311–324. doi: 10.1007/s10236-015-0809-y

Rudnick, D. L., & Davis, R. E. (1988). Frontogenesis in Mixed Layers. *Journal of Physical Oceanography*, *18*, 434–457. doi: 10.1175/1520-0485(1988)018<0434:FIML>2.0.CO;2

Salomon, F., Delile, H., Goiran, J.-P., Bravard, J.-P., & Keay, S. (2012). The Canale di Comunicazione Traverso in Portus: the Roman sea harbour under river influence (Tiber delta, Italy). *Géomorphologie : relief, processus, environnement*, *18*(1), 75–90. doi: 10.4000/geomorphologie.9754

Schoellhamer, D. H. (2011). Sudden Clearing of Estuarine Waters upon Crossing the Threshold from Transport to Supply Regulation of Sediment Transport as an Erodible Sediment Pool is Depleted: San Francisco Bay, 1999. *Estuaries and Coasts*, *34*(5), 885–899. doi: 10.1007/s12237-011-9382-x

Sharpe, P. J., & Baldwin, A. H. (2009). Patterns of wetland plant species richness across estuarine gradients of chesapeake bay. *Wetlands*, *29*(1), 225–235. doi: 10.1672/08-111.1

Shellenbarger, G. G., Downing-Kunz, M. A., & Schoellhamer, D. H. (2015). Suspended-sediment dynamics in the tidal reach of a San Francisco Bay tributary. *Ocean Dynamics*, *65*(11), 1477–1488. doi: 10.1007/s10236-015-0876-0

Sherwood, C. R., Jay, D. A., Harvey, R. B., Hamilton, P., & Simenstad, C. A. (1990). Historical changes in the Columbia River Estuary. *Progress in Oceanography*, *25*(1–4), 299–352. doi: 10.1016/0079-6611(90)90011-P

Shrestha, P., Su, S., James, S., Shaller, P., Doroudian, M., Firstenberg, C., & Thompson, C. (2014). Conceptual Site Model for Newark Bay—Hydrodynamics and Sediment Transport. *Journal of Marine Science and Engineering*, *2*(1), 123–139. doi: 10.3390/jmse2010123

Simoons, E. (2010). *Hydrodynamic analysis of the Johor River estuary* (Master's thesis). National University of Singapore and Delft University of Technology, Singapore, SG.

Simpson, J. E., & Linden, P. F. (1989). Frontogenesis in a fluid with horizontal density gradients. *Journal of Fluid Mechanics*, *202*, 1–16. doi: 10.1017/s0022112089001072

Simpson, J. H., Brown, J., Matthews, J., & Allen, G. P. (1990). Tidal straining, density currents, and stirring in the control of estuarine stratification. *Estuaries*, *13*(2), 125–132. doi: 10.2307/1351581

Simpson, J. H., & Nunes, R. A. (1981). The tidal intrusion front: An estuarine convergence zone. *Estuarine, Coastal and Shelf Science*, *13*(3), 257–266. doi: 10.1016/S0302-3524(81)80024-2

Skov, H., & Prins, E. (2001). Impact of estuarine fronts on the dispersal of piscivorous birds in the German Bight. *Marine Ecology Progress Series*, *214*, 279–287. doi: 10.3354/meps214279

Soulsby, R. L. (1990). Tidal-current boundary layers. In B. Le Mehaute & D. M. Hanes (Eds.), *Ocean Engineering Science* (Vol. 9, pp. 523–566). Cambridge, MA: Wiley and Sons.

Spaulding, M. L., & Swanson, C. (2008). Circulation and Transport Dynamics in Narragansett Bay. In A. Desbonnet & B. A. Costa-Pierce (Eds.), *Science for Ecosystem-based Management: Narragansett Bay in the 21st Century* (pp. 233–279). New York, NY: Springer. doi: 10.1007/978-0-387-35299-2_8

Speer, P. E., & Aubrey, D. G. (1985). A study of non-linear tidal propagation in shallow inlet/estuarine systems Part II: Theory. *Estuarine, Coastal and Shelf Science*, *21*(2), 207–224. doi: 10.1016/0272-7714(85)90097-6

Stommel, H., & Farmer, H. G. (1952). *On the nature of the estuarine circulation* (Tech. Rep. No. 52-88). Woods Hole, MA: Woods Hole Oceanographic Institution.

Stroup, E. D., Pritchard, D. W., & Carpenter, J. H. (1961). *Final Report on Baltimore Harbor Study* (Tech. Rep. No. XXVI). Baltimore, MD: Johns Hopkins University.

Suszkowski, D. J. (1978). *Sedimentology of Newark Bay, New Jersey* (Doctoral dissertation). University of Delaware, Newark, DE.

Sutherland, D. A., MacCready, P., Banas, N. S., & Smedstad, L. F. (2011). A Model Study of the Salish Sea Estuarine Circulation*. *Journal of Physical Oceanography*, *41*, 1125–1143. doi: 10.1175/2011JPO4540.1

Tran, N. K., & Haasis, H.-D. (2015). An empirical study of fleet expansion and growth of ship size in container liner shipping. *International Journal of Production Economics*, *159*, 241–253. doi: 10.1016/j.ijpe.2014.09.016

Traykovski, P. A., Geyer, W. R., & Sommerfield, C. K. (2004). Rapid sediment deposition and fine-scale strata formation in the Hudson estuary. *Journal of Geophysical Research: Earth Surface*, *109*(F2), F02004. doi: 10.1029/2003JF000096

van Maren, D. S., van Kessel, T., Cronin, K., & Sittoni, L. (2015). The impact of channel deepening and dredging on estuarine sediment concentration. *Continental Shelf Research*, *95*, 1–14. doi: 10.1016/j.csr.2014.12.010

van Maren, D. S., Winterwerp, J. C., Sas, M., & Vanlede, J. (2009). The effect of dock length on harbour siltation. *Continental Shelf Research*, *29*(11–12), 1410–1425. doi: 10.1016/j.csr.2009.03.003

van Maren, D. S., Winterwerp, J. C., & Vroom, J. (2015). Fine sediment transport into the hyper-turbid lower Ems River: the role of channel deepening and sediment-induced drag reduction. *Ocean Dynamics*, *65*(4), 589–605. doi: 10.1007/s10236-015-0821-2

Wang, T., Geyer, W. R., Engel, P., Jiang, W., & Feng, S. (2015). Mechanisms of Tidal Oscillatory Salt Transport in a Partially Stratified Estuary. *Journal of Physical Oceanography*, *45*, 2773–2789. doi: 10.1175/JPO-D-15-0031.1

Wang, T., Geyer, W. R., & MacCready, P. (2017). Total Exchange Flow, Entrainment, and Diffusive Salt Flux in Estuaries. *Journal of Physical Oceanography*, *47*, 1205–1220. doi: 10.1175/JPO-D-16-0258.1

Warner, J. C., Schoellhamer, D. H., Burau, J. R., & Schladow, S. G. (2002). Effects of tidal current phase at the junction of two straits. *Continental Shelf Research*, *22*(11–13), 1629–1642. doi: 10.1016/S0278-4343(02)00026-2

Warner, J. C., Schoellhamer, D. H., & Schladow, S. G. (2003). Tidal truncation and barotropic convergence in a channel network tidally driven from opposing entrances. *Estuarine, Coastal and Shelf Science*, *56*(3–4), 629–639. doi: 10.1016/S0272-7714(02)00213-5

Weisberg, R. H. (1976). The nontidal flow in the Providence River of Narragansett Bay: a stochastic approach to estuarine circulation. *Journal of Physical Oceanography*, *6*, 721–734. doi: 10.1175/1520-0485(1976)006<0721:TNFITP>2.0.CO;2

Winterwerp, J. C., & Wang, Z. B. (2013). Man-induced regime shifts in small estuaries—I: theory. *Ocean Dynamics*, *63*(11–12), 1279–1292. doi: 10.1007/s10236-013-0662-9

Winterwerp, J. C., Wang, Z. B., van Braeckel, A., van Holland, G., & Kösters, F. (2013). Man-induced regime shifts in small estuaries—II: a comparison of rivers. *Ocean Dynamics*, *63*(11–12), 1293–1306. doi: 10.1007/s10236-013-0663-8

Wolanski, E., & Hamner, W. M. (1988). Topographically Controlled Fronts in the Ocean and Their Biological Influence. *Science*, *241*(4862), 177–181. doi: 10.1126/science.241.4862.177

Woodruff, J. D., Geyer, W. R., Sommerfield, C. K., & Driscoll, N. W. (2001). Seasonal variation of sediment deposition in the Hudson River estuary. *Marine Geology*, *179*(1–2), 105–119. doi: 10.1016/S0025-3227(01)00182-7

Xu, J., Long, W., Wiggert, J. D., Lanerolle, L. W. J., Brown, C. W., Murtugudde, R., & Hood, R. R. (2012). Climate Forcing and Salinity Variability in Chesapeake Bay, USA. *Estuaries and Coasts*, *35*(1), 237–261. doi: 10.1007/s12237-011-9423-5

Yellen, B., Woodruff, J. D., Ralston, D. K., MacDonald, D. G., & Jones, D. S. (2017). Salt wedge dynamics lead to enhanced sediment trapping within side embayments in high-energy estuaries. *Journal of Geophysical Research: Oceans*, *122*(3), 2226–2242. doi: 10.1002/2016JC012595

Zhu, J., Wu, H., Li, L., & Qiu, C. (2018). Saltwater Intrusion in the Changjiang Estuary. In Y. Z. X. San Liang (Ed.), *Coastal Environment, Disaster, and Infrastructure—A Case Study of China's Coastline* (pp. 49–73). London, UK: IntechOpen. doi: 10.5772/intechopen.80903

Zimmerman, J. (1986). The tidal whirlpool: A review of horizontal dispersion by tidal and residual currents. *Netherlands Journal of Sea Research*, *20*(2–3), 133–154. doi: 10.1016/0077-7579(86)90037-2